CHAPTER 4.
EXPERIMENTAL RESULTS: VELOCITY PROFILES

4.1. Overview of the Experiments

Detailed measurements of velocity were made with ADCP and ADV instrumentation over bedforms in three separate experiments for this research. One set of data was collected from the Kankakee River above the Illinois-Indiana State Line Bridge, with the two remaining data sets collected from the Missouri River at St Charles, Missouri. Hydraulic and bedform characteristics for these three data sets are presented in table 4.1. The abbreviations for each data set is contained in table 4.1 and will be used for the remainder of this paper. The majority of the temporally averaged velocity and shear stress data is contained in the appendix to this report.

KANK-1 was collected on June 5, 2002, during a recession of a high-flow period. The flow just was below bankfull conditions and remained fairly steady during the duration of data collection (9.5 hours). Steadiness was determined from readings from a staff gage positioned on the right bank just downstream of the study reach. During the data-collection period, the water-surface elevation dropped .006 m. Water-surface slope was determined by comparing the water surface elevation at the study reach and the water surface elevation from the USGS streamflow-gaging station 17.3 km upstream at Shelby, Indiana (05518000). With the relatively uniform cross section of the Kankakee River in this reach, the water-surface slope is thought to be uniform.

Data Set	KANK-1	MO-1	MO-2	
Date	June 5, 2002	June 19, 2002	August 27, 2002	
Q	51.6 m^3/s	3,160 m^3/s	1,407 m^3/s	
S	0.000156	0.000161	0.00017	
<H>	1.84 m	6.46 m	4.87 m	
U	74.63 cm/s	152.05 cm/s	102.93 cm/s	
			Large	Small
H_d	0.25 m	1.25 m	1.1 m	0.32 m
λ	117.5 m	23.0 m	140 m	5.7 m
H_d/λ	0.002	0.05	0.008	0.056
H_d/<H>	1/7.36	1/5.02	1/4.4	1/15.2
λ/<H>	63.8	3.56	28.7	1.17
θ_S	0.20°	5.7°	0.72°	3.4°
θ_L	0.31°	7.8°	1.3°	14°-30°
L_S/L_L	1.54	1.09	1.90	1.5
(u_{*T})FB	5.31 cm/s	9.96 cm/s	9.01 cm/s	
(u_{*T})VP	4.91 cm/s	9.99 cm/s	8.244 cm/s	
Fr	0.168	0.2	0.149	
Re	$1.3X10^6$	$9.5X10^6$	$5.0X10^6$	
R_{ig}	38.3	33.2	53.8	
T	16.3°C	23.5°C	26.8°C	
D_{50}	0.31 mm	0.31 mm	0.31 mm	
k_c	11.22 cm	18.15 cm	69.04 cm	
f	0.0440	0.0343	0.0613	
n	0.025	0.029	0.036	
W_0	0.051	-0.077	-0.054	

Q, discharge; S, water-surface slope; <H>, mean depth; U, mean velocity; H_d, dune height; λ, dune length; θ_S , angle between horizontal and stoss side of bedform; θ_L, angle between horizontal and lee side of bedform; L_s, length of stoss side; L_L, length of lee side; (u_{*T})FB, shear velocity for the reach computed from the product of the water slope and mean depth; (u_{*T})VP, shear velocity for the reach computed from the slope of the reach-wise spatially averaged velocity profile; Fr, Froude number; Re, Reynolds number; R_{ig},. Gross Flow Richardson Number; T, water temperature; D_{50} , median diameter of the bed material; k_c, composite roughness height; f, Darcy-Weisbach friction factor; n, Manning's roughness coefficient; and W_0, Coles wake parameter for the reach-wise spatially averaged velocity profile

TABLE 4.1—General data for experiments KANK-1, MO-1, and MO-2

Detailed velocity measurements for the KANK-1 test were collected at 23 locations over the dune field (figure 4.1) for a sample time of approximately 10 minutes for most locations. The longitudinal location of the sample locations was down the middle of the channel. Less sample time resulted at some locations (in an effort to complete all locations before dark, four locations were sampled for 300 seconds, one location for 150 seconds, and one location for 100 seconds). The bedforms were asymmetric with superimposed large ripples. The bedforms were fairly two-dimensional in appearance, with the bedform crest running perpendicular to the stream direction for most of the stream width. The line of locations for collecting the velocity data was along the centerline of the river.

A 1200-kHz ADCP was used for the KANK-1 experiment. For locations 1-4, water mode 5, with a 5-cm depth cell setting was attempted, however, the data were poor (with missing data) (figure 4.2A), and by location 5, water mode 1, with 25-cm depth cells were used. These settings resulted in provided better data (figure 4.2B) than was collected for the previous settings in locations 1-4

A

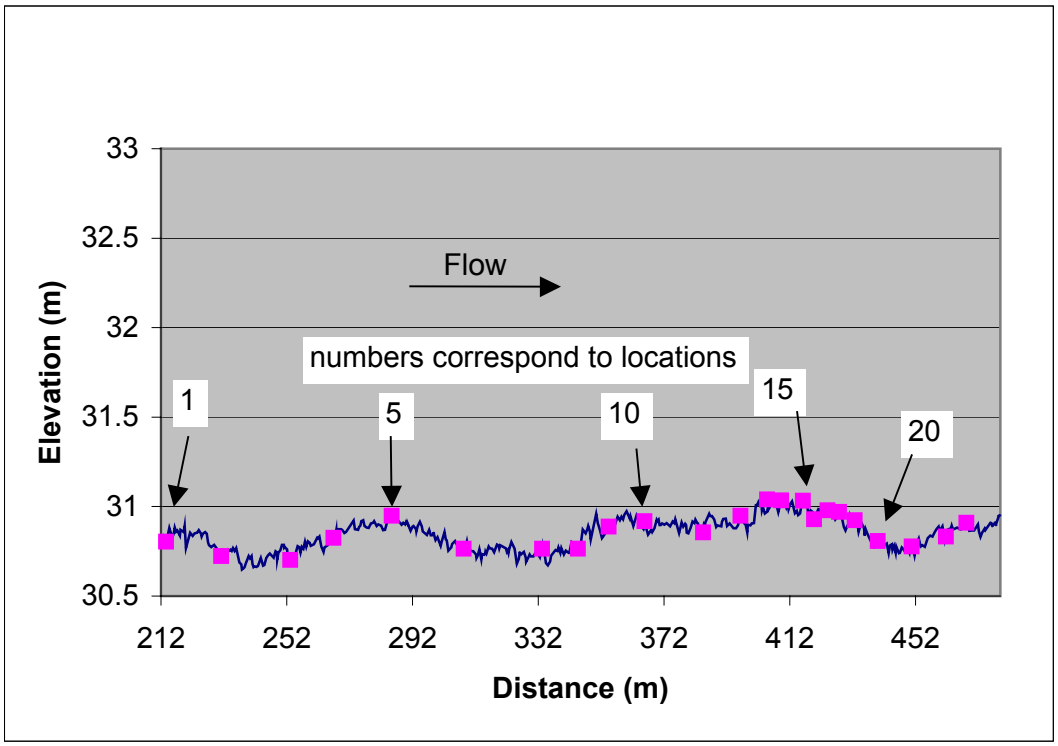

B

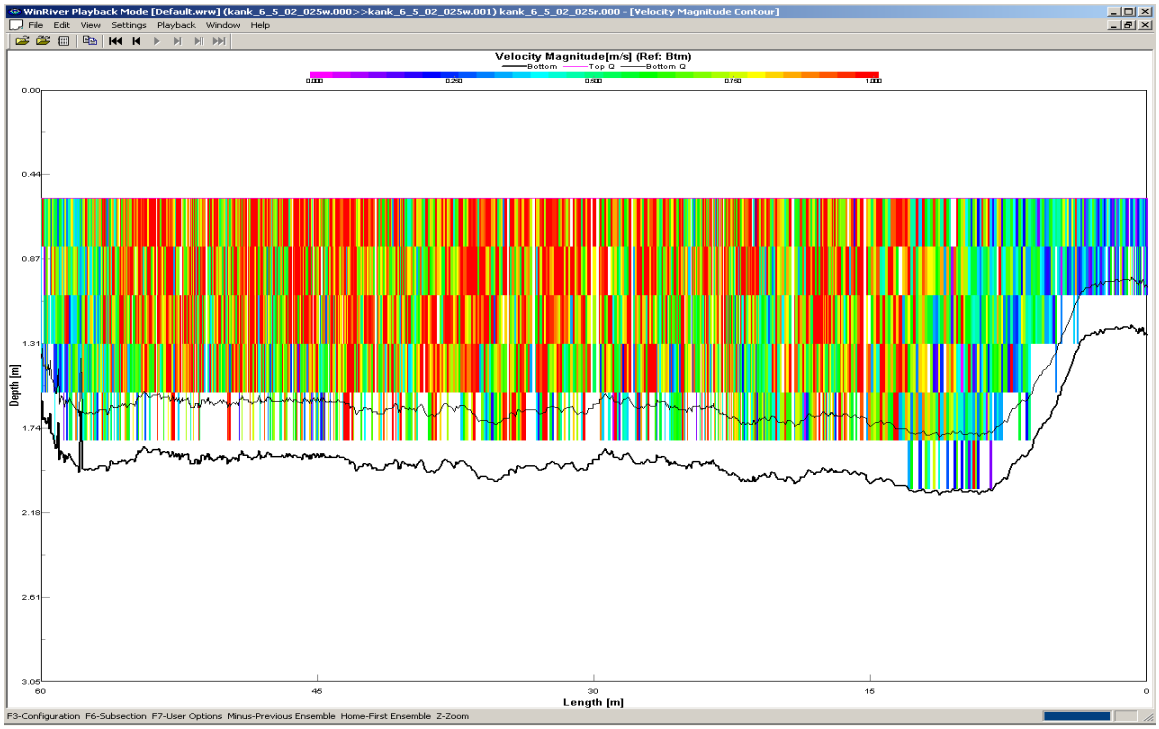

Figure 4.1—A) Locations for detailed velocity data collection in KANK-1 and B) typical cross section through the sampled reach

A

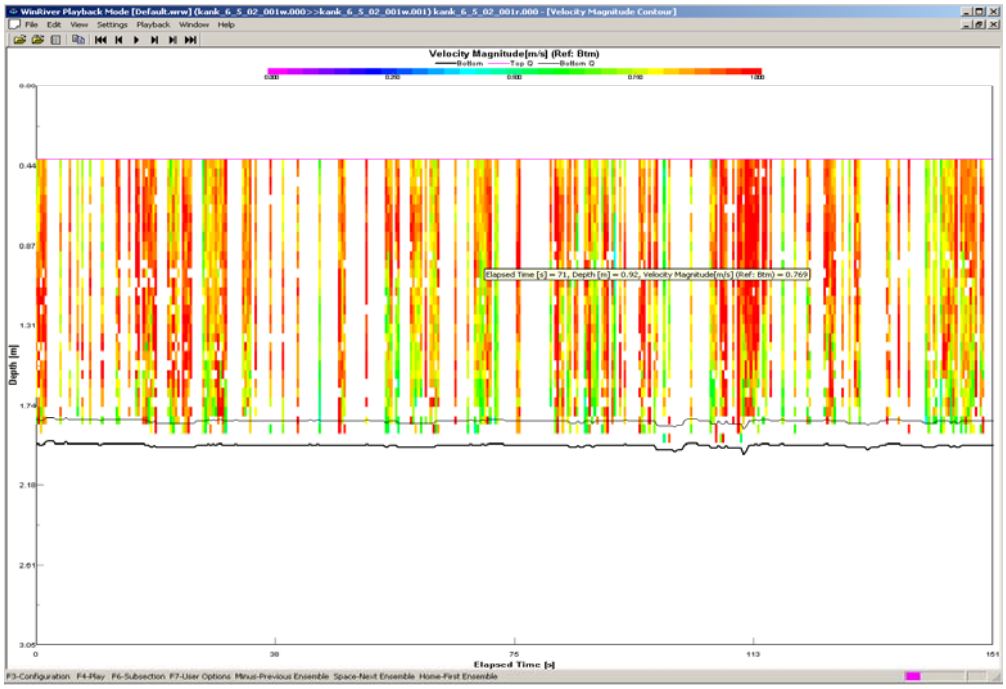

B

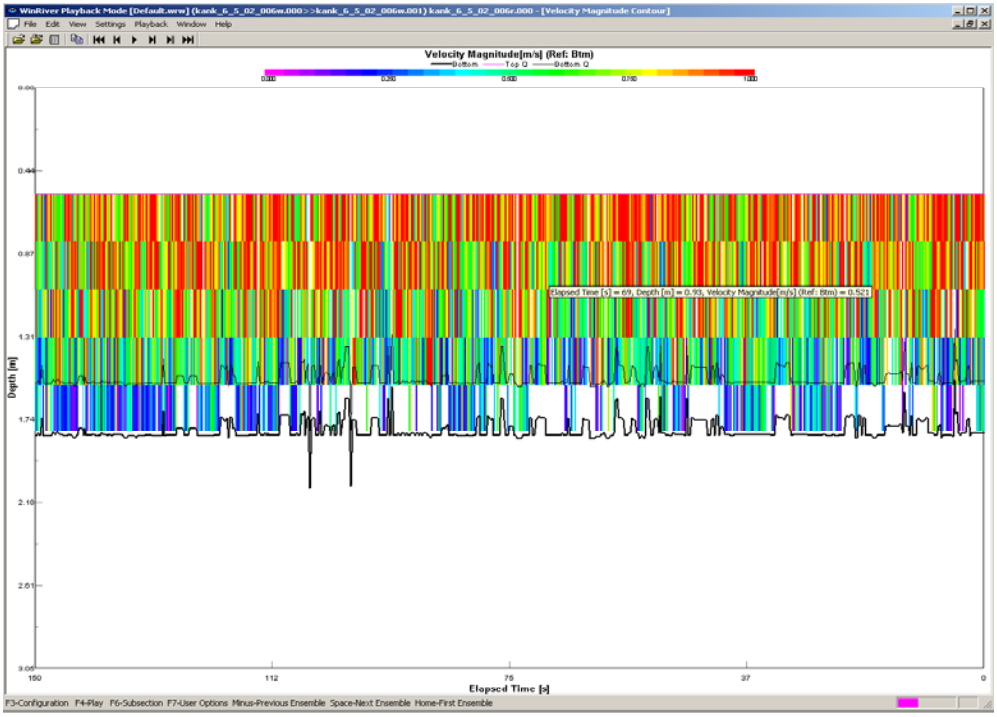

Figure 4.2--- ADCP output from the Kankakee River measurements June 5, 2002, in A) water mode 5 and B) water mode 1 for the 1200 kHz RDI Rio Grande Workhorse ADCP

ADV data were collected in each vertical of KANK-1 at two locations near the bed from the modified P-61 sampling frame (resting the sampler on the bottom of the river). The sample location of the bottom ADV was 30.5 cm below the upper ADV sample location. The bottom ADV sample location was set to be approximately 9.2 cm from the bed, assuming the bed and the P-61 are perfectly level. However, as discussed in Section 3.2.1, the initial distance indicated by the probe to the boundary was used to determine the elevation of the bottom probe from the boundary. A third ADV was mounted near the water surface on the ADCP frame to obtain a near-surface velocity data. The time-averaged ADCP and ADV data are shown in figure 4.3.

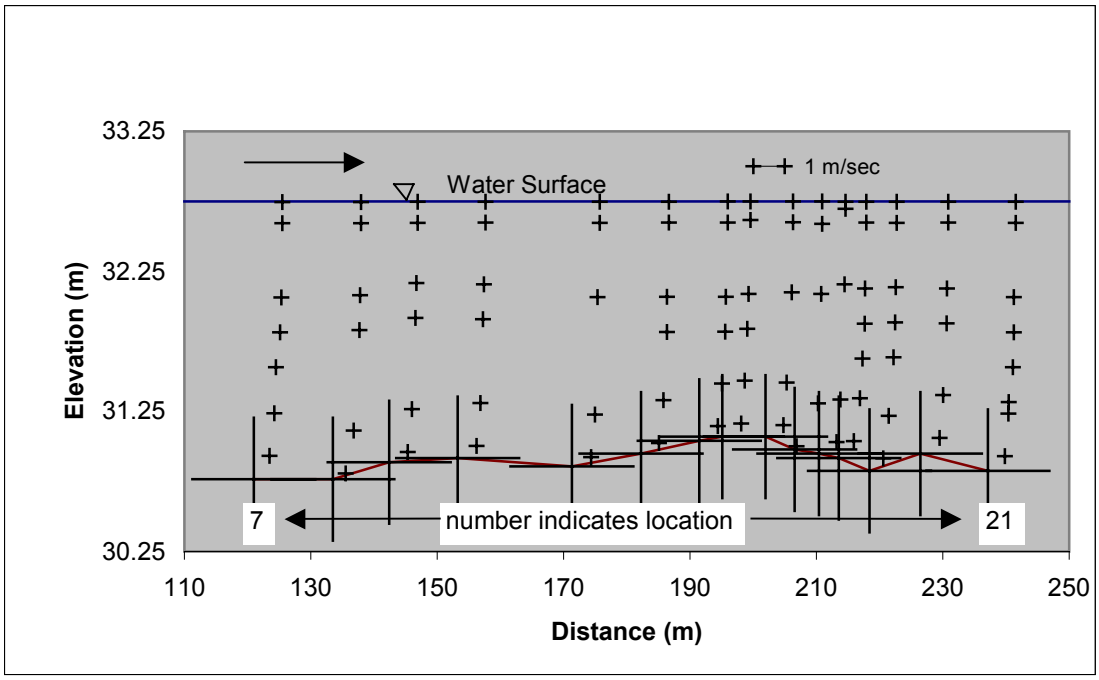

Figure 4.3—Streamwise velocity observations for KANK-1 at locations 7 - 21

Data set MO-1 was collected on June 19, 2002, during the recession to a slight rise on the Missouri River. A USGS streamflow-gaging station (06935965) is immediately

adjacent to the study reach. During the course of the experiment (approximately 8 hours), the water-surface elevation decreased .07 m with a corresponding decrease in water discharge of 56.6 m^3/s. Water-surface slope was determined by comparing the water-surface elevation at the gaging station at the study reach with water-surface elevations from National Weather Service water surface readings 53 km upstream at Washington, Missouri and from the Corps gaging station 44.6 km downstream at the confluence of the Missouri and Mississippi Rivers. The water-surface slope is most likely not uniform over this reach, however, as can be seen later, the bulk shear stress computed from the product of the water-surface slope, flow depth, and acceleration of gravity compares well with the bulk shear stress computed from the slope of the spatially averaged velocity profile. This agreement indicates that the water-surface slopes measured for the Missouri River data sets are acceptable.

Detailed velocity measurements for MO-1 were collected at 20 locations over the dune field (figure 4.4), along the approximate center of the channel. The dunes were fairly symmetric with no appearance of any superimposed features. The dunes appeared to be quasi two-dimensional for about 250 m across the width of the center of the stream, with a region of plane-bed conditions near the right bank side for about 100 m (figure 4.5). From the author's experience in surveying bedforms at a variety of locations along the Missouri and Mississippi Rivers, two-dimensionality of bedforms is rare and difficult to attain. Some of the "mounded" appearance of the bedforms is likely from the lack of detail in the survey cross sections. Survey transects were run parallel to the flow at approximately 20 m spacing, which gives the appearance of three-dimensionality than

actually present. The red line on figure 4.5 is the location that the data for MO-1 were collected on the following day (June 19, 2002).

At each location in MO-1, the sample time was approximately 10 minutes. A 600-kHz ADCP, with 25-cm depth cells, were used for this experiment. The bedforms present for MO-1 were short (23 m), resulting in a larger steepness ratio than in the other two data sets. Because of the ADCP beam spread , the depths reported from the ADCP were incorrect in areas with rapid bed elevation changes (such as near the crest and subsequent trough) (figure 4.6). The ADCP depths and subsequent locations of the velocity bins from the boundary were adjusted using the depth at that location determined from the 200-kHz survey Fathometer. The Fathometer data are noisy (figure 4.6) because of the instrument sensitivity was set too high; however, the bed elevation can be determined easily.

A

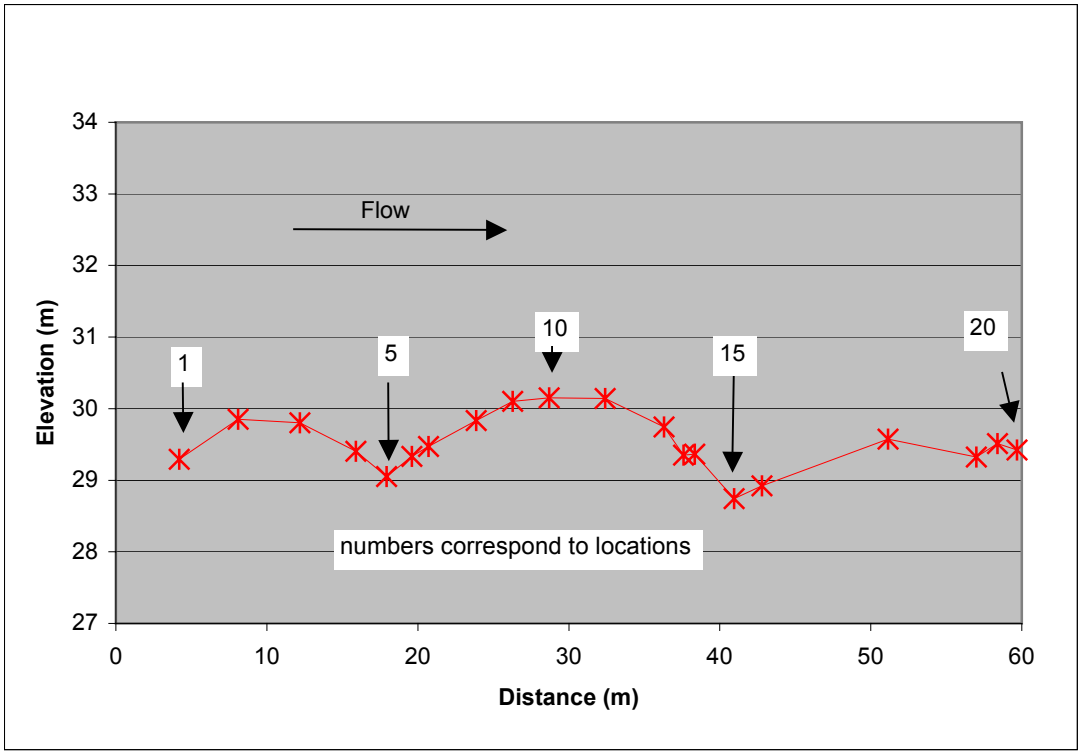

B

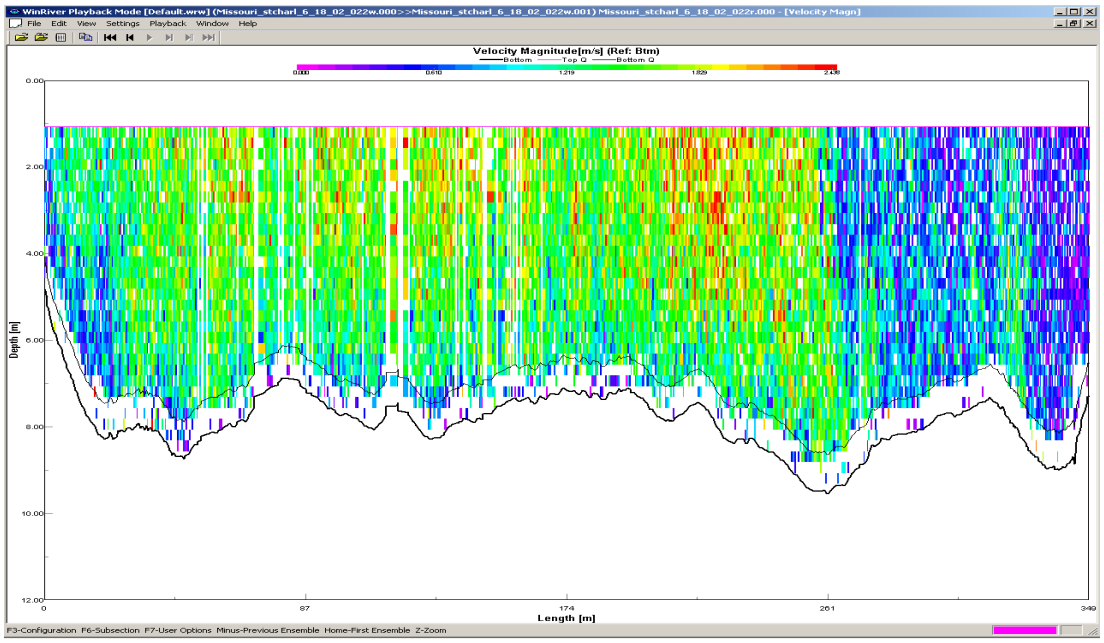

Figure 4.4—A) Locations for detailed velocity data collection in MO-1 and B) cross section (looking downstream) of the channel downstream of the detailed velocity data collection reach

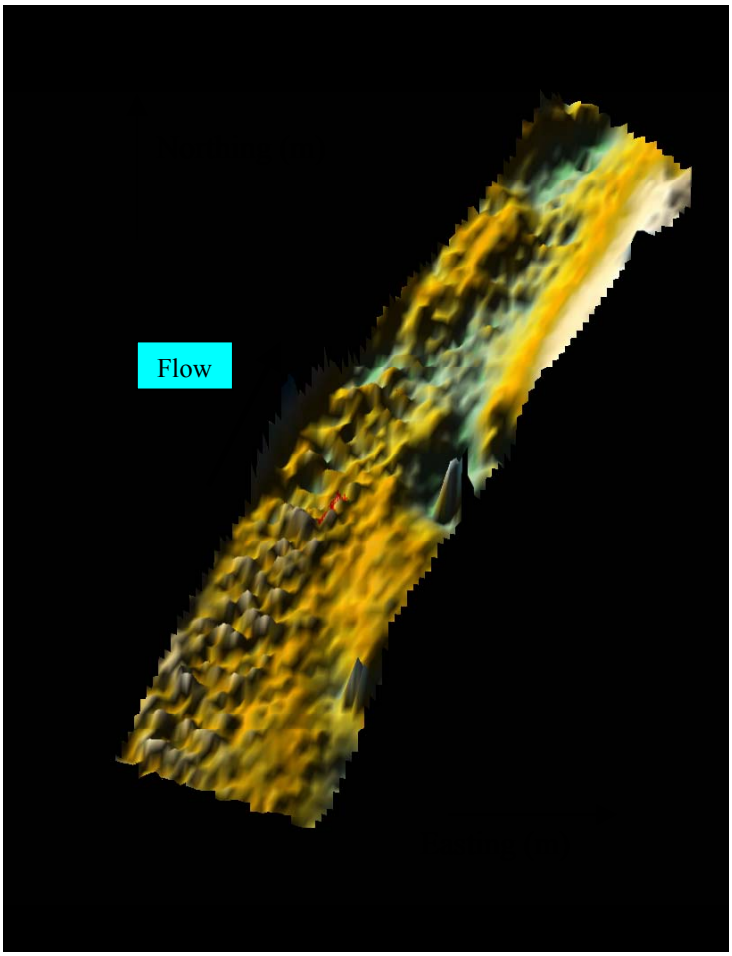

Figure 4.5—Three-dimensional view of the bedforms for the Missouri River at St Charles on June 18, 2002 (note that this is the day before the MO-1 data were collected with the red line being the approximate line where detailed data was collected for MO-1).

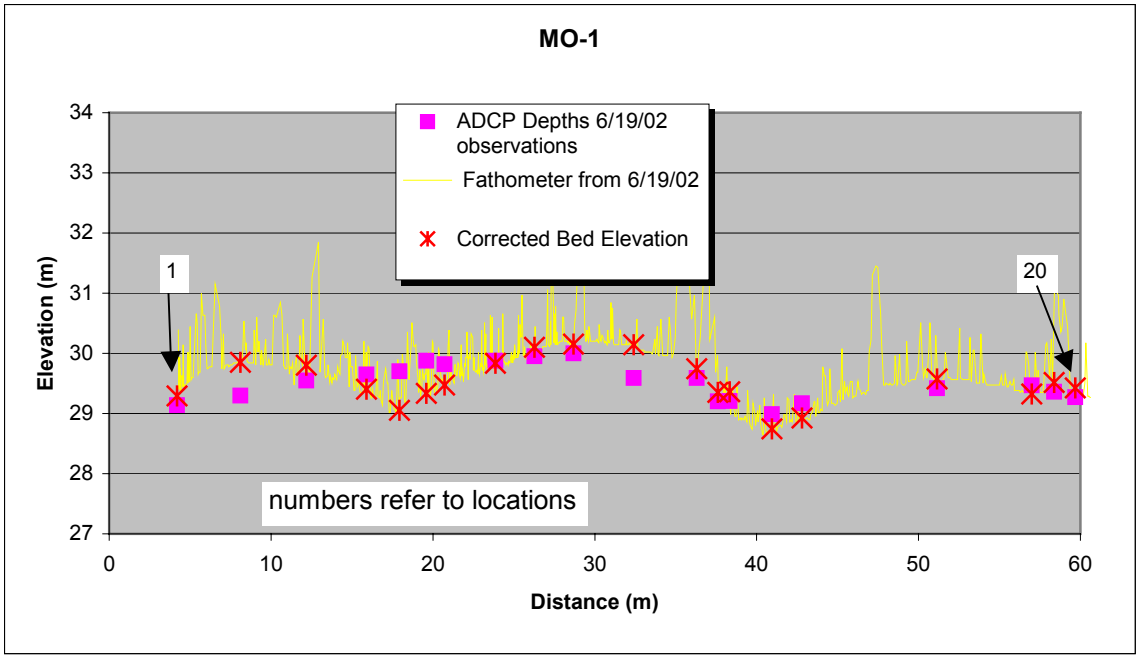

Figure 4.6--- ADCP reported depth and the depths from the Fathometer survey for MO-1

ADV data were collected at two locations near the bed using the modified P-61 sampling frame at each vertical of MO-1. These data were collected by resting the sampler on the river bottom. The sample location of the bottommost downward-looking ADV was 36.3 cm below the uppermost upward-looking ADV sample location. The bottom ADV sample volume was set to be approximately 5.7 cm from the bed with the P-61 sitting on the bed. When a boundary is within approximately 25 cm, the Nortek ADV has the capability to determine the sample distance from a boundary. Because of the heavy sand transport near the bed, this distance measuring capability failed to work for the bottommost ADV. Therefore, it was assumed that the lower ADV was 5.7 cm from the boundary and the upper ADV on the P-61 frame was 42 cm from the boundary. Furthermore, a majority (>50%) of the data from this bottommost ADV were filtered out

from the final data set because of low correlation among the three beams of the ADV (threshold was set at 70% correlation of three beams). An example of the appearance of the filtered ADV data from the bottommost probe for MO-1, location 5 is shown in figure 4.7. Data filtering was conducted using the WinADV32 software developed by the U.S. Bureau of Reclamation. .

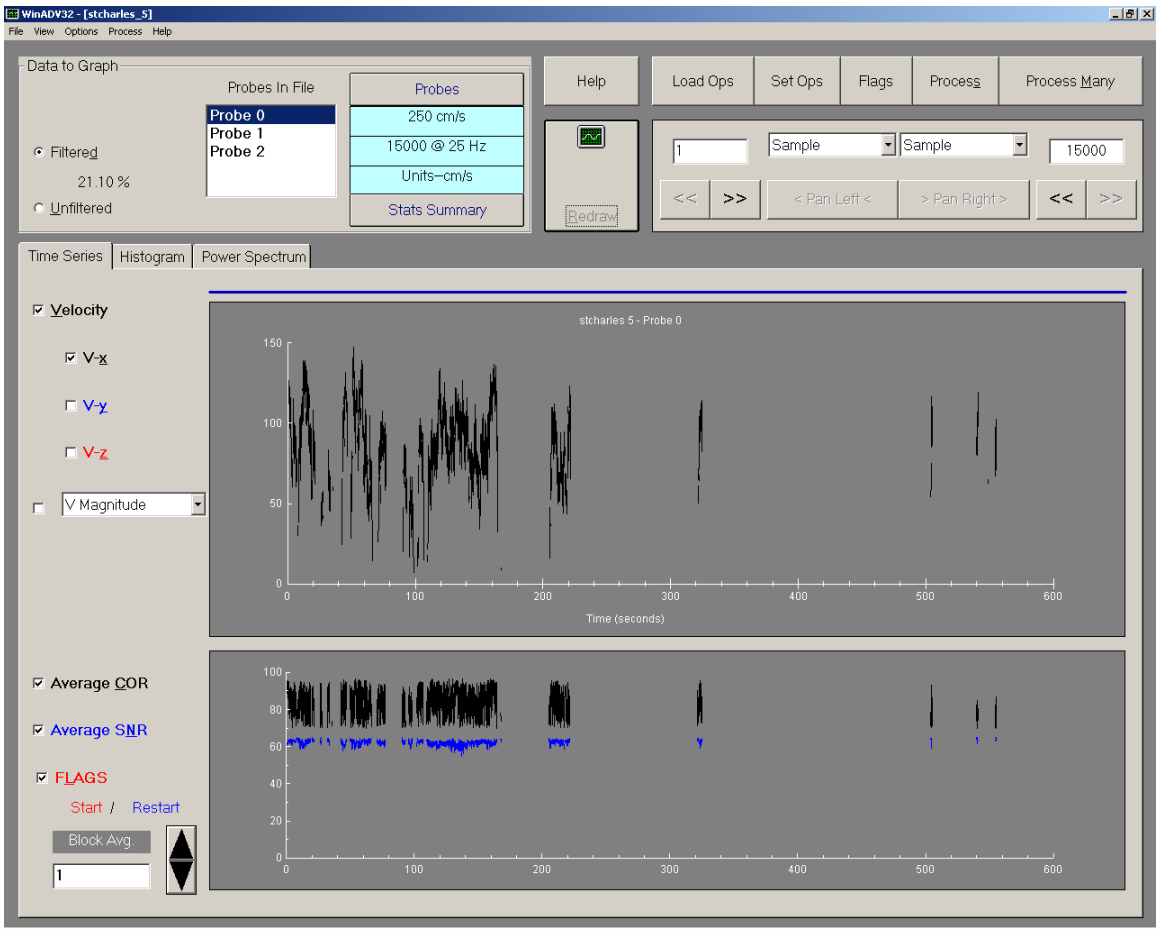

Figure 4.7---Time-series data from the lower ADV for MO-1, location 5

A third ADV was mounted near the water surface on the ADCP frame to obtain near-surface velocity data. During MO-1 data collection, the boat, although anchored, had to be canted at an angle to the flow to prevent the cable suspending the modified P-61 frame from coming off the pulleys because of the water speed. This positioning caused the measured velocities near the water surface to be lower than would have resulted if the boat had not been present. This result is indicated in many of the velocity readings from the near-water surface ADV when plotted with other data (example found in figure 4.8). The time-averaged ADCP and ADV data for MO-1 are shown in figure 4.9.

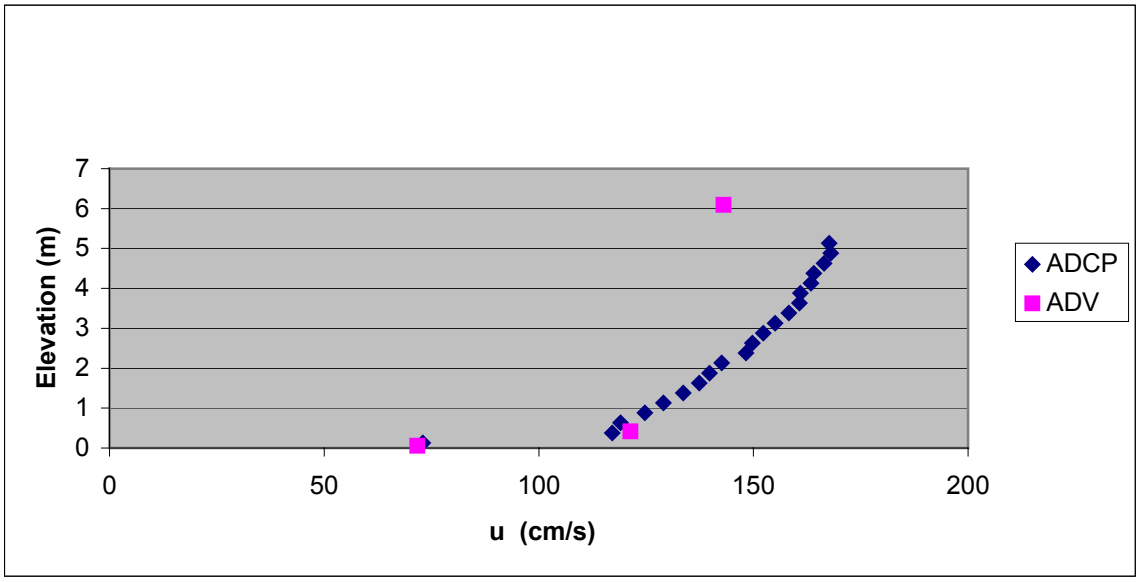

Figure 4.8—Time-averaged mean velocity profile for MO-1, location 2

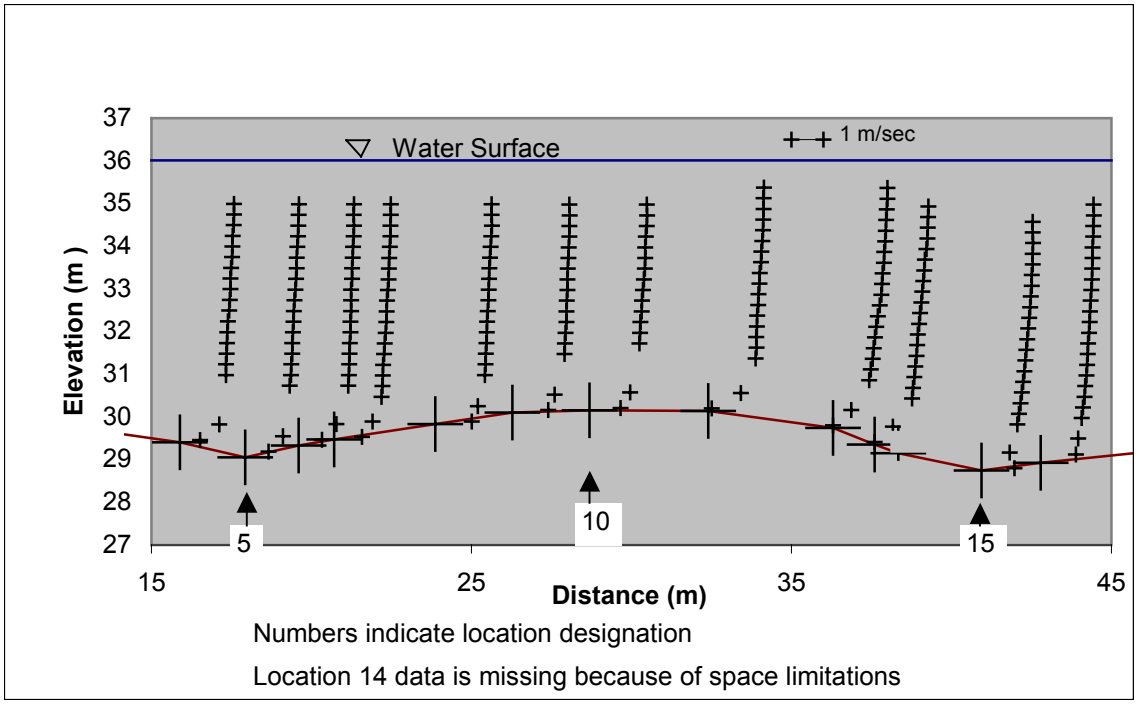

Figure 4.9—Streamwise velocity observations for MO-1, locations 4-16

Data set MO-2, utilizing the same stream reach on the Missouri River at St Charles as the MO-1 data set, was collected on August 27, 2002, during a period of fairly steady flow on the Missouri River. The water-surface elevation decreased 0.03 meters with a corresponding water discharge decrease of 17 m^3/s during the approximately 8.5-hours long experiment. Detailed velocity measurements for MO-2 were collected at 15 locations over the dune field (figure 4.10) longitudinally down the approximate center of the channel. The bedform is asymmetric with smaller superimposed bedforms .

A different scheme was used during the MO-2 experiment to collect data than the scheme previously used for the KANK-1 and MO-1 experiments. In the early design of the research experiments, emphasis had been placed on collecting simultaneous flow data

(using both the ADCP and the ADVs). When the original platform proved infeasible to deploy, the P-61 sampler was modified but only two ADV's could be used because of both space and hydrodynamic limitations (more equipment on the P-61 induced more drag making the sampler difficult to lower to the bed). Although not ideal, two ADV points were thought to be adequate for analysis. Data analysis on MO-1 data revealed that additional spatial detail was needed in the near bed region of flow (<1 m from the boundary), not only for the velocity profile but also for the Reynolds stresses. Therefore, the concurrent collection of ADV velocity data was abandoned in favor of collecting more detailed data. A single ADV was positioned on the modified P-61 frame. Velocity data then were collected with the ADV at approximately every 10 cm from the bed to around 1 m above the bed by raising the ADV through the water column and keeping track of position with the dial readout on the boat crane. ADV velocity data were collected approximately every meter from 1 m above the bed to the water surface. Sample times ranged from 60 seconds to 120 seconds for all data points except Locations 14 and 15, where because of darkness, the sample time was reduced to approximately 30 seconds per point. Approximately 25 to 30 minutes of concurrent ADCP data were collected during the time the ADV data were collected. In most cases, good agreement resulted between the ADV data and the ADCP data, particularly for points that were more than 1 m from the bed (figure 3.12). The time-averaged ADCP and ADV data for MO-2 are shown in figure 4.11.

A

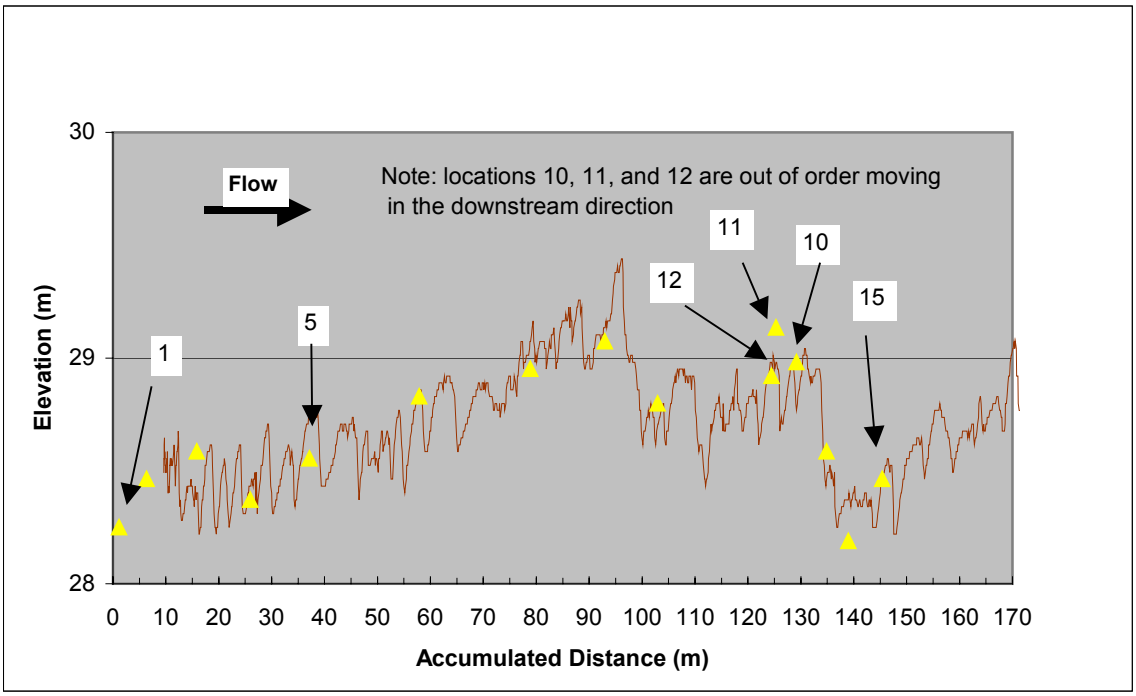

B

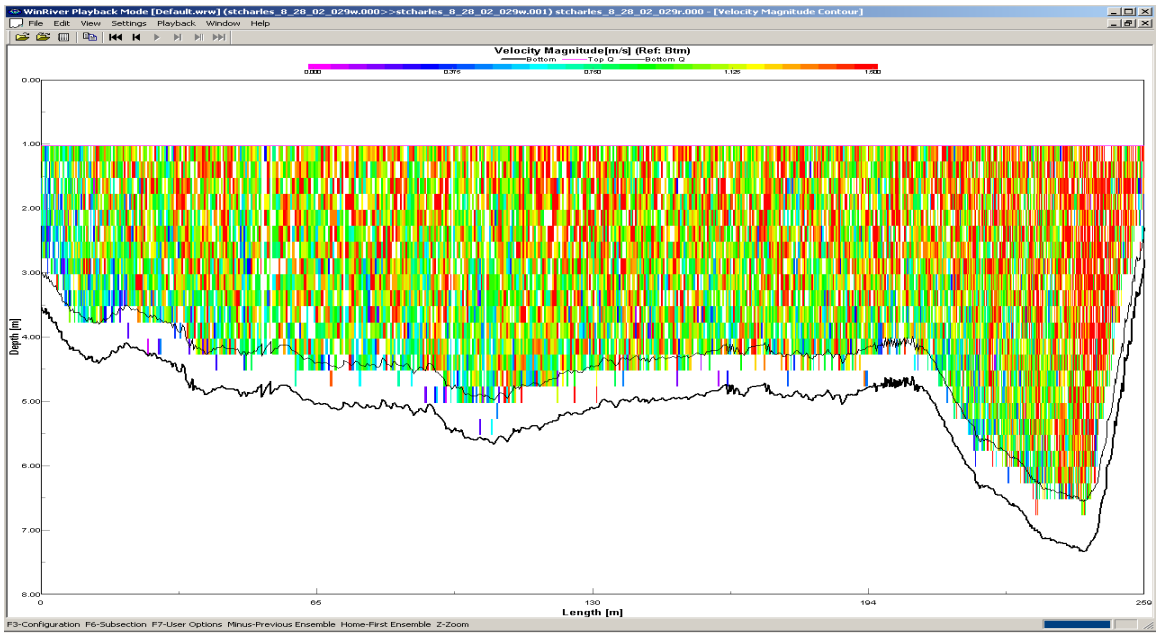

Figure 4.10---- A) Locations for detailed velocity data collection for MO-2 and B) cross section (looking downstream) of the channel downstream of the detailed velocity data collection reach

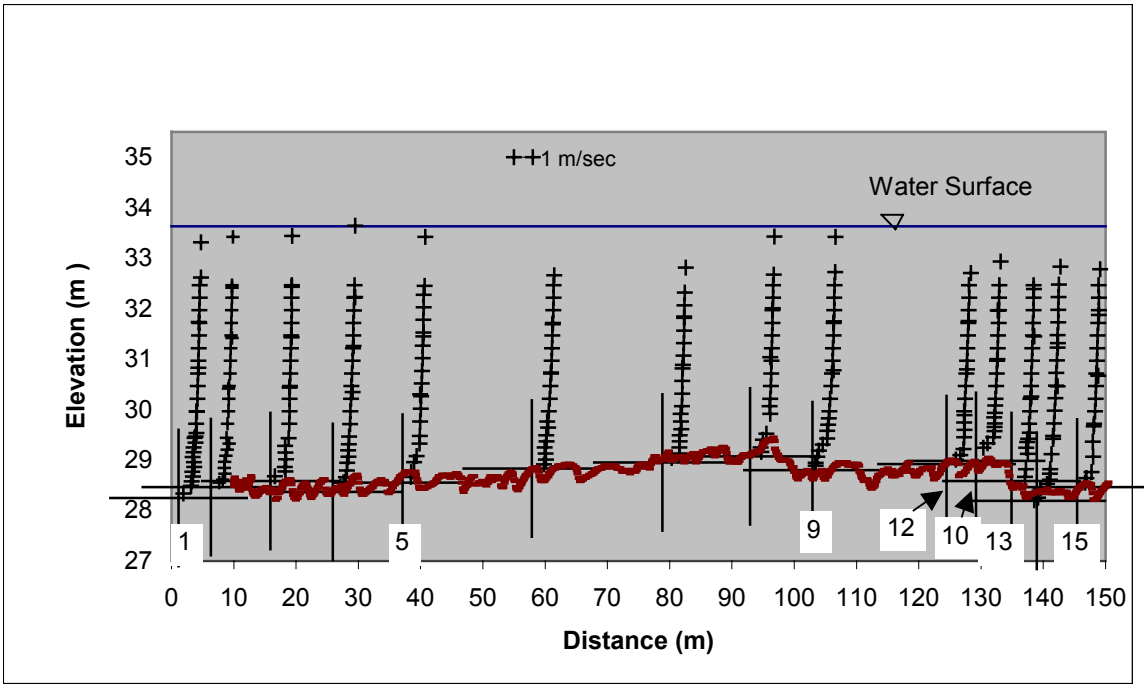

Figure 4.11--- Streamwise velocity observations for MO-2 at locations 1-15 (note: location 11 is omitted for clarity)

4.2 Overview of Data from Previous Studies

The field data collected in this research are compared with both laboratory flume studies and previous similar field studies. The laboratory studies found for comparison purposes include those by Lyn (1993), Nelson and others (1993), and Bennett and Best (1995), with the general data from these studies contained in table 4.2. Only data collected during two previous field studies were found to compare with data collected during the current study: Smith and McLean (1977) and Kostaschuk and Villard (1996), with the general data for these studies included in tables 4.3 and 4.4, respectively. Smith and McLean show little data at locations higher than 1 m above the bed, presumably because of both their interest in the near-bed processes and, possibly, also because of the

logistical difficulty in moving their measurement apparatus upward in the water column (only Smith and McLean (1977) experiments 69-W1 and 72-W1 show data above 1 m above the bed). There also are other details that are not readily available in their paper; thus, some fields in table 4.3 are left blank.

Each of the laboratory flume experiments utilized fixed bedforms (figures 2.19, 4.12, and 4.13 with clear water flows. Lyn (1993) ran three different bedform configurations, with only one configuration, case 3, being used in this research. Lyn's case 3 experiment (figure 4.12), has a series of fixed triangular bedforms positioned end-to-end. These bedforms have gradually sloping stoss sides. The configuration of the case 3 experiment is in contrast with the bedforms in case 1 and case 2, which were triangular elements spaced at regular interval with flat beds between the triangular elements.

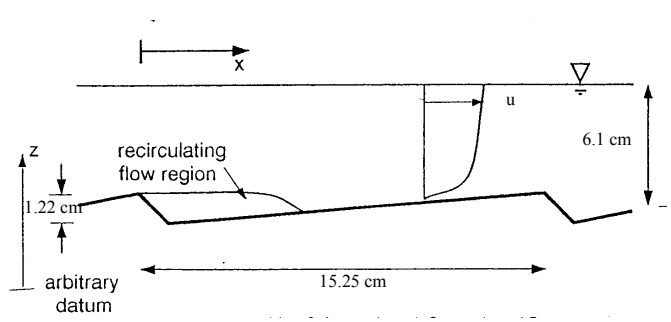

Figure 4.12—Bedform geometry of case 3 experiment from Lyn (1993)

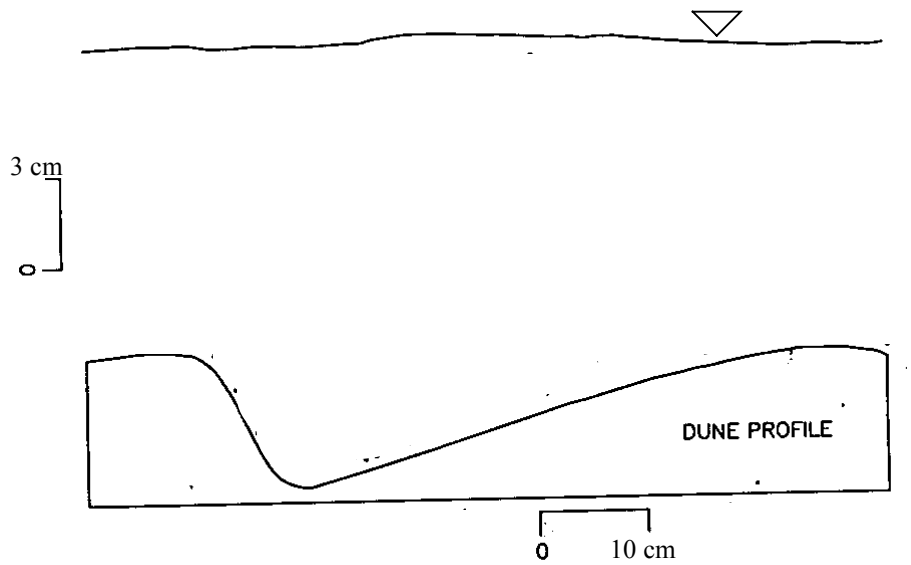

Figure 4.13—Bedform geometry of experiment from Bennett and Best (1995)

	Bennett and Best (1995)	Lyn (1993)	Nelson and others (1993)
<H>	11.6 cm	6.1 cm	19.5 cm
U	47.62 cm/s	56.28 cm/s	42.92 cm/s
H_d	4 cm	1.2 cm	4 cm
λ	63 cm	15 cm	80 cm
H_d/λ	0.06	0.08	0.05
H_d/<H>	1/2.9	1/5.08	1/4.88
λ/<H>	5.43	2.45	4.10
θ_S	4.19	4.18	3.07
θ_L	25.5	40.6	30.0
L_S/L_L	4.2	11.5	10.0
u_{*T}	4.1 cm/s	5.41 cm/s	3.74
Fr	0.46	0.71	0.36
Re	$5.7X10^4$	$3.4X10^4$	$9.9X10^4$
D_{50}	0.22 mm	0.25 mm	fine sand
k_c	0.46 cm	1.16 cm	2.37 cm

<H>, spatially averaged mean flow depth; U, mean velocity; H_d, dune height; λ, dune length; θ_S , angle between horizontal and stoss side of bedform; θ_L, angle between horizontal and lee side of bedform; L_s, length of stoss side; L_L, length of lee side; u_{*T}, shear velocity for the reach computed from velocity profile; Fr, Froude number; Re, Reynolds number; D_{50} , median diameter of the bed material; k_c, composite roughness height.

Table 4.2--- General data for flume experiments in the literature considered in this research

	Smith and Mclean (1977, 69-W1)	Smith and Mclean (1977, 69-W3)	Smith and McLean (1977, 71-W1)	Smith and McLean (1977, 71-W2)	Smith and McLean (1977, 72-W1)
Q	8000 m^3/s	8000 m^3/s	13,500 m^3/s	13,500 m^3/s	17,000 m^3/s
<H>	15.9 m	16.6 m	14.5 m	14.3 m	15.0 m
U	54.81 cm/s				145.7 cm/s
H_d	2.74 m	3.16 m	1.34 m	1.66 m	2.07 m
λ	74.3 m	82 m	82 m	80 m	96 m
H_d/λ	0.037	0.039	0.016	0.021	0.022
H_d/<H>	1/5.8	1/5.3	1/10.8	1/8.6	1/7.2
λ/<H>	4.67	4.94	5.66	5.59	6.40
θ_S					
θ_L					
L_S/L_L					
u_{*T}	3.67 cm/s	4.49 cm/s	9.98 cm/s	10.35 cm/s	10.79 cm/s
Fr	0.045				0.12
Re	$8.9X10^6$				$2.2X10^7$
R_{ig}	548	432	110	119	86.2
D_{50}					
k_c	30.9 cm	46.2 cm	139.8 cm	168.3 cm	196.5 cm
W_0	0.356	0.313	0.198	0.308	0.187

Q , water discharge; <H>, mean depth; U, mean velocity; H_d , dune height; λ, dune length; θ_S , angle between horizontal and stoss side of bedform; θ_L, angle between horizontal and lee side of bedform; L_s, length of stoss side; L_L, length of lee side; u_{*T}, shear velocity for the reach computed from velocity profile; Fr, Froude number; Re, Reynolds number; R_{ig}, Gross Flow Richardson Number; D_{50} , median diameter of the bed material; k_c, composite roughness height, and W_0, Coles wake parameter for the reach-wise spatially averaged velocity profile.

Table 4.3--- General data for field experiments conducted by Smith and McLean (1977)

	Kostaschuk and	Kostaschuk and	Kostaschuk and

	Villard (1996) June 21	Villard (1996) June 27	Villard (1996) June 29
<H>	11.27 m	11.09	12.76
U	182.9 cm/s	122.8 cm/s	151.8 cm/s
H_d	2.42 m	1.24 m	1.25 m
λ	37.2 m	29.9 m	33.6 m
H_d/λ	0..065	0.042	0.037
H_d/<H>	1/4.7	1/8.94	1/10.0
λ/<H>	3.3	2.70	2.63
θ_S	7.3	2.7	2.4
θ_L	7.5	18.7	18.9
L_S/L_L	1.02	7.17	8.17
u_{*T}	13.62 cm/s	11.81 cm/s	13.09 cm/s
Fr	0.17	0.12	0.14
Re	2.1 $X10^7$	$1.4X10^7$	$1.9X10^7$
Ri	66.1	81.9	63.7
D_{50}	0.33 mm	0.27 mm	0.32 mm
k_c	47.6 cm	184.8 cm	189.3 cm
W_0	0.121	0.0572	0.0779

Q , water discharge; <H>, mean depth; U, mean velocity; H_d, dune height; λ, dune length; θ_S , angle between horizontal and stoss side of bedform; θ_L, angle between horizontal and lee side of bedform; L_s, length of stoss side; L_L, length of lee side; u_{*T}, shear velocity for the reach computed from velocity profile; Fr, Froude number; Re, Reynolds number; R_{ig}, Gross Flow Richardson Number; D_{50} , median diameter of the bed material; k_c, composite roughness height, and W_0, Coles wake parameter for the reach-wise spatially averaged velocity profile

Table 4.4--- General data for field experiments conducted by Kostaschuk and Villard (1996)

4.3 Classification of Bedforms Present in Experiments

In studying flow over bedforms, it is important to classify the type of bedforms present to place flow results in proper context. The bedforms examined in this paper will be classified into two groups (both in the lower-flow regime): 1) bedforms that approximate equilibrium dunes and 2) bedforms that do not approximate equilibrium dunes (washed-out dunes (residual waves), developing dunes, bars, etc.).

An equilibrium dune is characterized by the following characteristics.

1. A non-symmetric ($L_S/L_L>1$) appearance.
2. Gradual stoss slopes (θ_S) leading up to a crest that abruptly changes to a sharp lee slope (θ_L), roughly approximating the angle of repose of the bed material ($\phi_{sand} \approx 30°$).
3. The height and wavelength of the bedform scale with flow depth (H_d~1/6 H; λ~$2\pi H$).

The KANK-1 bedform geometry characteristics (table 4.1) indicate a bedform height to flow depth ratio that is of the proper scaling for equilibrium dunes; however the wavelength is much larger than $2\pi H$, in addition to a small lee slope ($\theta_L << \phi$). Therefore, the KANK-1 bedforms could not be characterized as equilibrium dunes and are more likely washed-out dunes.

The MO-1 bedforms have bedform geometric ratios (table 4.1) that would imply that the bedforms are equilibrium dunes, however, the bedforms are too symmetrical (L_S/L_L=1.09) to be equilibrium dunes. These bedforms likely are developing dunes and not washed-out dunes, because as pointed out by the observations of Shen and others (1978) and Jordan (1965), bedforms typically become elongated for large flow depths when they are washed-out dunes.

Characterizing the MO-2 bedforms is difficult with the presence of smaller superimposed bedforms on a larger bedform. Both the smaller and larger bedforms are non-symmetric, but the bedform geometries are on both sides of the expected scale ratios for equilibrium

dunes (table 4.1). The lee slopes of the smaller bedforms are consistent with the angle of repose for sand (ϕ=30˚). Also, the composite roughness height scales between the smaller and larger bedform height, which indicates that the flow is experiencing form resistance. These bedforms are characterized as equilibrium dunes.

The laboratory bedforms of Bennett and Best (1995), Lyn (1993), and Nelson and others (1993) are all characterized as equilibrium dunes. All these bedforms are non-symmetric with gentle stoss slopes and steep lee slopes ($\theta_L > \phi$) (table 4.2). The bedform geometries all are within the expected ratios for equilibrium, with the exception of the geometries of the Bennett and Best (1995) experiments, where the bedform height to flow depth is 1/3. Nonetheless, all of the laboratory bedforms were considered to be equilibrium dunes.

The bedform geometries of the Smith and McLean (1977) experiments (table 4.3) all are characterized as equilibrium dunes. The bedform geometry ratios are within expected ratios for equilibrium dunes.

The Kostaschuk and Villard (1996) June 21 experiment had symmetric bedform geometries (table 4.4) and small lee slopes ($\theta_L << \phi$). The June 21 experiment was considered not to be equilibrium dunes, but rather washed-out dunes. The two remaining Kostaschuk and Villard (1996) experiments, June 27 and June 29, were asymmetric with bedform geometry ratios within the range of that expected for equilibrium dunes.

Therefore, the bedforms from these two experiments were considered to be equilibrium dunes.

Some of the more predominant available methods for prediction of bedform type and dimensions were discussed in Chapter 2. Kostaschuk and Villard (1996) evaluated some of the methods and found them poor for estimating the bedform geometry for large river field situations, largely because the majority of the data used to derive these methods is from laboratory studies. The bedform types predicted by selected methods are shown in table 4.5. Those graphs/methods developed using predominantly laboratory data (Simons and Richardson, 1966; Liu, 1957) predict an upper regime bedform type for the large river experiments (MO-1 and MO-2). This problem with predicting the bedform type also was found in other large river experiments (Jordan, 1965; and Shen and others, 1978). Van Rijn (1984C) reportedly using a range of data to develop his graph (flume data as well as large river data). Van Rijn's (1984C) method predicts the Missouri River bedforms to be in transition into the upper regime of bedforms. This prediction may be appropriate for the MO-1 data as the bedforms were not equilibrium dunes (see previous discussion); however, this prediction is not accurate for the MO-2 data. The Froude numbers for the MO-1 and MO-2 data are below any critical value for transition (table 4.1). It is apparent that current methods considered here are lacking to accurately predict the bedform type present in the field-scale experiments of this research.

Method	**KANK-1**	**MO-1**	**MO-2**
Simons and Richardson(1966)	dunes	upper regime	transition

Liu (1957)	dunes	plane bed/ antidunes	plane bed /stand.waves
Znamenskaya(1969)	ripples	ripples	ripples
Hill and others (1967)	flat bed/dunes	flat bed	flat bed
Vanoni (1974)	dunes	dunes	dunes
Van Rijn (1984)	dunes	transition	transition
Karim (1995)	ripples/dunes	ripples/dunes	ripples/dunes

Table 4.5—Predicted bedforms from selected methods in the literature

4.4. Structure of the Mean Velocity Profile

As previously described through laboratory experiments and conceptualization of flow over dunes, flow separation occurs near the crest of the dunes followed by a reattachment of the flow on the next downstream dune. At the reattachment point, a new internal boundary layer begins to grow within the wake region. Among the many questions of interest in reviewing the field data from these experiments are as follows.

1. Does the flow separate revealing some sort of wake zone (Nelson and others, 1993) or zone of re-circulation (Lyn, 1993)?
2. Will the velocity distribution be logarithmic in nature?
3. Are topographically induced acceleration effects of the bedforms present all the way to the water surface?

4. Is a wake effect present in the outer region of the velocity profile and can it be successfully modeled by a Coles wake type formulation?
5. How does bedform type affect the flow dynamics (equilibrium dunes versus other bedforms)?

The streamwise velocity profiles have been presented in figures 4.3, 4.9, and 4.11. Summary data for the individual locations sampled as part of these experiments are listed in tables 4.6-4.8. The data listed in these tables are from those locations (verticals) that were used in computing the spatial averages used later (for example, for KANK-1, locations 7 through 21 were used in the spatial averaging discussed in the next section). In these three experiments, MO-2 and MO-1 had a detectable flow separation (for MO-2 at location 14 (figure 4.14), the near bed velocity actually is negative). Results from the lee of dunes in KANK-1 and MO-1 are shown in figures 4.15 and 4.16, respectively. KANK-1 shows a decrease in velocity near the bed at Locations 18 and 19; however no flow separation is detected. These changes in the velocity profile, which change the mean velocity, satisfy continuity because of the changes in the local flow depth.

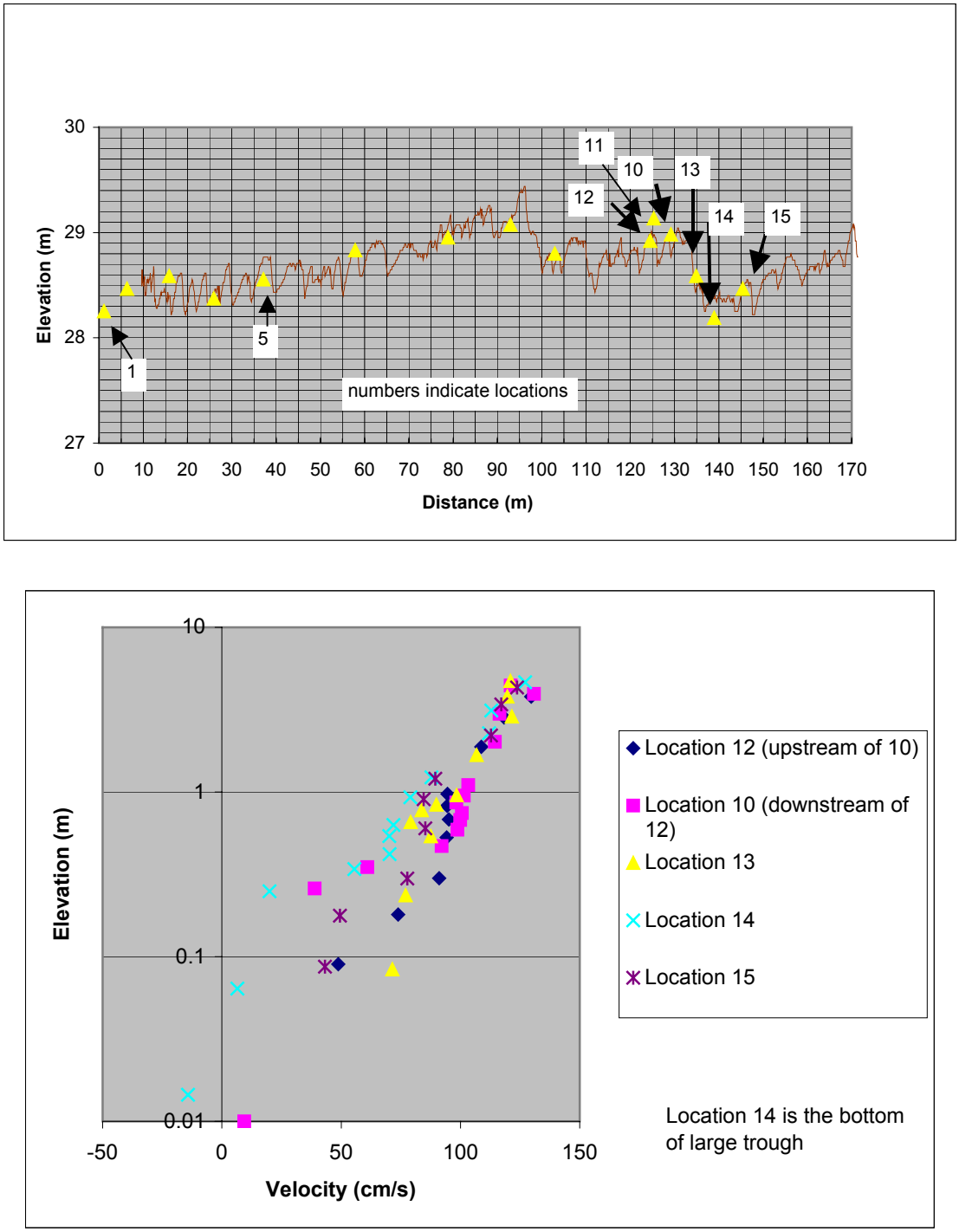

Figure 4.14—MO-2 velocity profiles at the crest and in the lee of the crest

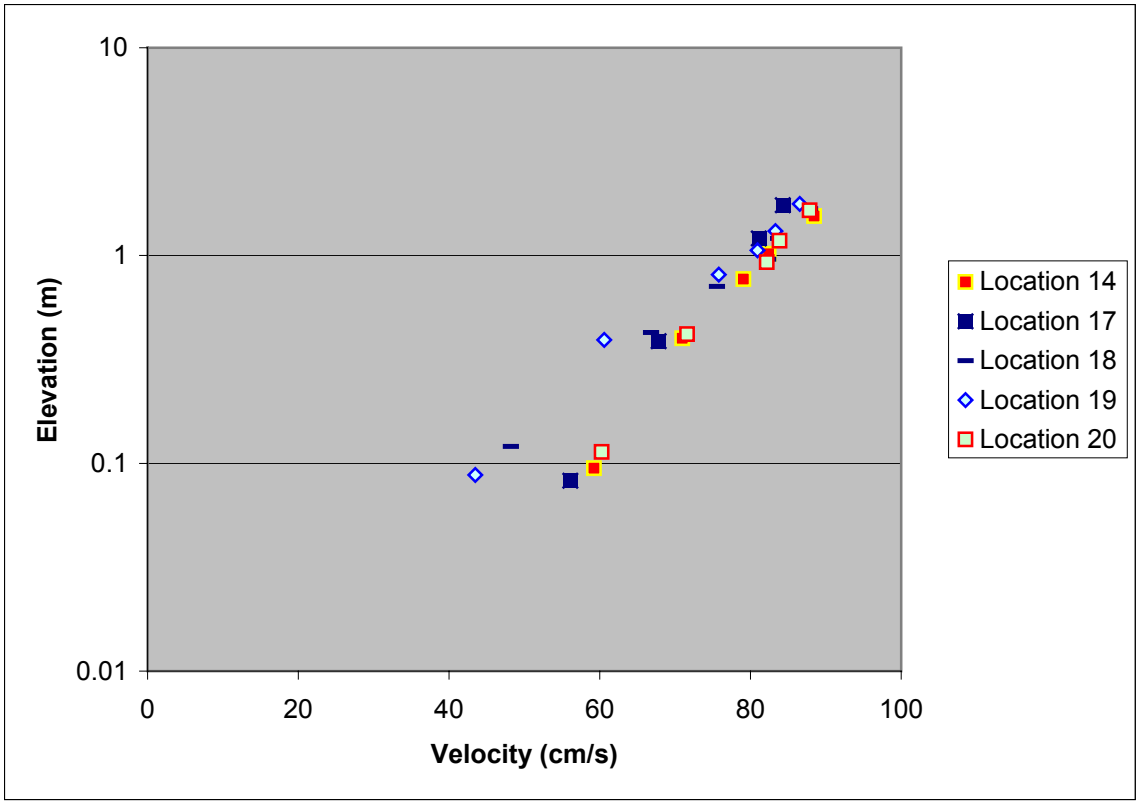

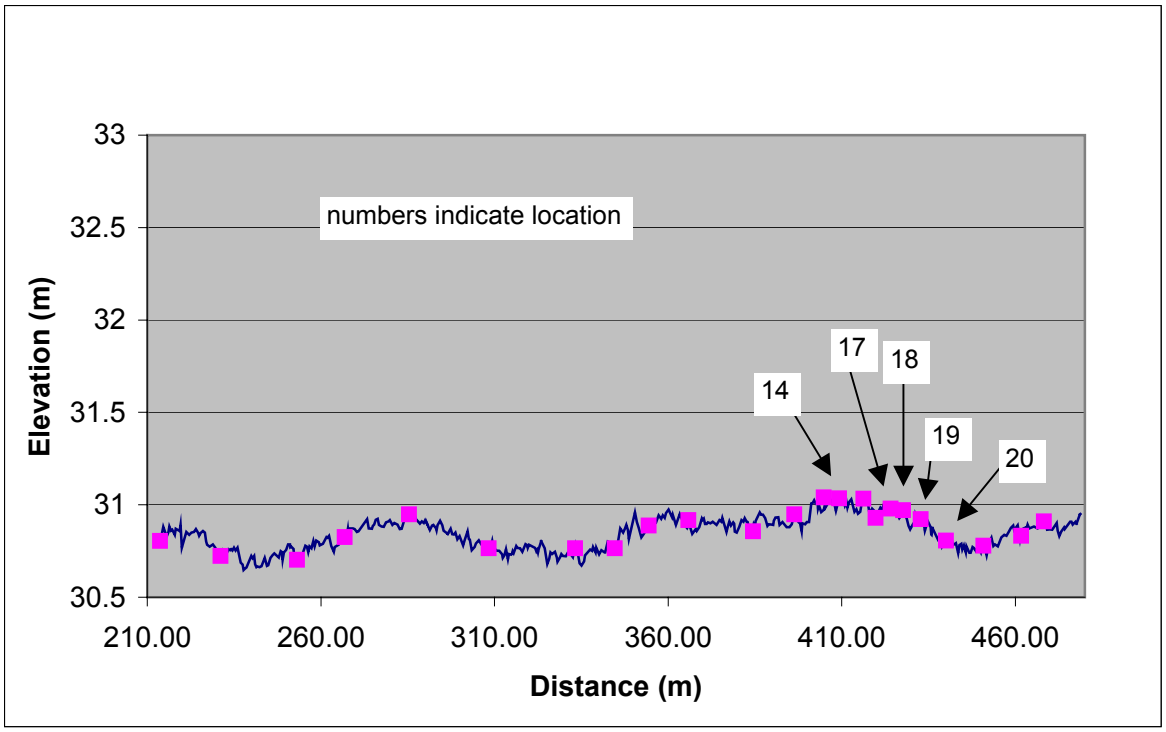

Figure 4.15—KANK-1 velocity profiles at the crest and in the lee of the crest

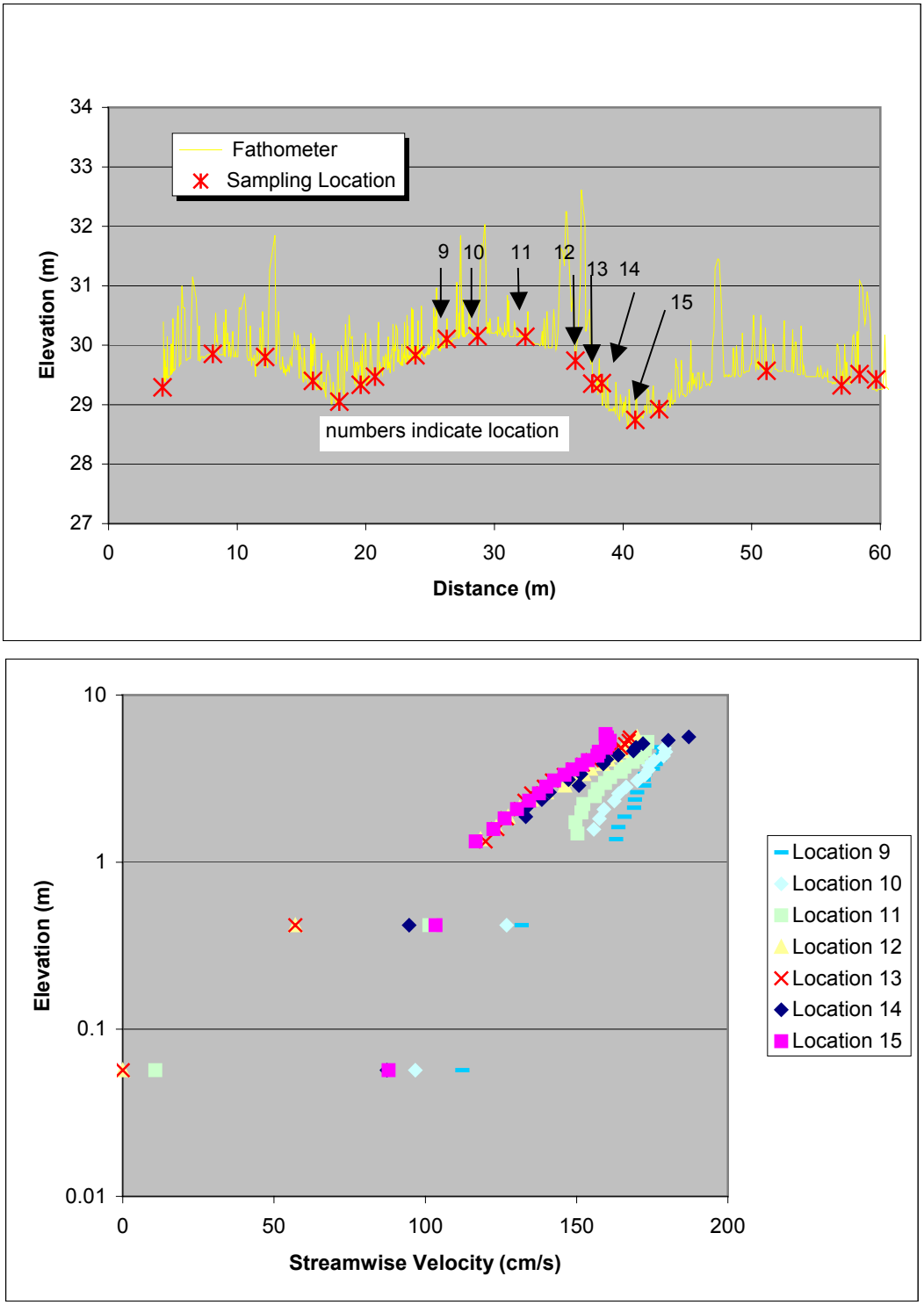

Figure 4.16—MO-1 velocity profiles at the crest and in the lee of the crest

Location	X (m)	X/λ	u_{*L} (cm/s)	U_m (cm/s)	H (m)	W_0
7	47.01	0.4	8.62	89.61	1.98	-0.003
8	58.76	0.5	6.23	88.74	1.98	-0.103
9	68.17	0.58	4.92	89.82	1.86	0.068
10	78.75	0.67	3.67	88.01	1.83	0.103
11	97.55	0.83	3.95	88.01	1.89	0.167
12	109.30	0.93	4.75	88.49	1.80	0.027
13	0	0	5.69	90.23	1.71	0.032
14	4.70	0.04	5.02	88.44	1.68	0.083
15	11.75	0.1	6.58	86.99	1.68	0.006
16	15.28	0.13	3.52	86.78	1.77	-0.036
17	18.80	0.16	4.79	84.27	1.80	-0.062
18	22.33	0.19	6.95	87.89	1.83	-0.073
19	27.03	0.23	7.95	86.52	1.92	-0.286
20	35.26	0.3	5.01	87.84	1.80	-0.007
21	45.84	0.39	7.22	88.10	1.92	-0.011

X is the distance from the previous bedform crest; λ is the dune length; u_{*L} is the local shear velocity for the outer layer; U_m is the maximum velocity in the vertical; H is the flow depth; and W_0 is the wake coefficient

Table 4.6—Data for experiment KANK-1

Location	X (m)	X/λ	u_{*L} (cm/s)	U_m (cm/s)	H (m)	W_0
5	8.43	0.37	6.91	169	6.96	-0.041
6	10.10	0.44	4.09	174	6.68	0.090
7	11.21	0.49	7.73	178	6.54	0.091
8	14.36	0.62	5.1	178	6.18	0.101
9	16.78	0.73	5.22	179	5.91	0.063
10	19.19	0.83	7.54	180	5.86	0.036
11	2.40	0.10	9.76	174	5.87	0.200
12	6.30	0.27	15.75	170	6.27	-0.058
13	7.60	0.33	10.46	168	6.66	-0.127
14	8.34	0.36	17.22	187	6.65	-0.033
15	10.94	0.48	13.06	162	7.27	-0.099

X is the distance from the previous bedform crest; λ is the dune length; u_{*L} is the local shear velocity for the outer layer; U_m is the maximum velocity in the vertical; H is the flow depth; and W_0 is the wake coefficient

Table 4.7—Data for experiment MO-1

Location	X (m)	X/λ	u_{*L} (cm/s)	U_m (cm/s)	H (m)	W_0
1	19.50	0.14	7.95	120	5.40	0.154
2	24.51	0.18	9.98	118	5.18	0.136
3	33.77	0.24	3.75	118	5.06	-0.251
4	43.54	0.31	8.96	119	5.27	0.040
5	54.41	0.39	7.39	122	5.09	-0.030
6	74.56	0.53	9.06	120	4.82	0.252
7	94.90	0.68	6.07	125	4.70	0.223
8	108.56	0.78	4.63	130	4.57	0.215
9	118.28	0.84	11.68	124	4.85	-0.186
12	139.18	0.99	8.50	130	4.73	0.205
11	0	0	9.67	121	4.51	0.154
10	3.76	0.03	7.44	131	4.66	0.201
13	9.28	0.07	7.77	122	5.06	-0.049
14	13.23	0.10	11.79	128	5.46	-0.087
15	19.50	0.14	10.21	124	5.15	0.067

X is the distance from the previous bedform crest; λ is the dune length; u_{*L} is the local shear velocity for the outer layer; U_m is the maximum velocity in the vertical; H is the flow depth; and W_0 is the wake coefficient

Table 4.8—Data for experiment MO-2

According to Nelson and others (1993), the distance between the crest and the downstream reattachment point averaged about 4 bedform heights, which follows the findings of Engel (1981). Lyn (1993) discussed the re-circulation region downstream of the dune crest and noted that in his laboratory results, the re-circulation region extended past the point of X/λ=0.25, which is defined in figure 4.17 (from Lyn, 1993). Data analysis from the current field experiments indicates that although there is flow separation, the spatial resolution of these experiments was insufficient to definitively ascertain the reattachment point (although attempts were made to have detailed velocity profiles closely spaced in the area immediately downstream of a bedform crest to fully characterize the separation). In MO-1 (figure 4.16), flow already has reattached by the

observation at location 14 ($X/\lambda = 0.36$), which is approximately 6 times the bedform height.

MO-2 data (figure 4.14) shows that flow is separated between locations 13 and 14 and reattaches by location 15 at $X/\lambda = 0.14$. Although not totally clear from the data presented in figure 4.14, it appears that flow separation may have occurred between location 11 and 10 (recall location 10 is downstream of 11). Because of the presence of the superimposed dunes, flow appears to detach and reattach at numerous points along the large bedform structure. For example, in figure 4.18 it could be inferred that flow detachment occurred between locations 8 and 9 (figure 4.14) because of the presence of a superimposed bedform. The velocity profile from location 9 shows the apparent effects of the upstream, superimposed bedform. It is likely that flow separation did occur, however, the detail of velocity measurements was not dense enough to detect this separation.

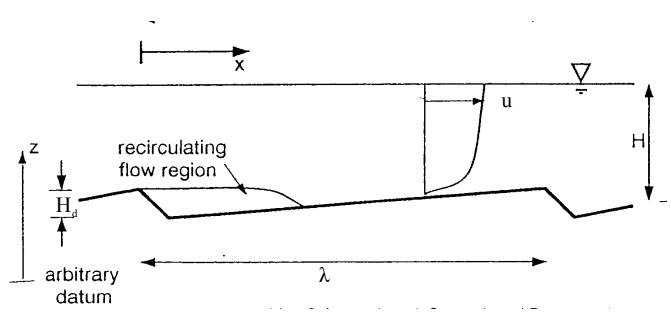

Figure 4.17—Definition sketch of flow and bedforms from Lyn (1993)

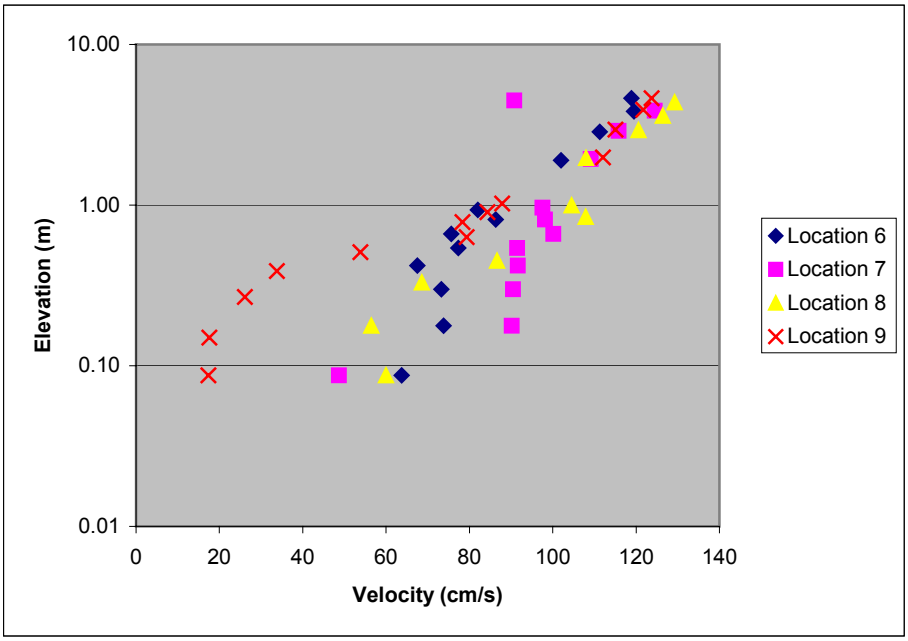

Figure 4.18—MO-2 velocity profiles for locations 6 - 9

MO-1 (figure 4.16) shows a marked decrease in velocity throughout the water column downstream of the bedform crest, which also is apparent for the MO-2 experiment (figure 4.14), however, not as pronounced. KANK-1 data (figure 4.15) show a velocity decrease in the near bed only, with no definite velocity change in the outer region. The question becomes whether the velocity decrease in MO-1 and MO-2 is wake-induced momentum defect (controlled by turbulence diffusion) or topographically induced deceleration (controlled by the pressure gradient and inertial forces). Nelson and Smith (1989B) delineate the various regions of flow over well-developed bedforms as characterized by different turbulence structures and length scales. The first region is where velocity and velocity fluctuations are wake-like (in the lee of the bedform near the bed and diffusing

outward). A second region with the scaling and velocity structure of a boundary layer and a third region that is wave-like, where the scaling parameters are closer to those of the bulk flow parameters of shear velocity and flow depth. In figure 4.16 (MO-1), it is noted that the velocity decrease is seen almost immediately throughout the water column directly downstream of the crest (location 12). Flow separation was noted in the MO-1 data, which would require the presence of wake-like flow features. However, the decrease of the velocity extending to the surface immediately downstream of the crest likely indicates that this is attributable to the pressure gradient (topographically induced), as intuitively, a wake-induced velocity decrease would require a longer distance downstream from the crest to be seen at the surface. Nelson and others (1993, p. 3,940) noted this same "wavelike" response of the flow to the bedforms in their laboratory results.

In regards to similarity and scaling of the mean velocity profile, velocity typically is scaled by shear velocity, while the length scale usually is a combination of some measure of the roughness and shear velocity divided by the kinematic viscosity for the inner region and the total depth for the outer region. These scales typically are referred to as inner and outer scales. For the shear velocity, both local and bulk (reach-averaged) shear velocity possibly could be used in scaling. The bulk shear velocity, u_{*T}, can be determined by two methods: 1) as the square root of the product of the mean flow depth, water-surface slope, and the gravitational constant and 2) as the slope of the best-fit line through the reachwise spatially averaged velocity profile (this profile will be explained in more detail later). In this report, method 1 is used to determine the bulk shear velocity

unless otherwise noted. The local shear velocity, u_{*L}, is computed at each vertical from the slope of the velocity distribution (note that in the figures which use local shear velocity, the local shear velocity changes for each location as it is locally computed). In computing the local shear velocity, the velocity data from in the range 0.2<z/H<0.5 was typically used as this range was found to provide the most reasonable values (i.e., smooth transition in local shear velocity along the longitudinal direction). The KANK-1 velocity data in defect form are shown in figure 4.19 without any scaling for the velocity, noting the scatter in the data for z/H <0.4. The same data scaled by bulk shear and local shear velocities are shown in figures 4.20 and 4.21, respectively. The collapse of the data is clear with a better collapse being evident for the local shear velocity than the bulk shear velocity. MO-1 and MO-2 also exhibit collapse of the data when scaled with shear velocity (although not as good in the near bed), as shown in figures 4.22-4.25, with the better collapse resulting when local shear velocity is used. Data from all three experiments from this research are plotted in defect form in figures 4.26 and 4.27.

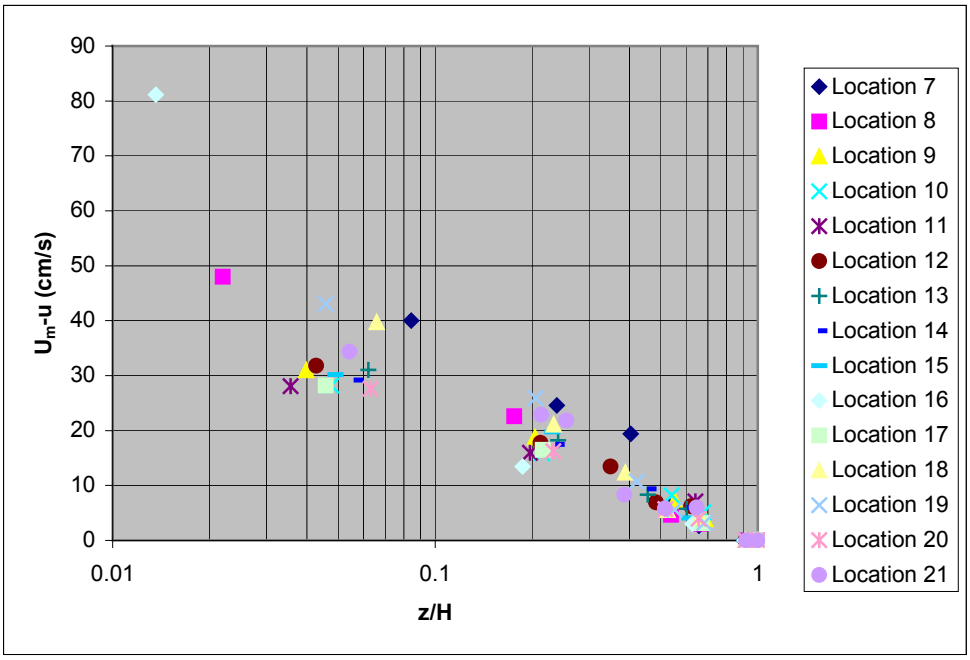

Figure 4.19—KANK-1 data plotted in velocity-defect form

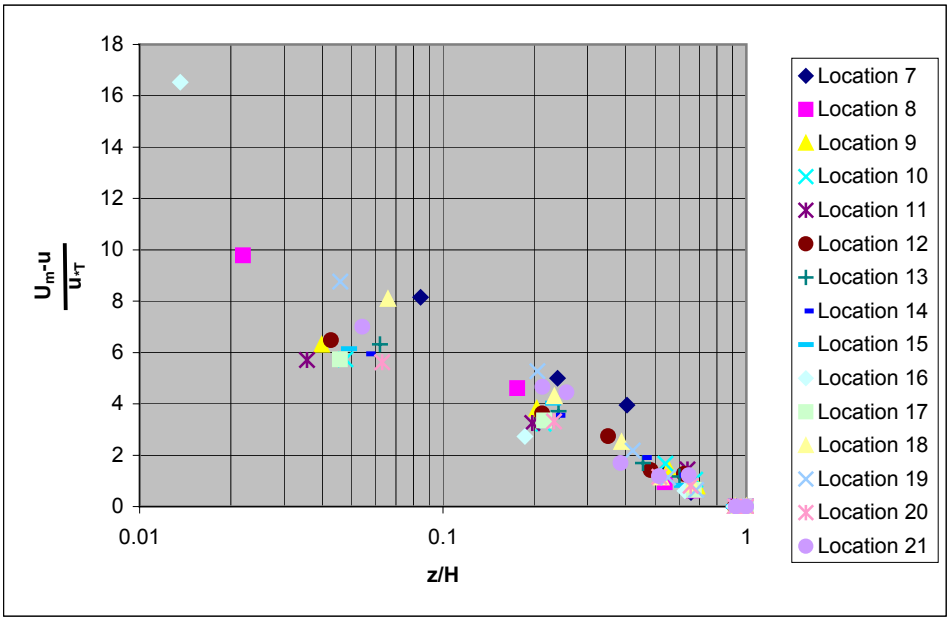

u_{*T} is computed from the slope of the velocity profile of the spatially averaged velocity profile

Figure 4.20—KANK-1 data plotted in velocity-defect form with bulk shear velocity as the scaling parameter

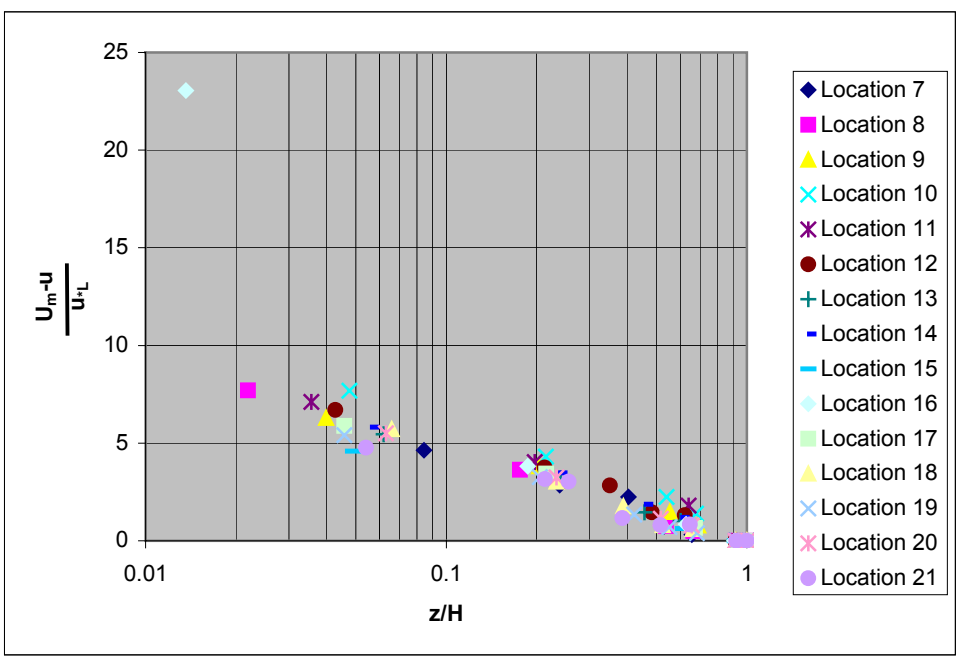

Figure 4.21—KANK-1 data plotted in velocity-defect form with local shear velocity as the scaling parameter

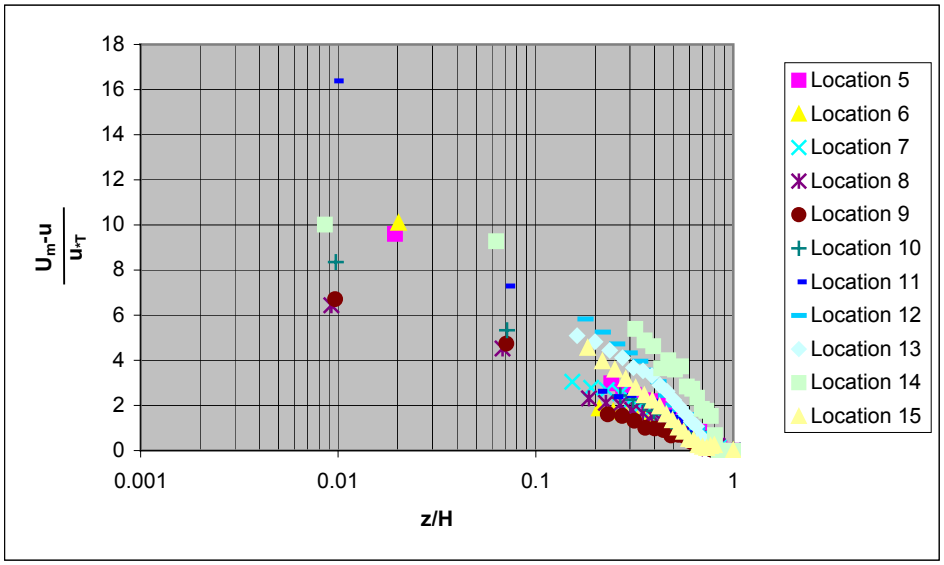

u_{*T} is computed from the slope of the velocity profile of the spatially averaged velocity profile

Figure 4.22—MO-1 data plotted in velocity-defect form with bulk shear velocity as the scaling parameter

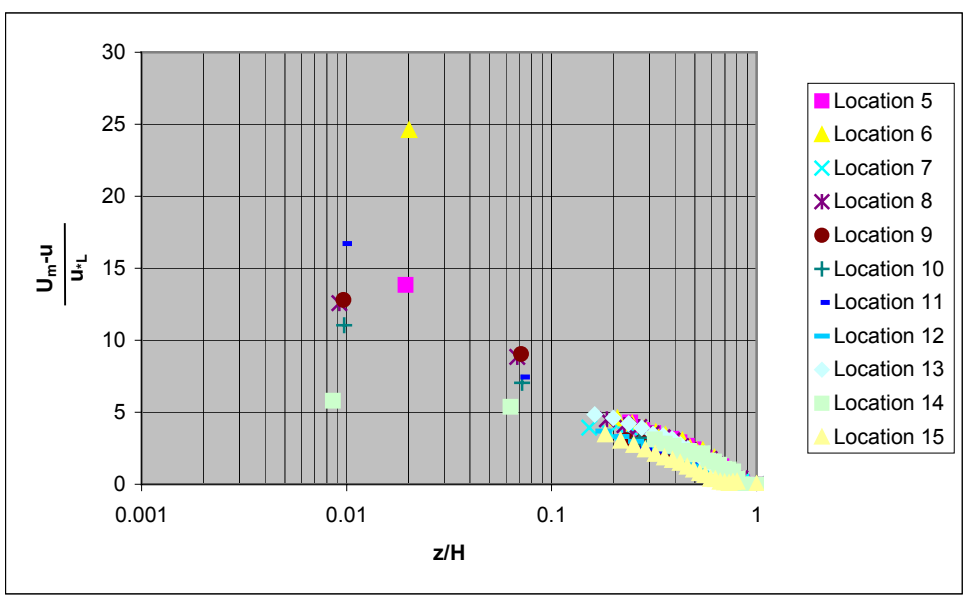

Figure 4.23—MO-1 data plotted in velocity-defect form with local shear velocity as the scaling parameter

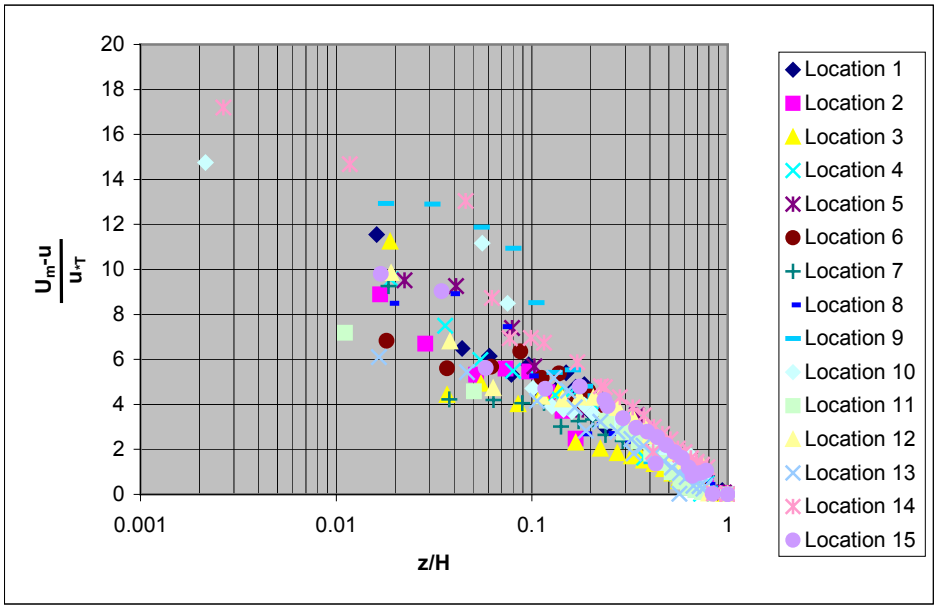

u_{*T} is computed from the slope of the velocity profile of the spatially averaged velocity profile

Figure 4.24—MO-2 data plotted in velocity-defect form with bulk shear velocity as the scaling parameter

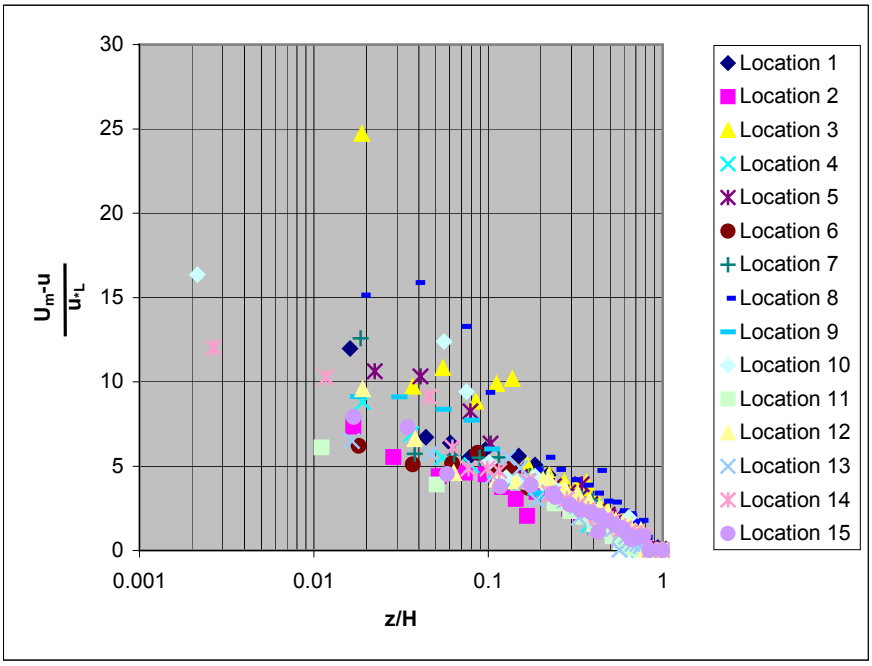

Figure 4.25—MO-2 data plotted in velocity-defect form with local shear velocity as the scaling parameter

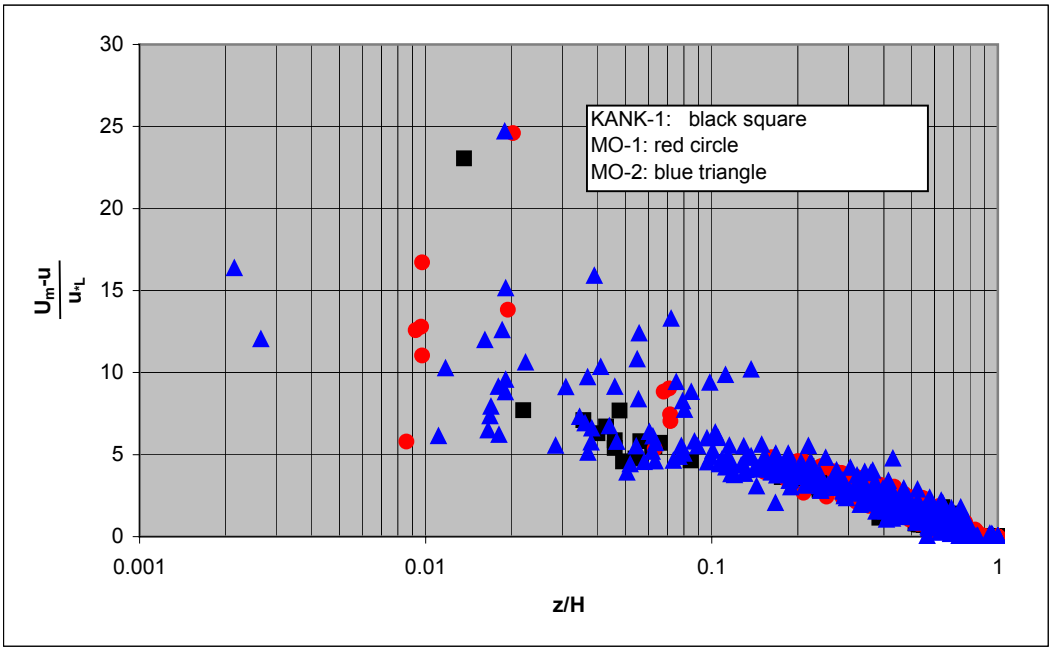

Figure 4.26—All local velocity data collected in KANK-1, MO-1, and MO-2 plotted in velocity-defect form and scaled by the local shear velocity

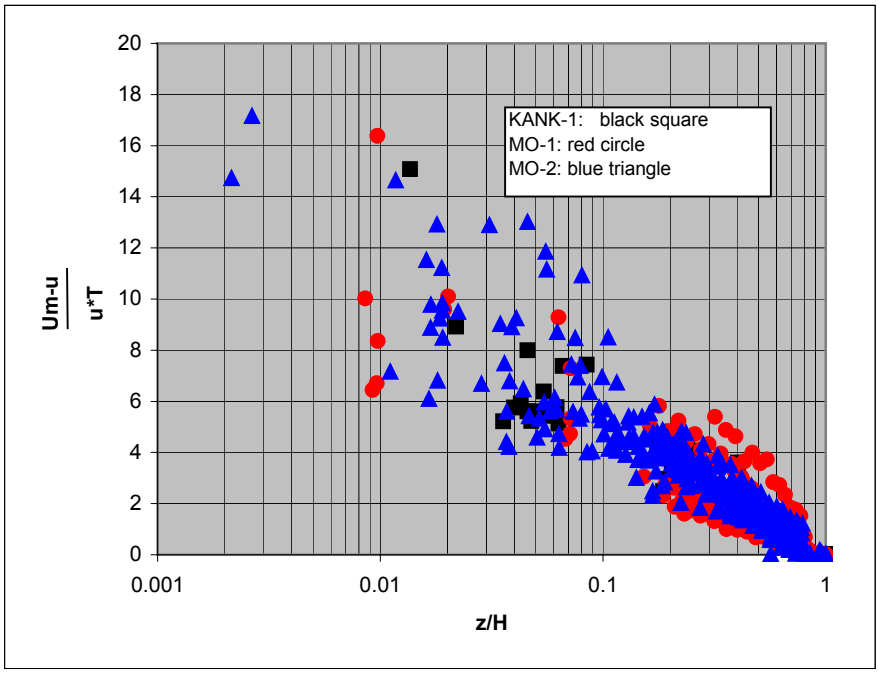

Figure 4.27—All local velocity data collected in KANK-1, MO-1, and MO-2 plotted in velocity-defect form and scaled by the bulk shear velocity

For KANK-1, the collapse of the data is good all the way to the bed (figure 4.21), which is not the case for either MO-1 or MO-2 in the area of z/H<0.15. This difference is not unexpected as KANK-1 had no flow separation, whereas both MO-1 and MO-2 had flow separation. The lack of near-bed (z/H<0.15) universal flow structure also was discussed by Lyn (1993), who noted that this region would "exhibit only weakly (if at all) any universal structure." Based on laboratory data, Fedele and Garcia (2001) postulate that within the internal layer (near-bed region), the lack of scaling occurs as "two major dynamic mechanisms are competing in producing and transporting turbulent properties with different relative importance at different locations along flow development (shear layer and wake diffusion, and wall turbulence)". This lack of scaling seems reasonable when examining the turbulent fluctuations from the MO-2 data set (figure 4.28). The streamwise turbulent fluctuations are similar with the wall-bounded shear flow relations given by Nezu and Nakagawa (1993) only for elevations where z/H >0.6; however, in the near bed (z/H<0.2) there is a lack of scaling.

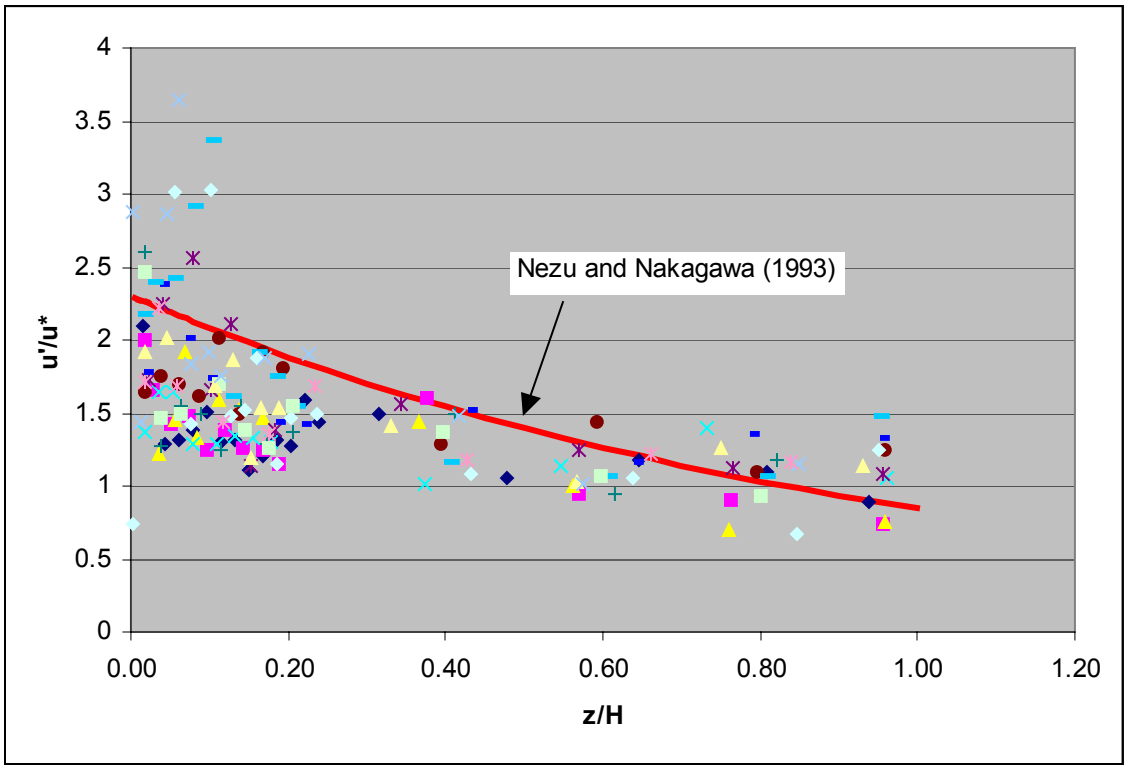

Figure 4.28—Streamwise turbulent fluctuations for MO-2

Coles wake coefficient (W_0) is computed for all the data (at each location) and presented in tables 4.6-4.8. W_0 depends on freestream pressure gradients in equilibrium boundary layer flow (Lyn, 1993), with negative W_0 occurring for favorable pressure gradients and positive W_0 for adverse pressure gradients. For flat-bed flows, W_0 has a range from 0 to 0.25 with a mean of approximately 0.2 (Nezu and Rodi, 1986).

The Coles wake coefficient varies from +0.167 on the stoss side of the crest for KANK-1 to –0.286 in the lee of the crest, with a mean value of –0.006. For MO-1, W_0 varied from 0.200 near the crest to –0.127 downstream of the crest, with an average value for all locations of 0.020. MO-2 had W_0 varying from 0.252 at a crest of a superimposed dune

to –0.251 in the lee of a superimposed bedform at location 3. An average of 0.070 was calculated for all MO-2 locations. In most cases, the wake coefficient was positive in locations where the bed was increasing (adverse pressure gradient) and negative in locations where the bed was decreasing (favorable pressure gradient). This result follows the theory outlined in the previous paragraph. There appears to be a lag, as the wake coefficient does not change from positive to negative until some point after the bedform crest (figure 4.29).

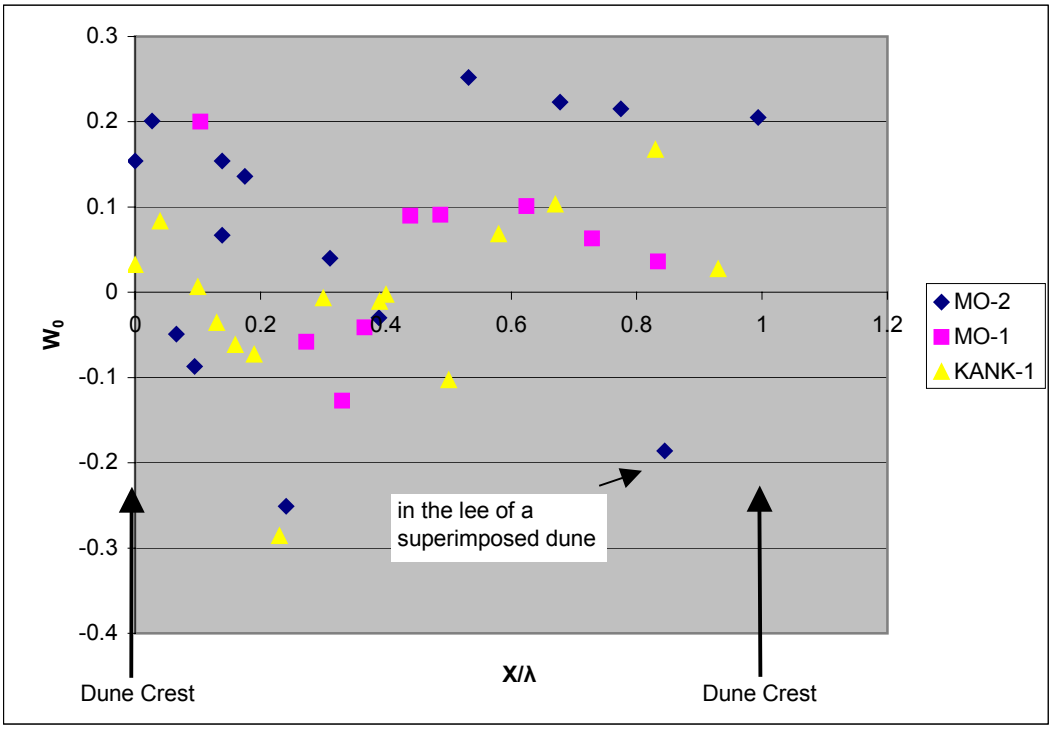

Figure 4.29—Variation of Coles wake coefficient with distance along the dune for all experiments

4.5. Spatially Averaged Velocity

As shown in the previous section, the velocity profile varies over the length of a bedform. For some applications, it is useful to determine a spatially averaged velocity profile. These spatial averages are an integration of all the flow effects over the bedform. Various investigators have done spatial averaging of both velocity and Reynolds stresses (Smith and McLean, 1977; Nelson and others, 1993; and Fedele and Garcia, 2001), with two different methods used: 1) averaging along lines of constant elevation above a datum and 2) averaging along lines equidistant from the boundary. Averaging along lines equidistant from the boundary was used in this research because this method better captures the boundary effects in the flow structure. Averaging along lines of constant elevation above the datum causes elimination of data in the bedform trough, as there is not enough other data at that elevation to average against. When comparing data at each location, the observations in the vertical were not exactly coincident to the same distance above the bed for all locations, therefore, averaging took place in blocks (or bands) above the bed. For example, for the MO-2 data, the bands were 10 cm deep up to 1 meter above the bed, then the bands were 1 meter deep to the water surface. An example illustration of this averaging is included in the appendix (figure 8.1).

Spatial averages for KANK-1, MO-1 and MO-2 are given in figures 4.30 A,B, and C, respectively. A single log-linear line has been fit to each of these data sets. The single

log-linear relation probably is justified for KANK-1 and MO-1 data sets; however, the MO-2 data set likely has a two-segment, log-linear relation.

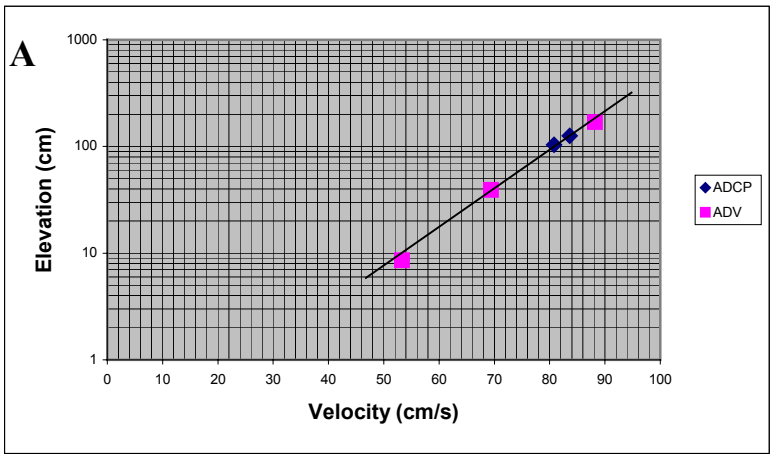

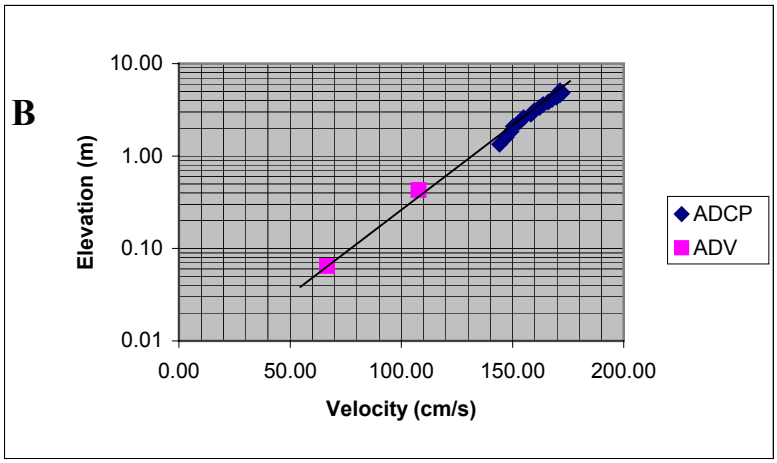

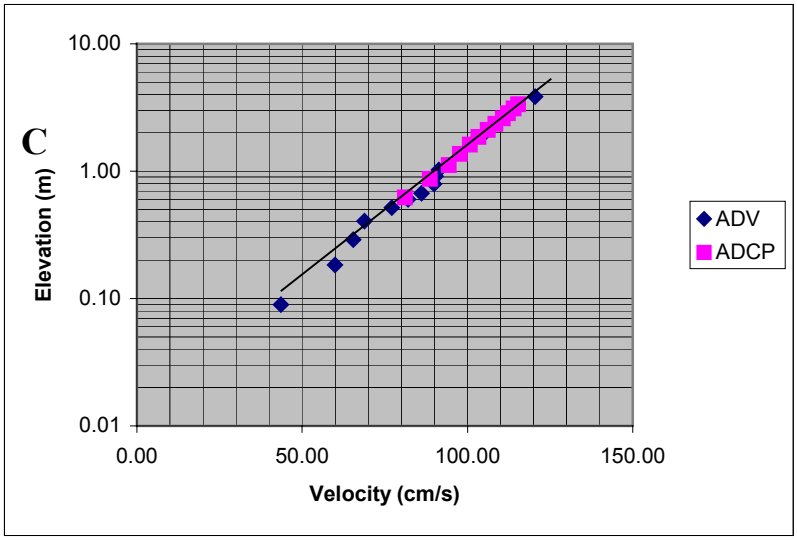

Figure 4.30-Spatially averaged velocity profile for A) KANK-1, B) MO-1, and C) MO-2

For flow over bedforms, the inner length scale is the composite roughness height, k_c, which is an amalgam of both grain and form resistance, and can be computed in the following steps.

1. Take the law of the wall (equation 2.75) and present it in the form

$$\frac{u}{u_*} = \frac{1}{\kappa}\ln z - \frac{1}{\kappa}\ln k_c + B(\frac{u_* k_c}{\nu}) \quad , \qquad [4.1]$$

where $B(\frac{u_* k_c}{\nu})$ is the Roughness function from Nikuradse's data (Schlichting, 1979, p. 620) and $\frac{u_* k_c}{\nu}$ is the Roughness Reynolds Number.

2. Define from equation 4.1

$$C_1 = -\frac{u_*}{\kappa}\ln k_c + B(\frac{u_* k_c}{\nu})u_* \qquad [4.2]$$

and rearrange terms yielding

$$k_c = \exp\left\{\left(B - \frac{C_1}{u_*}\right)\kappa\right\} \quad . \qquad [4.3]$$

3. C_1 is computed from a regression of the velocity profile data, recalling from step 1 that the law of the wall can be written as

$$u = \frac{u_*}{\kappa}\ln z + C_1 \quad , \qquad [4.4]$$

where the intercept (for z = 1) of the regression fit to the line is equal to C_1. Note that u_* also could be computed in this step.

4. An iteration technique then is used by assuming an initial value of roughness (k_c), solving for Roughness Reynolds Number, determining B from Nikuradse's data plot (Schlichting, 1979, p. 620), and computing k_c by equation 4.2 (step 2), then compared with the initially assumed value. If the initially assumed value is not sufficiently close, the new computed k_c is used to compute Roughness Reynolds Number and the process is repeated.

Another method used in this study is that of Fedele's (1998) extrapolation of the Brownlie (1981) equation, which involves utilizing equation 2.94 as

$$\frac{1}{\sqrt{f}} - 2\log\left[\frac{2H}{k_c}\right] = 1.74 \quad , \qquad [2.94]$$

where the total[1] friction factor, f, is computed from

$$f = \frac{8g}{U^2} HS \quad , \qquad [4.5]$$

where the depth, H, has been substituted for the hydraulic radius, R_h.=H Alternatively, the graph presented by Brownlie (1981) (figure 4.31) could be used instead of equation 2.94 to determine k_c.

[1] Note the the word total is used here as in the presence of bedforms. The friction factor can be partitioned into that attributable to form resistance and that attributable to grain resistance (see equation 2.42).

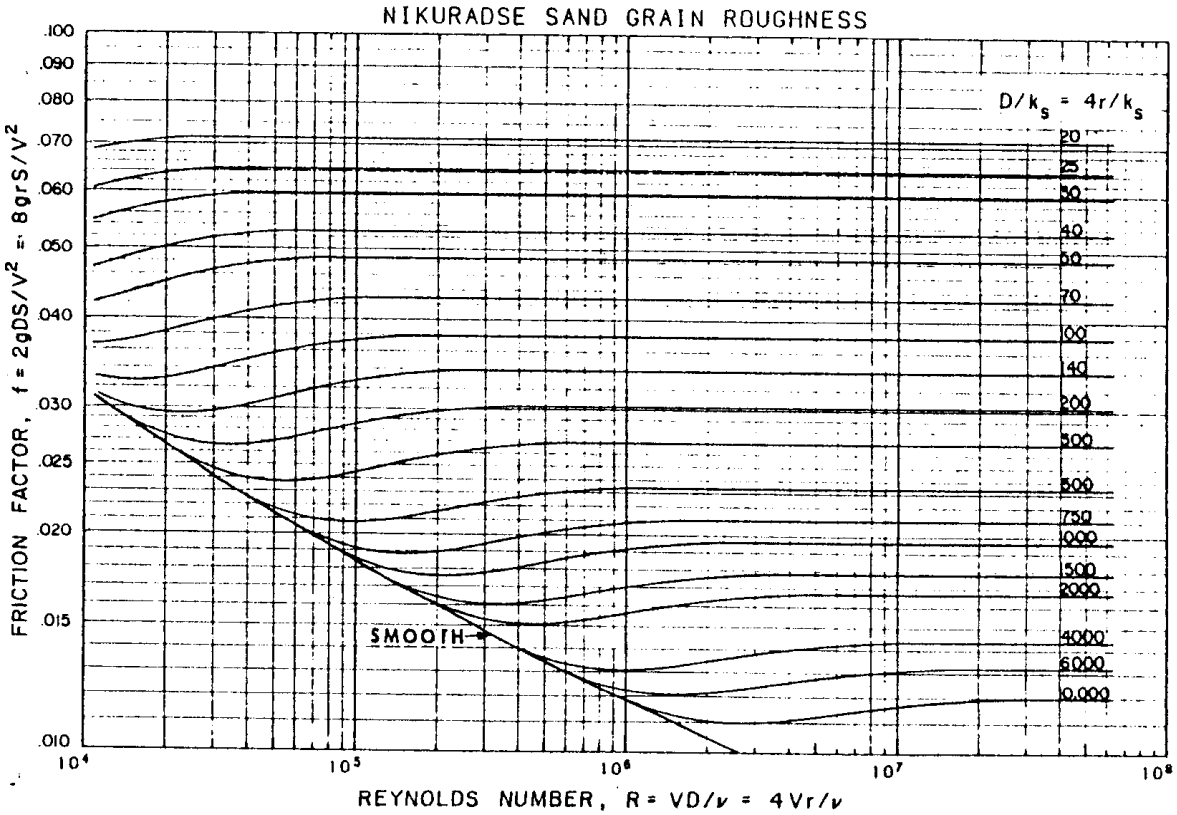

Figure 4.31—Friction factor diagrams (from Brownlie, 1981)

The results of the two methods for computing the composite equivalent roughness along with the total friction factor are presented in table 4.9. In examining the values for k_c derived from both methods, only the value for MO-2 scales with the bedform height (the superimposed value), with the composite roughness values for KANK-1 and MO-1 being much smaller. This result implies that the flows for KANK-1 and MO-1 were experiencing very little form resistance. With the small bedform steepness and lee slope of KANK-1, the topographic changes in the bed elevation are not abrupt enough to cause the typical form drag losses. With the relatively symmetric and closely spaced bedforms of MO-1, the flow is affected by the bedforms as if they were large roughness elements.

Experiment	H_d	λ	f	k_c^A	k_c^B
KANK-1	25 cm	117.5 m	0.0440	3.73 cm	11.22 cm
MO-1	125 cm	23 m	0.0343	13.02 cm	18.15 cm
MO-2					
large bedform	110 cm	140 m	0.0613	32.2 cm	69.04 cm
superimposed bedform	32 cm	5.7 m			

[A] composite roughness height computed from the spatially averaged velocity profile;
[B] composite roughness height computed from the Fedele (1998) extrapolation of the Brownlie (1981) work

Table 4.9—Roughness estimates for KANK-1, MO-1, and MO-2

Examining the data to determine similarity characteristics, the data can be plotted in logarithmic form with the composite roughness height as the length scaling parameter and the bulk-shear velocity as the velocity-scaling parameter. For all data plots, the composite roughness heights used are those from the velocity-profile computation method. This log-linear form is presented in figure 4.32 and shows good collapse of the data. The velocity data can also be presented in dimensionless velocity defect form using outer scales; average flow depth and bulk shear velocity (figure 4.33). This collapse is better than the log-linear plot, with the added benefit that no knowledge of equivalent composite roughness is needed. Note that the absence of any universal flow structure near the bed, observed in the local velocity data from MO-1 and MO-2, is not apparent in the spatial average. Although not as good a collapse as the outer region, the collapse of the data in close proximity to the bed is remarkable. The wake coefficients computed for the log-wake law for the spatially averaged data for these experiments are listed in table 4.1.

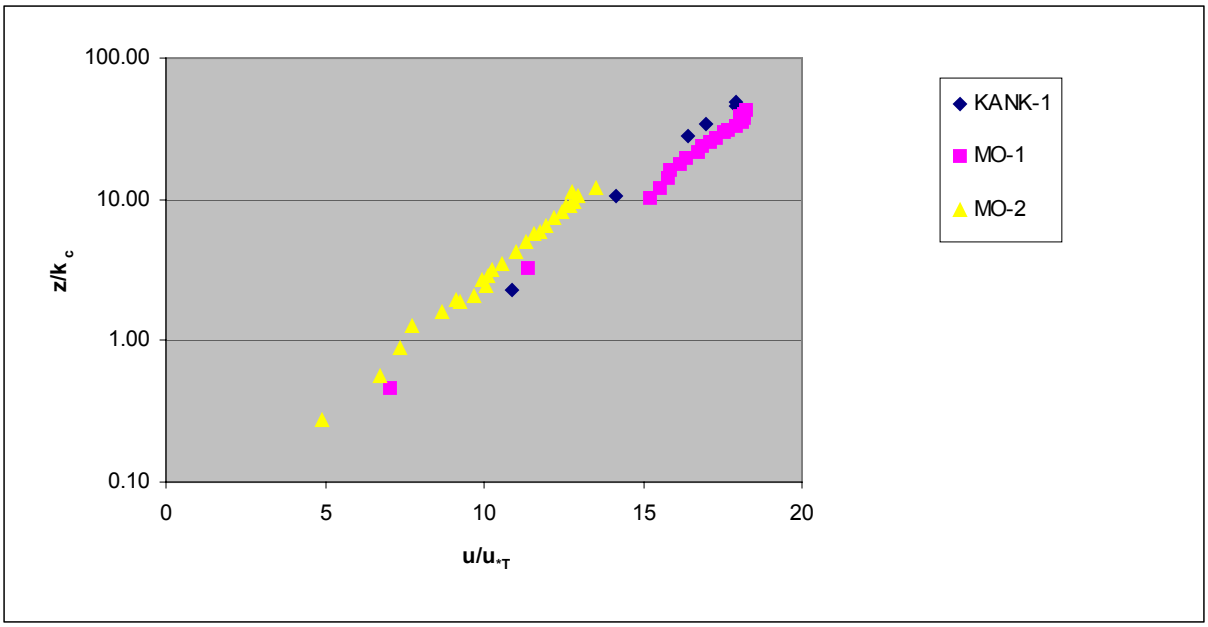

Figure 4.32—Log-linear dimensionless velocity plot

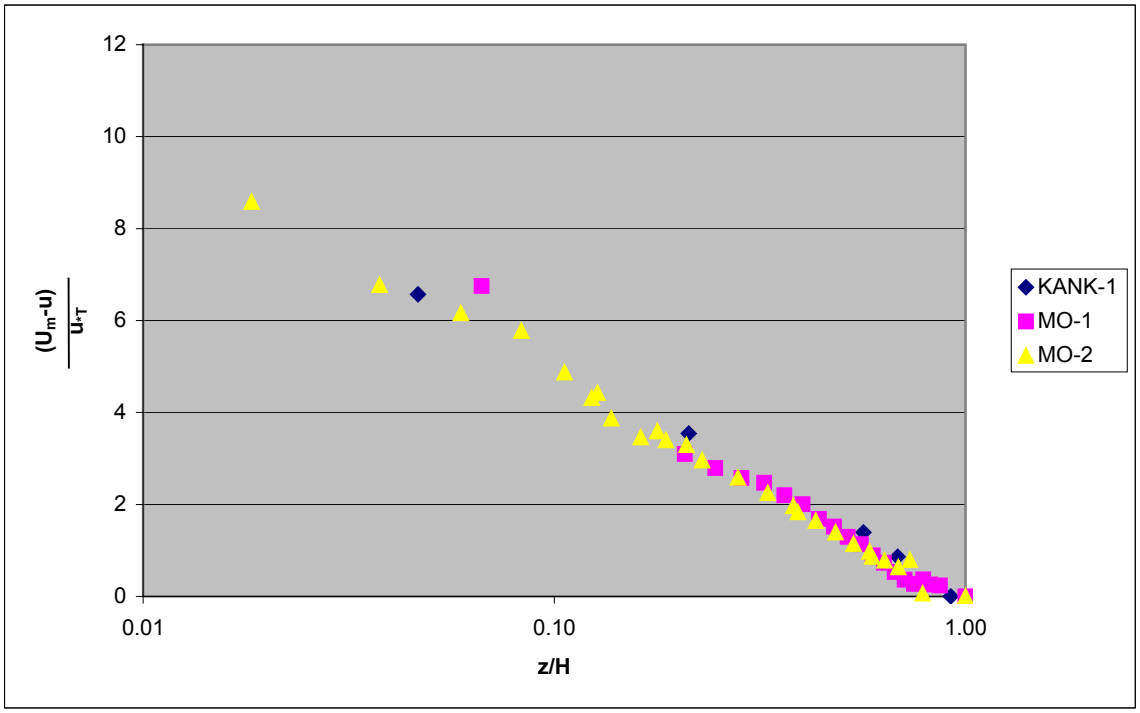

Figure 4.33—Spatially averaged velocity data plotted in velocity-defect form

4.6. Comparison of Field Data with Flume Data and Previous Field Studies

The spatial averages of all field and laboratory data sets considered in this research, plotted in velocity-defect form, are shown in figure 4.34, whereas only the field data collected in this research and the laboratory data plotted in velocity-defect form are shown in figure 4.35. The field-scale data collapse well when plotted in outer region scales. The laboratory data, whereas following a linear plot in defect form, do not collapse as well as the field data. The field (collected in this research) and laboratory data plotted in inner scales is shown in figure 4.36. A plot of all field and laboratory data considered during this research are shown in figure 4.37. The composite roughness height (k_c) is the inner length scale. When plotted in these inner scales, the collapse of the field data appears to deteriorate, whereas the laboratory data collapse appears to neither improve nor deteriorate. This apparent lack of collapse of laboratory-scale data reveals an apparent sensitivity to boundary conditions (bedform geometry ratio, bedform to flow depth ratio, etc.) in both the inner and outer flow regions. The field-scale data have good collapse in the outer region scales and, thus, much less sensitivity in the flow field to bedform boundary conditions. In the inner region scales, both field-scale and flume-scale flows appear to be sensitive to bedform boundary conditions.

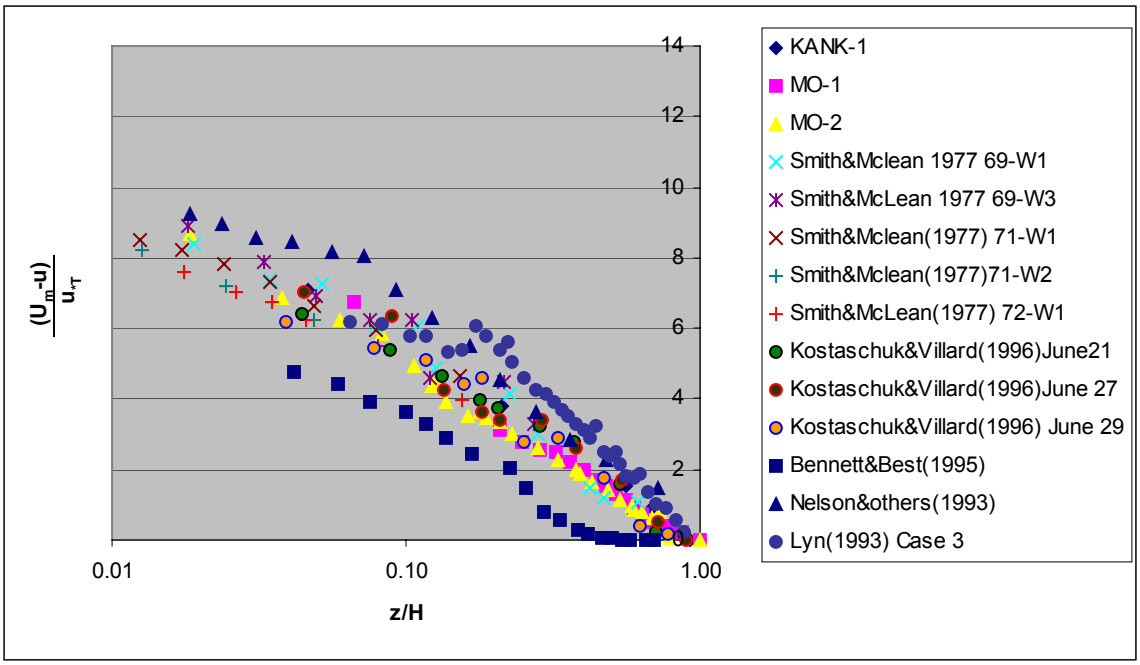

Figure 4.34—Laboratory and field data considered in this research plotted in velocity-defect form

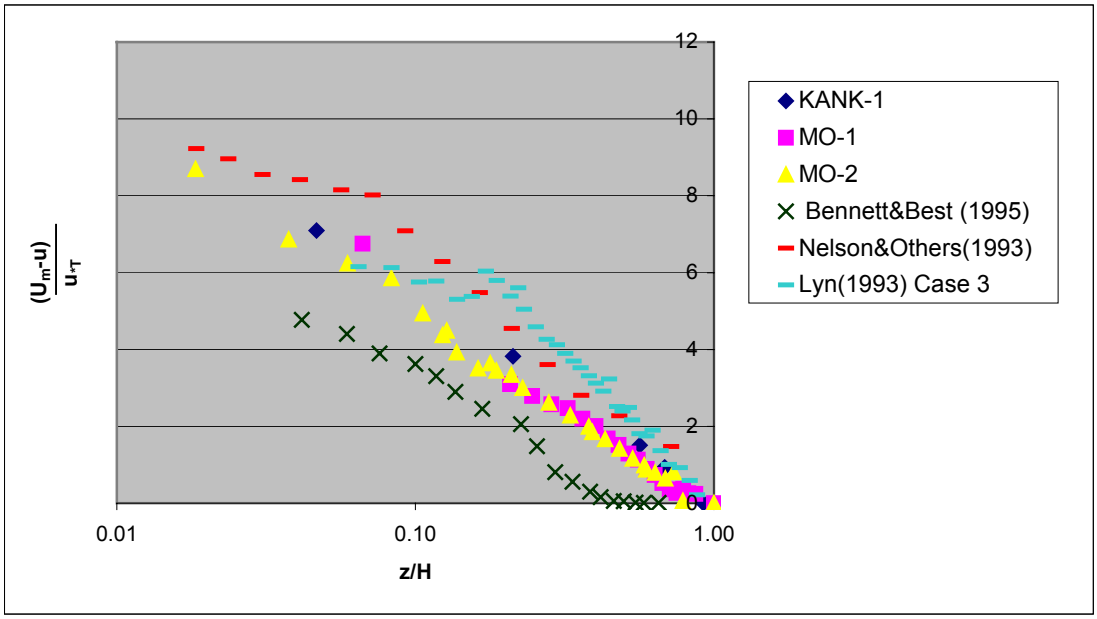

Figure 4.35—Laboratory and selected field data collected in this research plotted in velocity-defect form

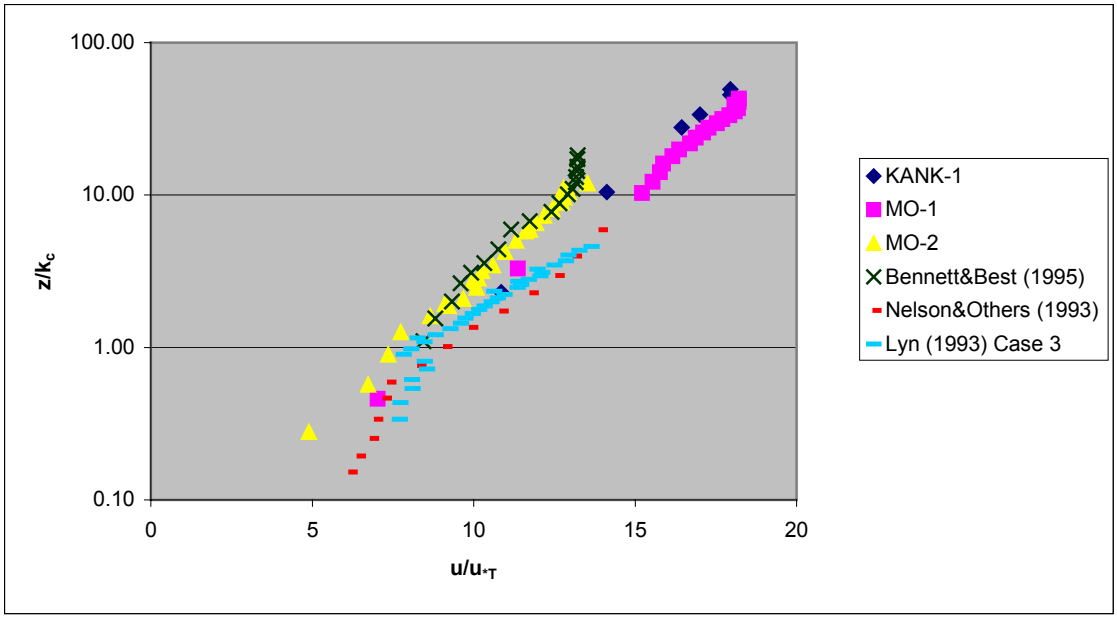

Figure 4.36—Laboratory and selected field data plotted in log-linear form with composite roughness height as the similarity parameter

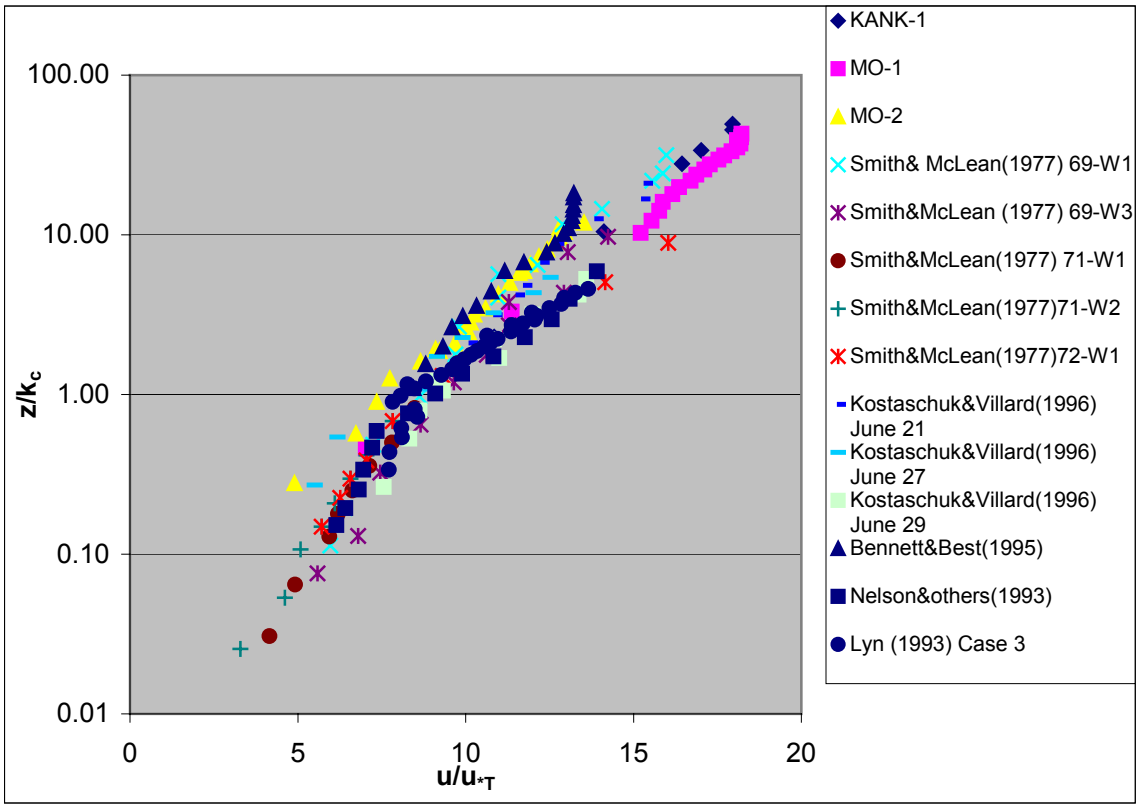

Figure 4.37—Laboratory and field data plotted in log-linear form

When examining the spatially averaged data, the flume data (figure 4.36), the Smith and McLean data (figure 4.38), the MO-2 data (figure 4.36), and the Kostaschuk and Villard (1996) data of June 27 and June 29 (figure 4.39) have two linear segments in log-linear form, with the breakpoint approximately at $z=k_c$. These results are in contrast to the KANK-1 and MO-1 data (figure 4.36) and that of the Kostaschuk and Villard (1996) data for June 21 (figure 4.39), where a single log-linear segment describes the velocity profile. All the data sets with two segment log-linear forms have bedforms that approach equilibrium dune conditions, whereas the remaining data sets (KANK-1, MO-1, and Kostaschuk and Villard June 21;1996) are not classified as equilibrium dunes.

According to Nelson and Smith (1989A), the composite roughness height, k_c, describes "the extraction of momentum from the flow by both skin friction and form drag". As the log-linear velocity profile breakpoint occurs at approximately the composite roughness height for both field- and laboratory-scale flows with bedforms characterized as equilibrium dunes, the portion of the momentum extracted by the bedforms is similar for the field and laboratory scale.

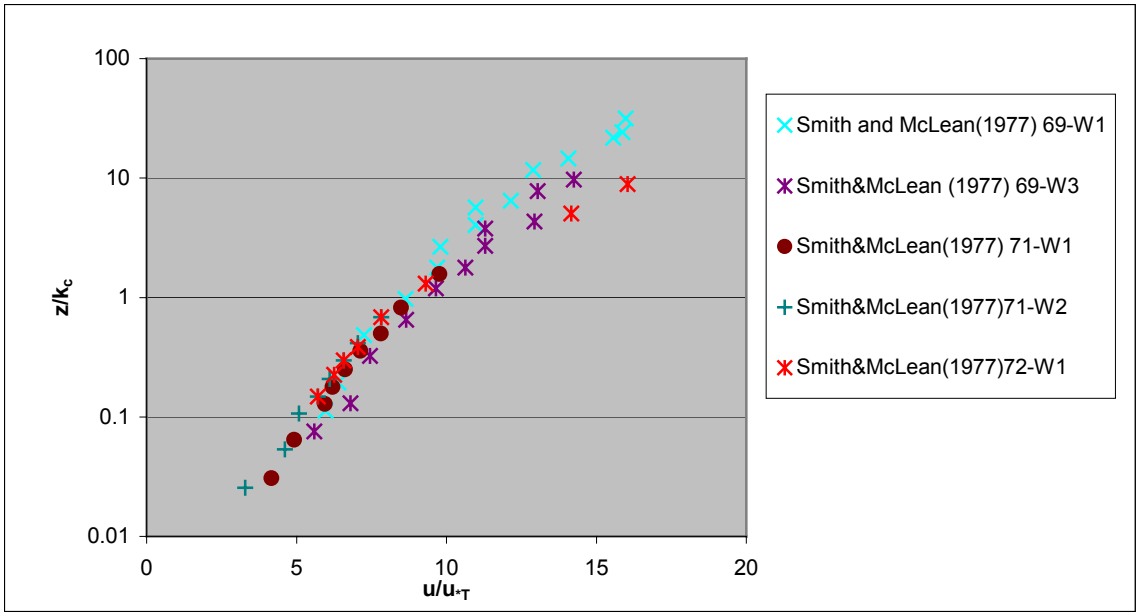

Figure 4.38—Smith and McLean (1977) data plotted in log-linear form

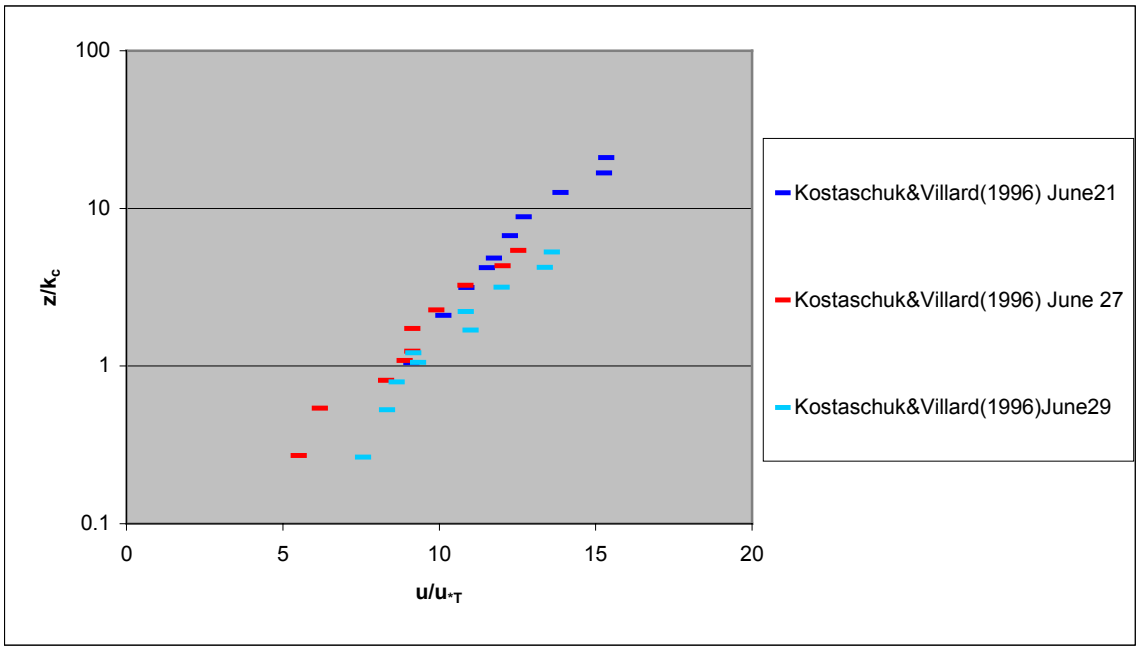

Figure 4.39—Kostaschuk and Villard (1996) data plotted in log-linear form

The local velocity profiles at two discreet points along a dune profile, near the crest and in the trough, are shown in figures 4.40 and 4.41, respectively. The laboratory results collapse well on the field data near the crest. The laboratory results for Lyn (1993)

collapse well with the field data in the trough; however, the results of Bennett and Best (1995) do not collapse well in this region. This result likely is attributable to the larger ratio of dune height to flow depth for the Bennett and Best (1995) data. This good collapse of the Lyn (1993) laboratory data at both the crest and the trough indicate that the flume does a reasonably good job of simulating field velocity profiles in the outer region over bedforms of similar geometry and flow.

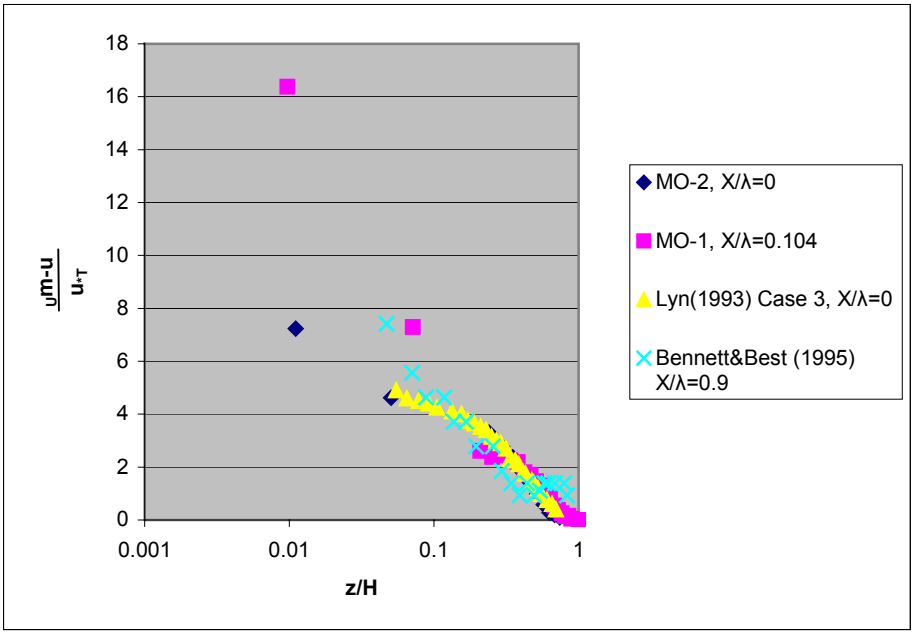

Figure 4.40—Local velocity data collected near the bedform crests plotted in velocity defect form

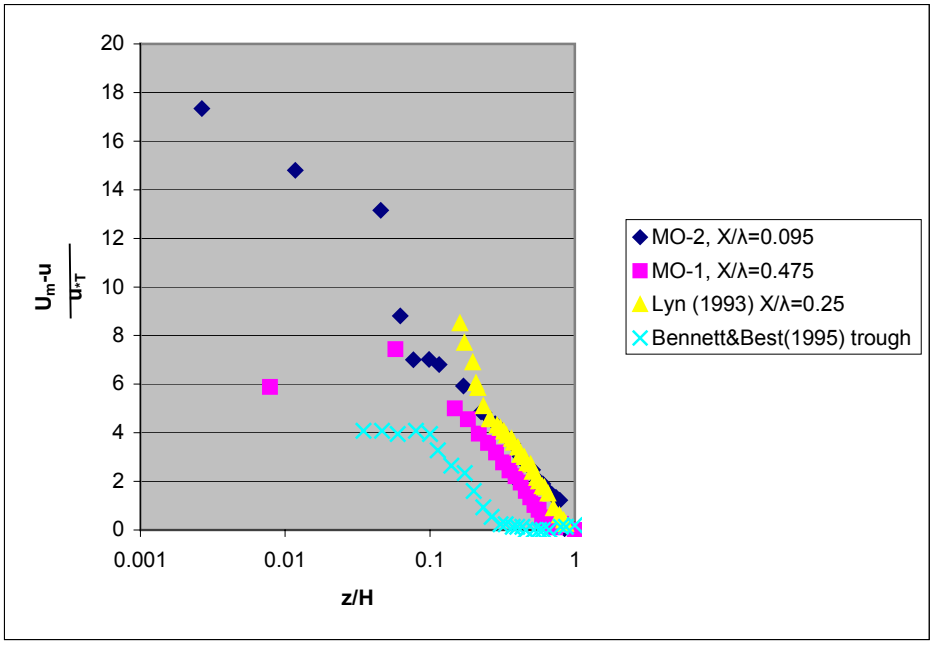

Figure 4.41—Local velocity data collected in the bedform trough plotted in velocity defect form

4.7. Evaluation of Existing Models for Spatially Averaged Velocity

Models are available that attempt to estimate the spatially averaged velocity profile. Among these are the models of Smith and McLean (1977) and Nelson and Smith (1989A). The work of Fedele and Garcia (2001) also is included, although that work never was intended as a stand-alone velocity model, but rather a conceptualization for alluvial roughness. Each model considered in this research will be explained, followed by application and comparison of each model results to field data. Although it is fully acknowledged in each study that the mechanics of the flow in the interior region (near the bed) involves a complex interaction of the wake propagating after the flow separation at the dune crest, topographically induced flow acceleration (pressure gradients), and a

redeveloping boundary layer, all the models use logarithmic approximations to appropriate regions of the flow field in a piecewise fashion. These regional logarithmic approximations are then joined under some condition of matching.

4.7.1 Existing Models

The strategy of all the models is to determine both the shear velocity (u_*) and roughness parameter (z_0) for each flow region and the location in the flow field where the fields meet (match). Nelson and Smith (1989A) note that near the boundary, a similarity region is present where the local velocity scales with the local grain shear velocity. In the flow field away from the boundary (outer region), the local velocity scales with the overall total (bulk) shear velocity (that is the shear velocity averaged over a large part of the dune field). The different scales of superimposed bedforms determine the number of required segments. A different method is used in each model for determining a value for the number of segments. Once these parameters are known, the standard log-linear velocity model could be applied to the various regions. Smith and McLean (1977), however, use a numerical modeling approach starting from the well-known, one-dimensional constitutive equation for the shear stress as

$$\tau = \rho K \frac{\partial u}{\partial z} \quad , \qquad [4.6]$$

and divide by the boundary shear stress yielding

$$\frac{K}{u_*^2}\frac{\partial u}{\partial z} = \frac{\tau}{\tau_0} = 1 - \varepsilon \quad , \qquad [4.7]$$

where K is the eddy viscosity and ε = z/H. Equating the shear-stress ratio to 1-ε implies that an equilibrium shear-stress distribution with a monotonically decreasing shear stress away from the bed is present in the presence of bedforms (Fedele and Garcia, 2001). As Smith and McLean (1977) were interested in the effect of stratification because of sediment on the flow field, they derived a closure form for the eddy viscosity as

$$K = \kappa u_* H f_2(\varepsilon)(1 - \alpha\beta R_i) \quad , \qquad [4.8]$$

where

$$f_2(\varepsilon) = \varepsilon + 1.32892\varepsilon^2 - 16.86321\varepsilon^3 + 25.22663\varepsilon^4 \qquad \text{for } \varepsilon \le 0.3 \quad ,$$

$$f_2(\varepsilon) = 0.160552 + 0.075605\varepsilon - 0.1305618\varepsilon^2 - 0.1055945\varepsilon^3 \qquad \text{for } 0.3 \le \varepsilon \le 1 \quad ,$$

α is the ratio of eddy diffusitivity of mass to that of momentum, β is a constant equal to 4.7 (+/- 0.5), R_i is the gradient Richardson number given by

$$R_i = \left[\frac{-(\rho_s - \rho)g}{\rho}\frac{\partial c}{\partial z}\right]\left(\frac{\partial u}{\partial z}\right)^{-2} \quad , \qquad [4.9]$$

where c is the volumetric suspended-sediment concentration. Using the currently available methods, it has been the author's experience that sediment concentration data collected in the field can have as much as 100-percent error. This fact coupled with the previously mentioned problems with collecting sediment concentration data as part of

this research make it impossible for computing reliable gradient Richardson numbers for the field data collected in this research. Therefore, for the present purposes of evaluating any of these models, stratification is not considered.

The use of the full Smith and McLean (1977) model, starting with the non-dimensionalized constitutive equation (equation 4.7) utilizing a Runga-Kutta finite-difference scheme, is presented in figure 4.42 for the data from MO-1. In addition, the model parameters fit to the simple log-linear velocity equations for each region also are shown. The full model does not have the benefit of stratification incorporated, which would result in greater values of velocity for each elevation [2] (figure 4.43 from Coleman, 1986); thus, resulting in a better match with observed field data; however, simply using the log-linear velocity profile with the Smith and McLean (1977) parameters provides a good fit. In addition, when using the full model, constraints are placed on the model by the assumptions of the validity of both the equilibrium shear-stress distribution assumption (equation 4.7) and the validity of the relation for the eddy viscosity (equation 4.8). Therefore, the full model of Smith and McLean (1977) was not utilized for the reasons stated above (lack of accurate sediment data and additional model assumptions). Rather, the parameters important to the log-linear velocity equations for each region and the computed matching locations were computed using the rationale of Smith-McLean (1977) and then utilized in simple log-linear velocity equations to produce a "modeled" estimate of the velocity profile. This also was the approach in the Nelson and Smith

[2] Coleman (1986) states: "Apparently, the effect of the suspended-sediment is to decelerate the flow in the high-concentration region near the channel bed. Continuity then requires a compensating acceleration in the upper part of the flow."

(1989) and Fedele and Garcia (2001) models. In all models considered, there will be a minimum of two regions. For each region, n, the log-linear velocity equation will be

$$\frac{u}{(u_*)_n} = \frac{1}{\kappa}\ln\left[\frac{z}{(z_0)_n}\right] \quad , \qquad [4.10]$$

where $(u_*)_n$ is the shear velocity for region n and $(z_0)_n$ is the roughness parameter for region n. The location where the two regions meet (or match) will be designated $(z_*)_{n,n+1}$.

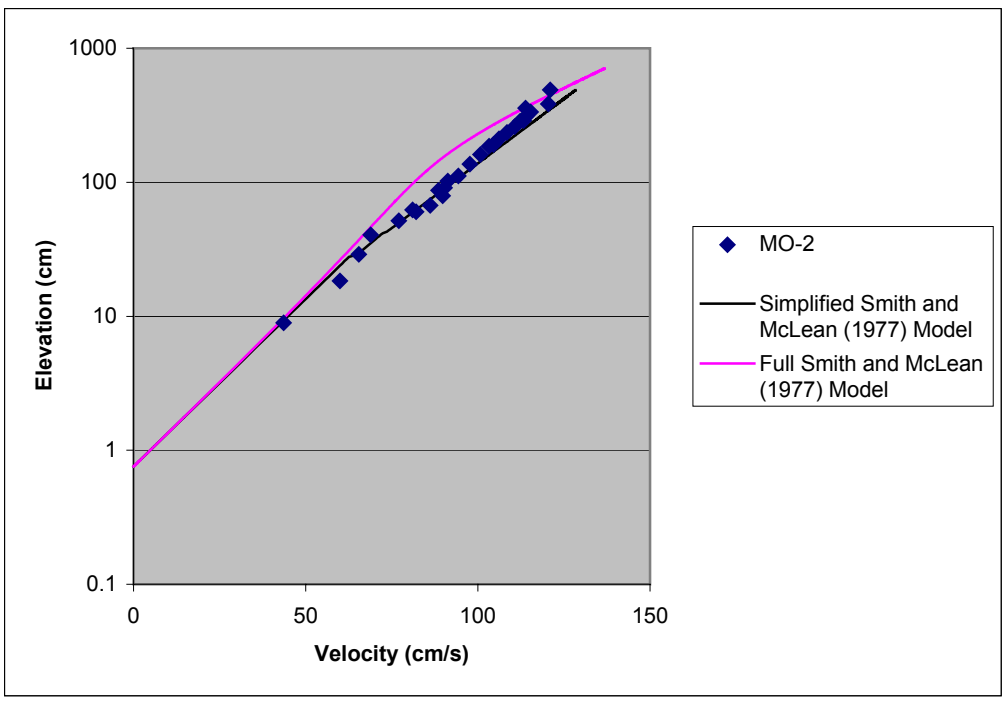

Figure 4.42—Comparison of the full model of Smith and McLean (1977) and a simplified log-linear version using the parameters of the Smith and McLean (1977) model

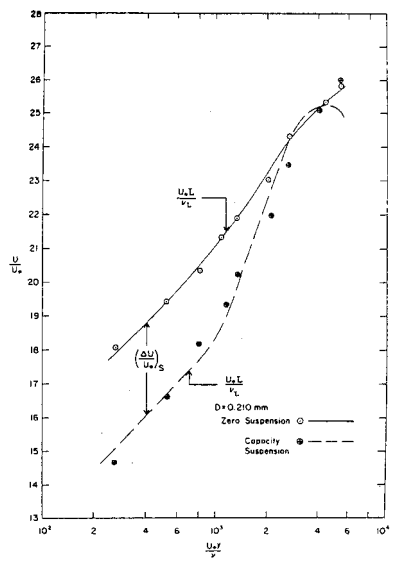

Figure 4.43—Velocity profiles for clear water and a capacity suspension of 0.210 mm sand (from Coleman, 1986)

Smith and McLean (1977) begin deriving their procedure by assuming that at the matching level, the velocity equations for each region can be equated as

$$\frac{(u_*)_n}{(u_*)_{n+1}} = \frac{\ln\left(\left(z_*\right)_{n,n+1} \Big/ \left(z_0\right)_{n+1}\right)}{\ln\left(\left(z_*\right)_{n,n+1} \Big/ \left(z_0\right)_n\right)} \quad . \qquad [4.11]$$

Obviously, equation 4.11 cannot be applied without relations for the unknown terms. In beginning to define some of these terms, Smith and McLean (1977) borrow from the work of Arya (1975) on Arctic winds and sea ice, which equated z_* with the height of the internal boundary layer of each pressure ridge. Also, Smith and McLean follow the

work of Elliot (1958), which identified the thickness of the internal boundary layer, to formulate the following equation for $(z_*)_{n,n+1}$

$$\frac{(z_*)_{n,n+1}}{(z_0)_n} = \frac{5a_0}{9}\left[\frac{\lambda}{(z_0)_n}\right]^{4/5} \quad , \qquad [4.12]$$

where a_0 is constant ranging from 0.6 to 0.9 and λ is the bedform wavelength. For the purposes of applying the model here, a_0 was set to 0.54 as it appeared that simulated results better fit the measured data. When the flow is insufficient to produce sediment transport, the value for z_0 for the bottommost region is equivalent to the roughness parameter given by the work of Nikuradse (Schlichting, 1979, p 621). For sediment-transporting flows, Smith and McLean (1977) propose that the roughness parameter is related to the bedload saltation height, which followed the reasoning of Owen (1964), who proposed this concept for wind-induced bedload transport. Smith and McLean (1977) use a balance of the potential energy at the top of the sand-grain trajectory with the maximum kinetic energy. Then, they reason that the kinetic energy of a sediment particle leaving the bed is proportional to the force exerted on the grain (as it leaves the bed) along the distance of acceleration. They scale this work by the excess bed shear stress (τ_0-τ_{cr}) to arrive at the following equations for the roughness parameter in the bottommost region as

$$z_0 = z_N \qquad \tau_0 < \tau_{cr} \quad , \qquad [4.13a]$$

$$z_0 = \alpha_0 \frac{(\tau_0 - \tau_{cr})}{[(\rho_s - \rho)g]} + z_N \qquad \tau_0 > \tau_{cr} \quad , \qquad [4.13b]$$

where z_N is the roughness length parameter computed by the work of Nikuradse, τ_{cr} is the critical shear stress , and α_0 is a constant of proportionality equal to 22.8 for the original work by Owen (1964).

The relations between the inner-layer (grain-dominated) shear velocity and the outer-layer (grain- and form-affected) shear velocity (total shear velocity) utilize the shear-partition approach of Einstein (1950) and the approach of Nelson and Smith (1989A) introduced in Chapter 2. Accordingly, shear is partitioned as

$$\tau_0 = \tau_0' + \tau_0'' \quad , \qquad [2.41]$$

which when being consistent with the nomenclature used in this discussion becomes

$$\tau_{n+1} = \tau_n + \tau_0'' \quad ,$$

and utilizing the form drag closure of equation 2.52

$$\tau_0'' = \frac{1}{2}\rho C_d \frac{H_d}{\lambda} U_r^2 \quad ,$$

where U_r is related to the undisturbed velocity (if the bedform was not present). Smith and McLean reason that U_r is equal to the velocity at the height $(z_*)_{n,n+1}$ and noting that

$$(u_*)_n = \sqrt{\tau_0' / \rho} \quad , \qquad [4.14a]$$

$$(u_*)_{n+1} = \sqrt{\tau_0 / \rho} \quad , \qquad [4.14b]$$

by substitution of the appropriate terms into equation 2.52 yields

$$\tau_{n+1} - \tau_n = \frac{\rho C_d}{2} \left[\frac{(u_*)_n}{\kappa} \ln \frac{(z_*)_{n,n+1}}{(z_0)_n} \right]^2 \frac{H_{d,n+1}}{\lambda_{n+1}} \quad . \qquad [4.15]$$

Substitution from equation 4.12 into equation 4.15 (using equation 4.14) and rearranging, the ratio of the shear velocity from one region to another yields

$$\frac{(u_*)_{n+1}}{(u_*)_n} = \left\{ 1 + \frac{C_d}{2\kappa^2} \frac{H_{d,n+1}}{\lambda_{n+1}} \left[\ln\left(a_1 \left(\frac{\lambda_{n+1}}{(z_0)_n} \right)^{4/5} \right) \right]^2 \right\}^{1/2} \quad , \qquad [4.16]$$

where a_1=(5/9)a_0. To utilize these equations to solve for the parameters used in generating the velocity profile, one must assume values for C_d and a_0, and know the bedform dimensions along with the total shear stress (τ_0=τ_{n+1}) for the reach. An iterative solution scheme is then employed to solve for the parameters as follows.

1. Assume a value for τ_n to allow for computation of $(z_0)_n$ by equation 4.13 (note: $\tau_n = \tau_0'$ and $\tau_n = \rho(u_*)_n^2$) .
2. Compute $(z_*)_{n,n+1}$ using equation 4.12 .
3. Compute the ratio of shear velocities using equation 4.16 .
4. Compute $(z_0)_{n+1}$ using equation 4.11 .
5. Compute the form stress (τ_0'') using equation 2.52 with the velocity at z_* for U_r.
6. Compute total shear stress by adding the assumed value of τ_n with the form stress (τ_0'') to compute τ_0. Determine if this value of τ_0 matches the known total shear stress (computed as the product of the average water depth, water-surface slope, and the unit weight of water). If the value doesn't match, assume another τ_n, and resume with step 2. (Note: $\tau_{n+1} = \tau_0$ and $\tau_{n+1} = \rho(u_*)_{n+1}^2$)

The method of Nelson and Smith (1989A) is similar to the Smith and McLean (1977) method with three exceptions: 1) they assume the matching level to be equal to the height of the bedforms (H_d), 2) the method for computing the bottommost roughness parameter $(z_0)_n$ is different, and 3) the reference velocity used in the form drag closure (equation 2.52) is the average velocity from the bed to the top of the bedform at level H_d that would have resulted if the bedform was not present.

The roughness parameter, $(z_0)_n$, is computed using a scheme detailed in Dietrich and Whiting (1989) where they relate the height of the bedload layer to the roughness parameter as

$$(z_0)_n = \alpha_1 \delta_b + z_N \quad , \qquad [4.17]$$

where α_1 is an empirical constant approximately equal to 0.077, z_N is the roughness parameter computed by the work of Nikuradse (Schlichting, 1979, p. 621), and δ_b is the bedload-layer height, that is computed as

$$\delta_b = \frac{1.2D(1-\cos\phi)\left[\tau_0 / \tau_{cr}\right]}{1+0.2\left[\tau_0 / \tau_{cr}\right]} \quad , \qquad [4.18]$$

where ϕ is the angle of friction of the bed material (sand≈20˚-30˚) and D is the diameter of the bed material. Nelson and Smith (1989A) proceed to simplify the estimate for the bottommost roughness layer as

$$(z_0)_n \approx 0.20D \quad . \qquad [4.19]$$

When computing the reference velocity, computing the average velocity between the bed and the top of the bedform yields

$$U_r = \frac{(u_*)_n}{\kappa}\left[\ln\left(\frac{H_d}{(z_0)_n}\right) - 1\right] \quad . \qquad [4.20]$$

Therefore, the form drag shear stress is computed as

$$\tau_0'' = \frac{C_d \rho (u_*)^2{}_n}{2\kappa^2}\frac{H_d}{\lambda}\left[\ln\left(\frac{H_d}{(z_0)_n}\right) - 1\right]^2 \quad . \qquad [4.21]$$

Matching the profiles at the height of the bedform, the following formulation occurs for the roughness parameter for the upper region as

$$(z_0)_{n+1} = H_d\left[\frac{H_d}{(z_0)_n}\right]^{-1/\gamma_D} \quad , \qquad [4.22]$$

where

$$\gamma_D = \left[\frac{\tau_{n+1}}{\tau_n}\right]^{1/2} = \left[1 + \frac{C_d}{2\kappa^2}\frac{H_d}{\lambda}\left(\ln\frac{H_d}{(z_0)_n} - 1\right)^2\right]^{1/2} \quad . \qquad [4.23]$$

As with Smith and McLean (1977), to utilize the Nelson and Smith (1989A) model, a value for C_d must be assumed and bedform dimensions along with the total bed shear stress must be known. The steps for computing the parameters are listed below.

1. Compute $(z_0)_n$ using equation 4.17 or 4.19.
2. Compute γ_D using equation 4.23.

3. Compute $(z_0)_{n+1}$ using equation 4.22.
4. Assume a value for τ_n (note: $\tau_n = \tau_0'$ and $\tau_n = \rho(u_*)_n^2$) .
5. Compute the form stress (τ_0'')using equation 4.21.
6. Compute the total shear stress by adding the assumed value of τ_n with the form stress (τ_0''). Determine if this value matches the known total shear stress (usually computed as the product of the average water depth, water slope and the unit weight of water). If this value does not match, another value for τ_n must be assumed and resume with step 5. (Note: $\tau_{n+1} = \tau_0$ and $\tau_{n+1} = \rho(u_*)_{n+1}^2$)

Fedele and Garcia (2001) introduce the concept of the equilibrium level (ε_e), whereby at this location, they assume the velocity profiles from the two flow regions match, there is negligible vertical momentum transfer, and the velocity at this equilibrium level is equal to the vertically averaged mean velocity. The two regions of flow, and the associated velocity and shear stress distributions are shown in figure 4.44. The peak-shear stress is assumed to occur at the equilibrium level with the value of the shear stress at that point being equal to the form shear stress. The shear-stress value in its intersection with the bed is equal to the grain shear stress (τ_n).

Under the assumptions shown in figure 4.44, the internal region ($k_s \leq z \leq \varepsilon_e$) has the following expressions as

$$\tau(z) = (\tau_0'' - \tau_n)\frac{z - k_s}{\varepsilon_e - k_s} + \tau_n \quad , \qquad [4.24]$$

$$\frac{du}{dz} = \frac{(u_*)_n}{\kappa z} \quad , \qquad [4.25]$$

noting that k_s is equal to $30(z_0)_n$. For the external region ($\varepsilon_e < z \leq H$), the following equations apply as

$$\tau(z) = \tau_0''\left[1 - \frac{(z - \varepsilon_e)}{(H - \varepsilon_e)}\right] = \tau_0''\left[\frac{(H - z)}{(H - \varepsilon_e)}\right] = \tau_0''\left[\frac{H}{H - \varepsilon_e} - \frac{z}{H - \varepsilon_e}\right] \qquad [4.26]$$

$$\frac{du}{dz} = \frac{(u_*)_{n+1}}{\kappa z} \quad . \qquad [4.27]$$

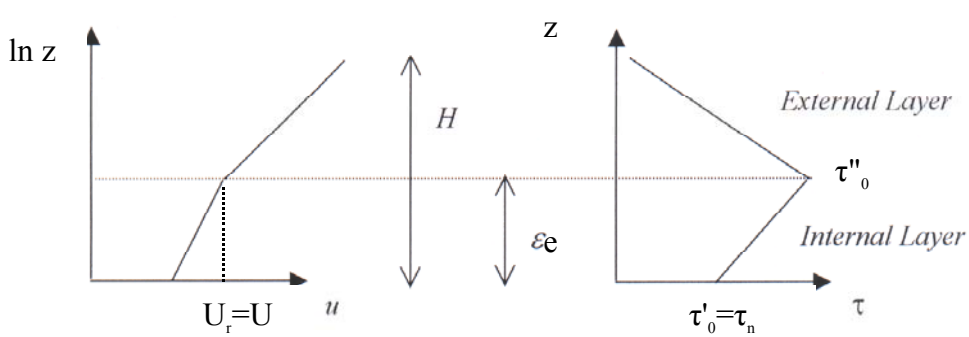

Figure 4.44—Spatially averaged flow over a dune (from Fedele and Garcia, 2001)

Fedele and Garcia (2001) express the formulation of the energy dissipated by the mean motion in terms of the water-surface slope for equilibrium (between flow and sediment transport) from Yen (1992) as

$$S_e \gamma q = \int_H \tau(z) \frac{du}{dz} dz = \int_{k_s}^{\varepsilon_e} \tau(z) \frac{du}{dz} dz = \int_{\varepsilon_e}^{H} \tau(z) \frac{du}{dz} dz \quad , \qquad [4.28]$$

where S_e is the energy slope that can be equated with the water slope in most cases, γ is the unit weight of water, and q is the unit discharge. Using equations 4.24 - 4.27 to integrate equation 4.28 yields

$$S_e \gamma q \kappa = (u_*)_n \left[(\tau_0'' - \tau_n) \frac{(\varepsilon_e - k_s)}{\varepsilon_e} + \tau_n \ln\left(\frac{\varepsilon_e}{k_s}\right) \right] + (u_*)_{n+1} \tau_0'' \left[\left(\frac{H}{H - \varepsilon_e}\right) \ln\left(\frac{H}{\varepsilon_e}\right) - 1 \right] . \qquad [4.29]$$

To compute form shear stress, they assume that the reference velocity (U_r) is equal to the vertically averaged mean velocity as

$$\tau_0'' = \frac{1}{2} \rho C_d \frac{H_d}{\lambda} U^2 \quad . \qquad [4.30]$$

This assumption by Fedele and Garcia (2001), which will be discussed later in Chapter 5, is based on the assumption that the turbulence production becomes negligible above the

equilibrium level (ε_e). Furthermore, Fedele and Garcia (2001) reason that because they assume internal equilibrium at ε_e, a force balance is required at this level such that

$$\int_{k_s}^{\varepsilon} \tau(z)dz = \int_{\varepsilon}^{H} \tau(z)dz \quad . \qquad [4.31]$$

From figure 4.44, equation 4.31 can be integrated to yield

$$(\tau_0'' + \tau_n)\varepsilon = \tau_0''(H - \varepsilon) \quad . \qquad [4.32]$$

To use the work of Fedele and Garcia (2001) as a velocity model, a value of C_d is assumed, the mean velocity is estimated, and the bedform dimensions must be known. The steps for computing the parameters are listed below.

1. Compute τ_0'' (form shear stress) by equation 4.30.
2. Assume a value for τ_{n+1} (note: $\tau_{n+1} = \tau_0$ and $\tau_{n+1} = \rho(u_*)_{n+1}^2$) .
3. Compute $\tau_n = \tau_{n+1} - \tau_0''$ (note: this is the shear partition formula; equation 2.41 and $\tau_n = \tau_0'$ and $\tau_n = \rho(u_*)_n^2$).
4. Compute ε_e using equation 4.32 .
5. Compute k_s from the log-linear velocity profile equation (equation 2.75) with the assumptions that at z = ε, u = U (vertically averaged

mean velocity), and the shear velocity is $(u_*)_n$, that can be computed from τ_n in step 3.

6. Compute both the left-hand-side and right-hand-side of equation 4.29 to determine if they match. If these sides do not match, go back to step 2.

4.7.2 Evaluation of Models

Each method was applied to the field data from this research as well as those of Smith and McLean (1977) and Kostaschuk and Villard (1996). The relative performances of the three models with the field data are shown in figure 4.45.

The Fedele and Garcia (2001) model consistently overpredicts velocity magnitudes. This overprediction is assumed to result because of the assumption inherent in the rationale that the form drag shear stress can be computed using the mean velocity as the reference velocity. This model consistently computed form drag shear stresses that were much higher than overall shear stresses computed by the product of the average depth, the water slope and the unit weight of water, resulting in overprediction of shear velocities for both regions of the flow.

To examine the validity of the assumption that the matching level has a local velocity that corresponds to the vertically averaged mean velocity, the collected field data can be examined (figure 4.30). The MO-1 data do not clearly indicate a matching level; however, the more detailed MO-2 data indicate that at what could be interpreted as a

point of matching for two different regions of flow (z = 42 cm), the velocity at this point (u = 69 cm/s) does not equal the vertically averaged mean velocity (U = 102.9 cm/s). The difference between the velocity at the matching point and the vertically averaged mean velocity also is indicated in data from Smith and McLean (1977), where the mean velocity for data set 69-W1 was 56.4 cm/s (table 4.8) but the velocity at the matching location was < 44 cm/s at an elevation of 169 cm above the bed (figure 4.46). The assumption of the mean velocity corresponding to the matching location, and the subsequent assumption that the reference velocity in the form drag closure is the mean velocity, are most likely the largest causes of the poor fit of the Fedele and Garcia (2001) model to the field data. As discussed previously, Fedele and Garcia (2001) never intended for their model to be a stand-alone velocity-profile model.

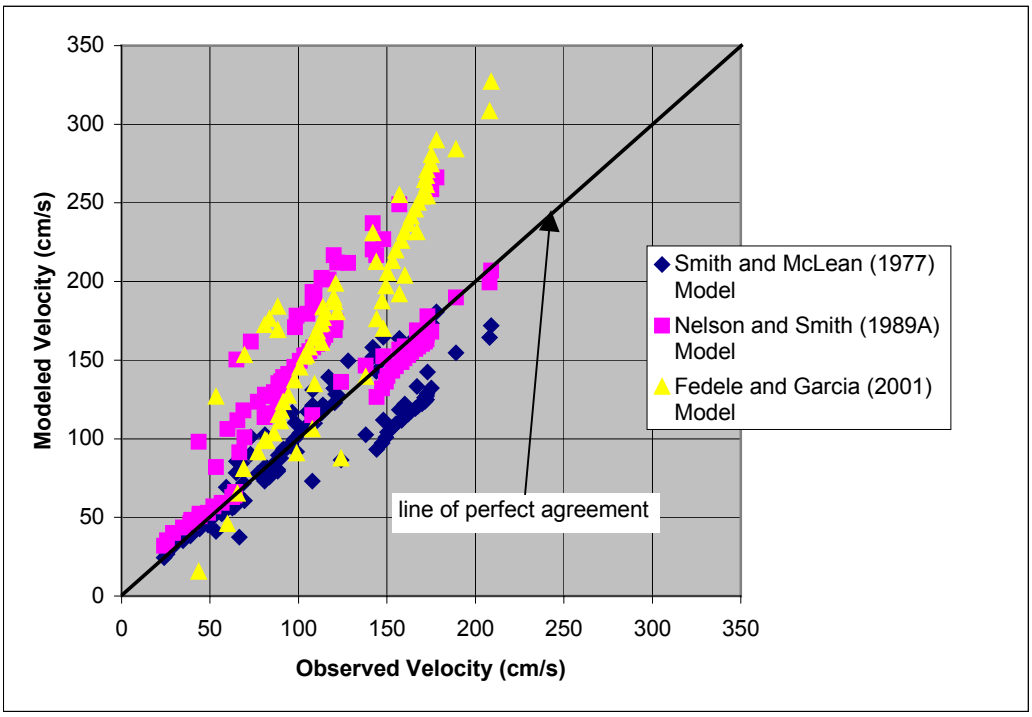

Figure 4.45—Comparison of all field data with results from three velocity distribution models

It would appear, from reviewing figure 4.45, that both Smith and McLean (1977) and Nelson and Smith (1989A) models have poor fits. Both models are sensitive to the estimate of the roughness parameter for the bottommost region $(z_0)_1$ (figure 4.47). The roughness parameter estimated from both methods for the field data sets are listed in table 4.10. It can be seen that the Smith and McLean method consistently provides a larger estimate of $(z_0)_1$.

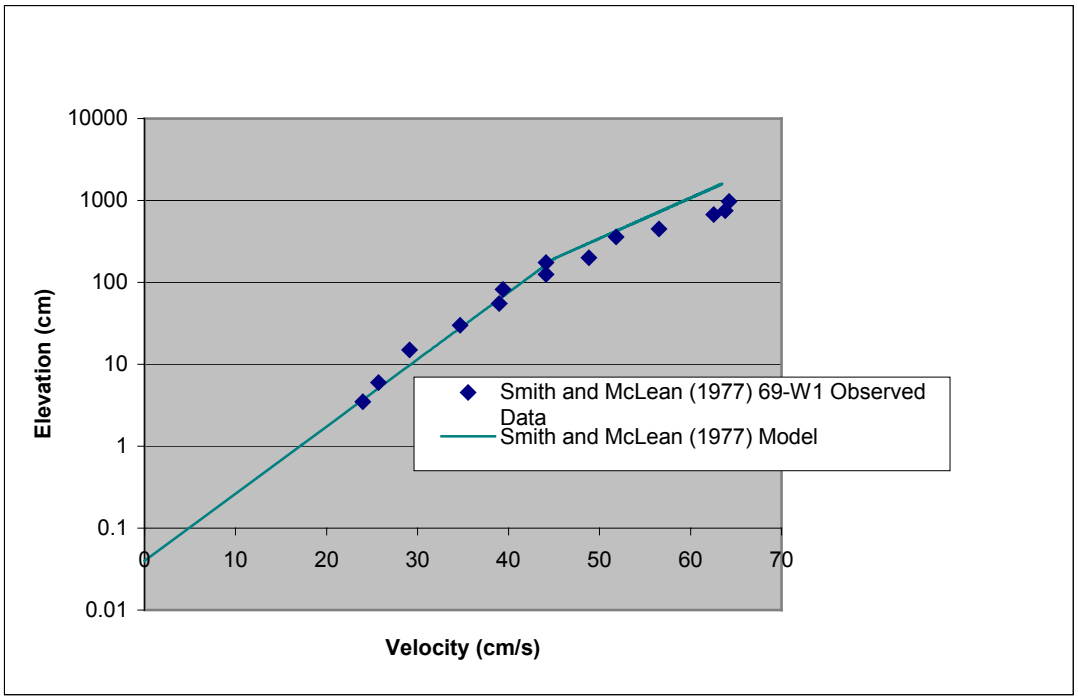

Figure 4.46—Spatially averaged velocity profile from Smith and McLean (1977) 69-W1 data set

Upon further examination of model results, it was noted that by dividing the field data sets into two separate groups by the rationale described in Section 4.3: 1) data sets with bedforms that approach an equilibrium dune situation (MO-2; Kostaschuk and Villard

(1996), June 27;, Kostaschuk and Villard (1996), June 29; Smith and McLean (1977), 69-W1; and Smith and McLean (1977), 72-W1) and 2) data sets with no bedforms that approach an equilibrium dune situation (KANK-1; MO-1; and Kostaschuk and Villard (1996), June 21), there was marked improvement in the each models relative performance when selectively applied. The Smith and McLean (1977) model best described those data sets with bedforms that could be characterized as equilibrium dunes (figure 4.48), whereas the Nelson and Smith (1989A) model best described those data sets with bedforms that could not be characterized as equilibrium dunes (figure 4.49). KANK-1 data was not described well by either modeling scheme.

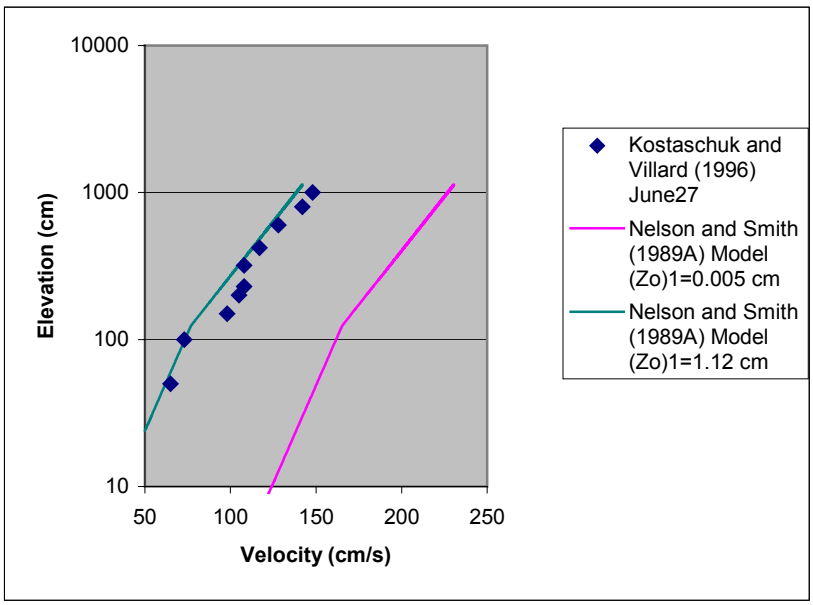

Figure 4.47—Velocity profiles estimated by the Nelson and Smith (1989A) model with different estimates of $(z_0)_1$ (0.005 cm is the estimate of $(z_0)_1$ given by the Nelson and Smith (1989A) model, and 1.12 cm is the estimate of $(z_0)_1$ given by the Smith and McLean (1977) model, but used in the Nelson and Smith (1989A) model)

Model		**$(z_0)_1$ (cm)**	
Simulation	**S-M**	**N-S**	**N-S^A**

KANK1	0.347	0.00247	0.0062
MO-1	0.674	0.0004	0.0062
MO-2	0.866	0.00273	0.0062
S-M69-W1	0.0471	0.00194	0.005
S-M72-W1	1.053	0.00244	0.005
K-V June 21	1.174	0.00248	0.005
K-V June 27	1.12	0.0025	0.005
K-V June 29	1.526	0.00248	0.005

S-M, Smith and McLean (1977); N-S, Nelson and Smith (1989A); K-V, Kustaschuk and Villard (1996); $(z_0)_1$, roughness parameter for the bottommost region; A, This value is the simplified value, assuming that $(z_0)_1 \approx 0.20D$

Table 4.10—Bottommost-region roughness parameter estimated by the models of Smith and McLean (1977) and Nelson and Smith (1989A)

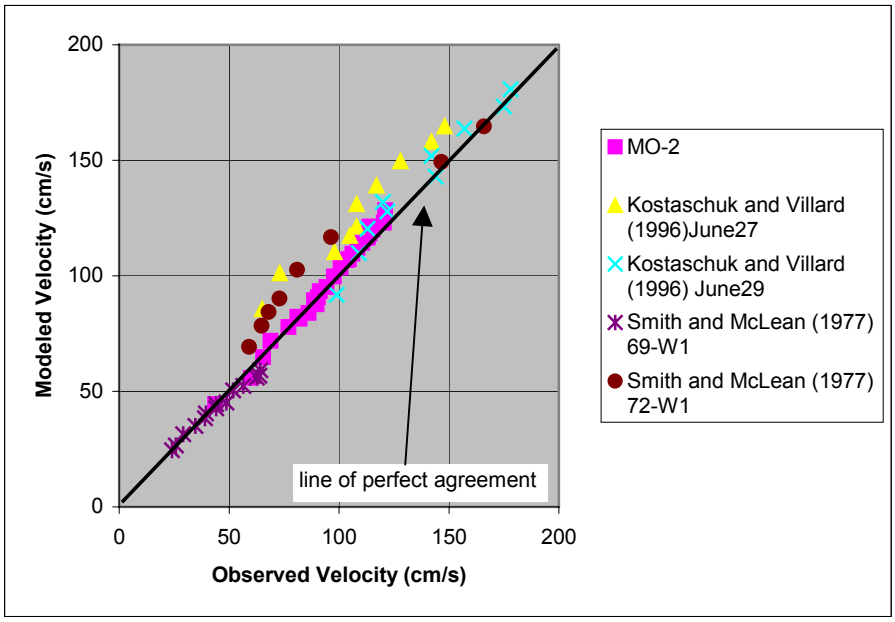

A

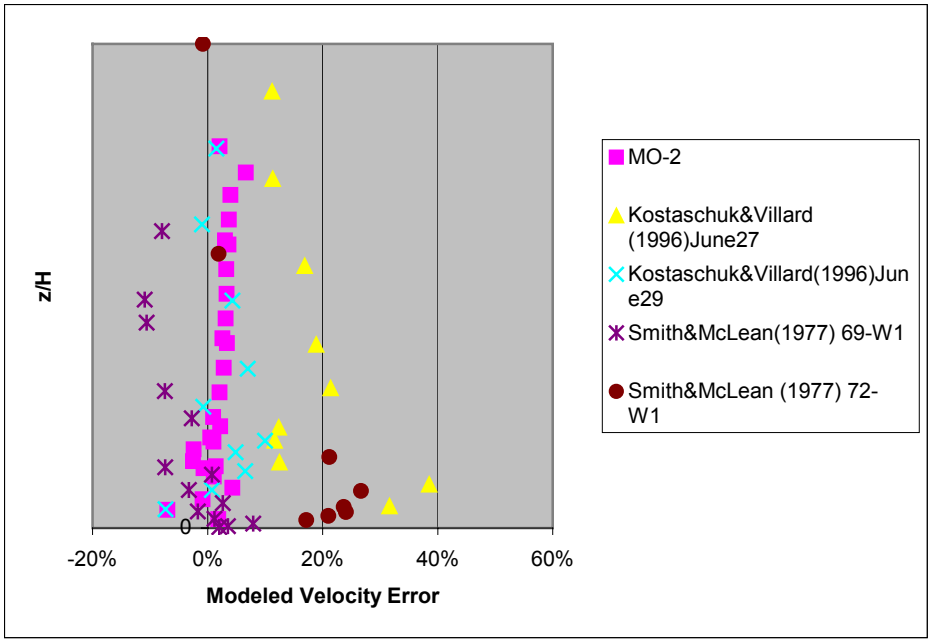

B

Figure 4.48—A) Observed and modeled velocities for the Smith and McLean (1977) model, and B) percent error by dimensionless depth

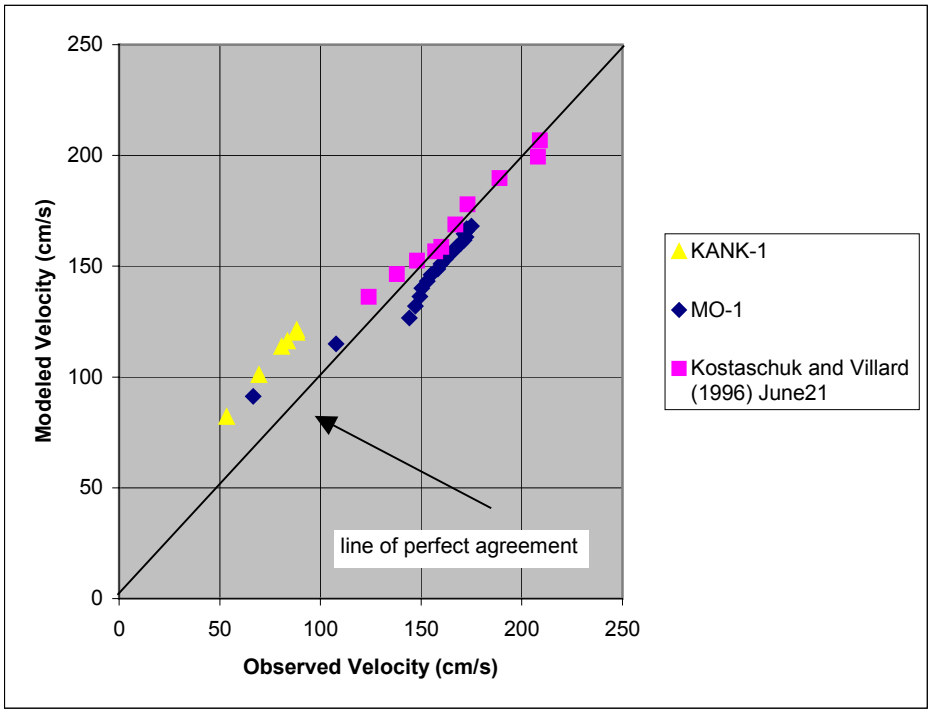

A

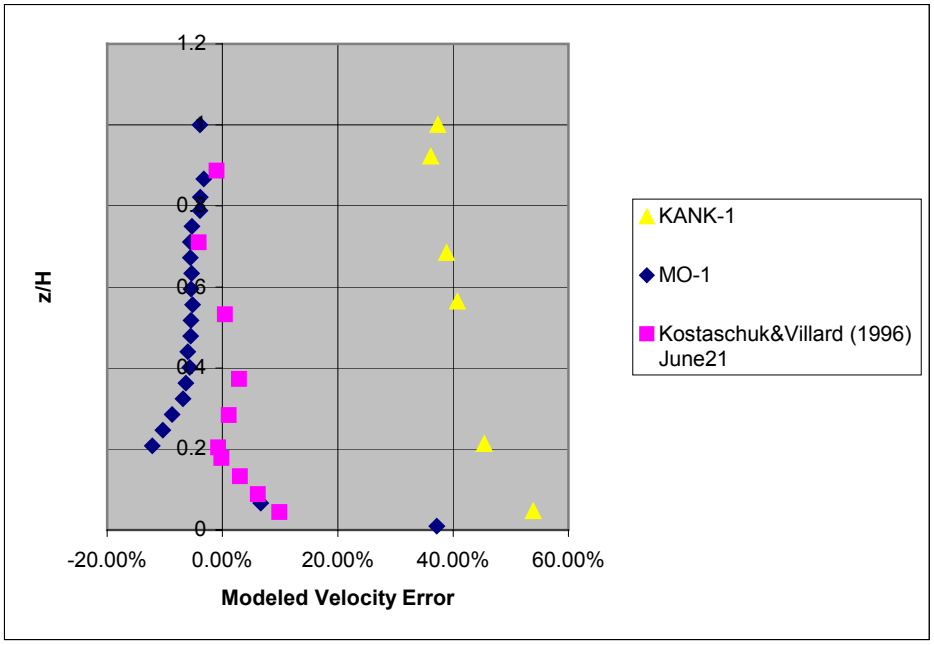

B

Figure 4.49—A) Observed and modeled velocities for the Nelson and Smith (1989A) model, and B) percent error by dimensionless depth

When bedforms approach equilibrium conditions, the non-symmetric dunes induce flow separation. As this separation occurs, the momentum extracted near the bed (and throughout the flow) no longer just results because of the saltating grains but also because of the dunes themselves. Therefore, the roughness parameter $(z_0)_1$ has to increase to reflect this. The Smith and McLean (1977) model produces a larger estimate of $(z_0)_1$, and, thus, the model performs better when dunes start to evolve into the regime where the flow is affected by form roughness from the dunes as a large part of the overall resistance. The Nelson and Smith model has a consistently smaller estimate of $(z_0)_1$, as compared to the Smith and McLean (1977) model, of the order of grain-only roughness with form roughness being a negligible part of the bottommost roughness parameter.

4.8 Spatially Averaged Velocity-Defect Model

In formulating or adapting any model for spatially averaged velocities, the purpose for the model should be considered. If the detailed vertical distribution of velocity information is necessary for applications such as sediment-load estimates, then the accuracy of point velocities is more important than would be the case if the application only required a vertically averaged mean velocity, such as for computing water discharge. As was presented in the previous section, a combination use of the Smith and McLean (1977) and Nelson and Smith (1989A) models could be used, with the model selection based on the type of bedforms present. As was demonstrated , this model can provide fairly accurate estimates of velocity. However, with uncertainty in predicting the dune geometry (see Chapter 2), which is a requirement of the models, the application of these models remains problematic. Therefore, it is worthy to examine a simplified and practical approach to estimating the spatially averaged velocities.

Nikuradse's work first revealed that the velocity-defect law is applicable to the bulk of the flow depth, which is unaffected by the grain-roughness scale (Perry and others, 1969) (grain roughness is termed 'k' type roughness by Perry and others (1969), as opposed to 'd' type roughness, which is not represented in alluvial flows). Examination of those velocity data collected from experiments where equilibrium dunes were present (MO-2, Smith and McLean (1977), and Kostaschuk and Villard (1996)), indicate that a multi-segment, log-linear velocity profile is typically present. One could deviate from the

observed multi-segment form for the reachwise spatially averaged velocity profiles over bedforms and assume that a single log-linear velocity profile could suffice. Obviously, ignoring the multi-segmentation of the velocity profile would most likely result in an increased error, however, the relative ease of application may make some of the increased error acceptable. In addition, as has been demonstrated from some of the present field data, a single log-linear fit is reasonable (figures 4.30A,B).

As has been previously mentioned in Section 2.2.2.4, the log law only accounts for the wall shear stress, and does not include pressure and inertia terms (which are important in flow over dunes). A wake term can be added in the form previously presented as

$$\frac{u}{u_*} = \frac{1}{\kappa}\ln\left(\frac{u_* z}{\nu}\right) + A + w(\frac{z}{H}) \quad , \qquad [2.86]$$

where A is the constant for the typical logarithmic velocity profile (A=5.5 for smooth boundaries and A=$8.5 - \frac{1}{\kappa}\ln\left(k_s u_* / \nu\right)$ for completely rough flow), and w(z/H) is a wake function from Coles (1956) having the form

$$w(\frac{z}{H}) = \frac{2W_0}{\kappa}\sin^2\left(\frac{\pi}{2}\frac{z}{H}\right) \quad , \qquad [2.87]$$

where W_0 is the Coles wake parameter, expressing the strength of the wake function.

In an attempt to further simplify the velocity model, the defect form of the log-linear velocity model could be used to eliminate one of the most difficult (and sensitive) velocity model parameters, the roughness parameter (k_s). Equation 2.86 can be put in velocity defect form as

$$\frac{U_m - u}{u_*} = -\frac{1}{\kappa}\ln\left(\frac{z}{H}\right) + \frac{2W_0}{\kappa}\cos^2\left(\frac{\pi z}{2H}\right) \quad . \qquad [2.89]$$

The parameters to be estimated for application of this model are U_m, u_*, and W_0. The inclusion of the wake parameter gives the added benefit of adding some non-linearity (in log-linear space) to the velocity profile, which has been shown to occur in the spatially averaged velocity profile over bedforms (figure 4.37).

As the data from this research have been found to collapse well when plotted in defect form when the bulk shear velocity is used as the similarity parameter (figure 4.33), the reach-averaged bulk shear velocity will be used and can be computed from the reach-averaged total shear stress computed in equation 2.55 knowing that

$$\rho u_*^2 = \tau_0 = \rho g \langle H \rangle S \quad , \qquad [2.55]$$

which allows that the bulk shear velocity be given by

$$u_{*T} = u_* = \sqrt{g \langle H \rangle S} \quad , \qquad [4.33]$$

where S is the water surface slope and <H> is the spatially averaged mean flow depth. U_m would have to be supplied, which is not unreasonable given that in simple applications such as streamgaging, instrumentation is available that can remotely sense surface velocities.

On the other hand, Coles wake parameter (W_0) needs to be estimated. Coleman (1986) established that the wake parameter varies with sediment concentration. Through examination of the momentum equations (equation 2.85), it is known that inertial and pressure terms affect the wake parameter.

In an attempt to arrive at a relation for W_0 and inertial/pressure influences, W_0 was plotted against measures of bedform geometry that possibly could be considered surrogates for pressure and inertia parameters. As can be seen from figures 4.50 –4.52, no definitive relation could be found (W_0 was computed according to the method of Julien (1995) and described in Section 2.2.2.4). It is interesting to note that the values of W_0 for the present field data are lower (even negative for both MO-1 and MO-2) than those of Smith and McLean (1977) and Kostaschuk and Villard (1996).

The effect of sediment on the wake parameter can be represented in terms of the gross flow Richardson number that is defined from Coleman (1986) as

$$R_{ig} = \frac{gH(\rho_s - \rho)}{\langle \rho \rangle U_m^2} \quad , \qquad [4.34]$$

where $\langle \rho \rangle$ is the vertically averaged, sediment-water mixture density. A relation was defined to determine W_0 from the Richardson number (figure 4.5). One data set from each of the three investigations, Smith and McLean (1977), 69-W1; Kostaschuk and Villard (1996), June 29; and MO-2; was not used in construction of figure 4.53, therefore these data could be used as a verification data set.

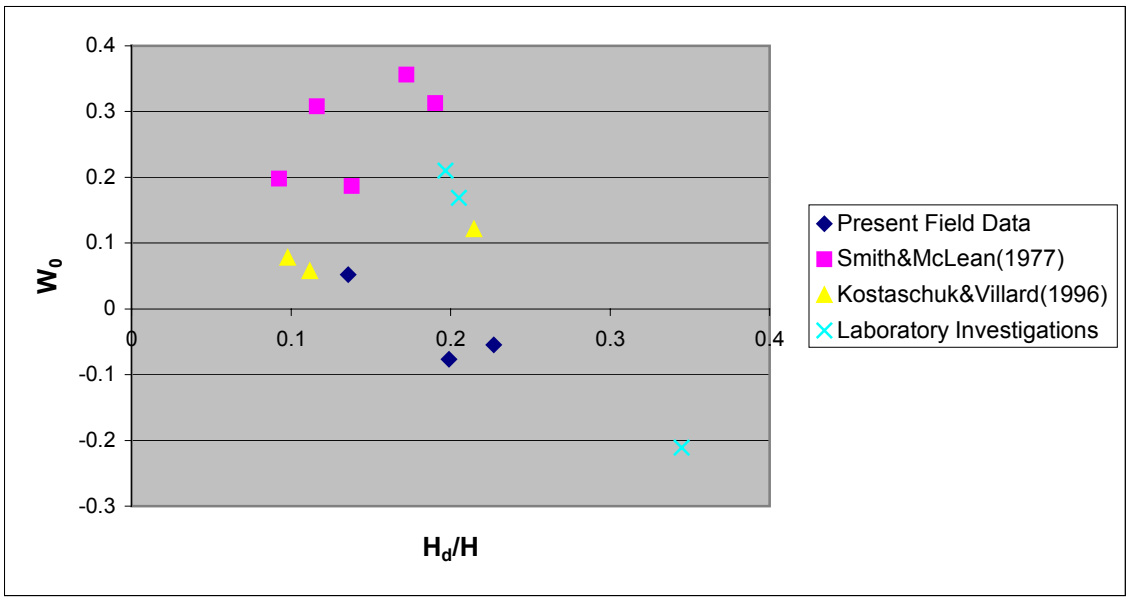

Present Field Data includes KANK-1, MO-1, MO-2; Laboratory Investigations includes: Nelson and others (1993), Lyn (1993) Case 3, and Bennett and Best (1995)

Figure 4.50—Coles wake parameter as a function of the ratio of bedform height to flow depth

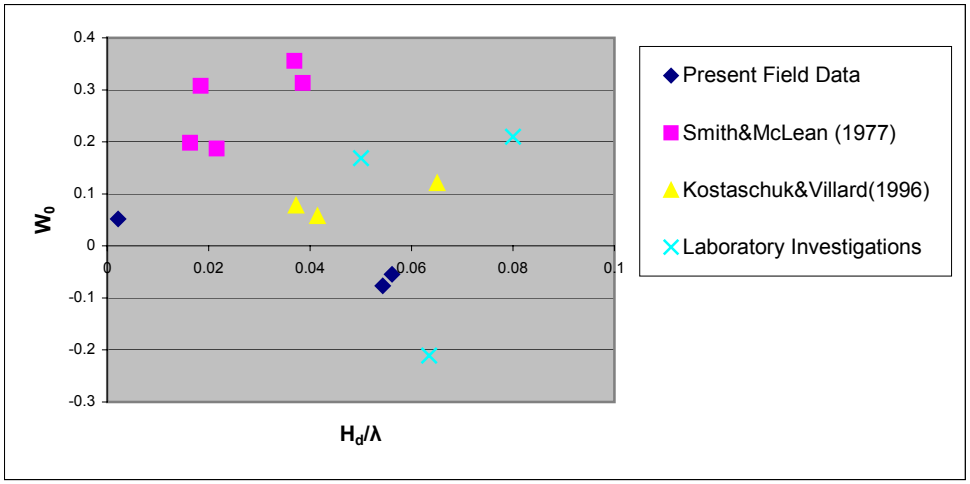

Present Field Data includes KANK-1, MO-1, MO-2; Laboratory Investigations includes: Nelson and others (1993), Lyn (1993) Case 3, and Bennett and Best (1993)

Figure 4.51—Coles wake parameter as a function of the ratio of bedform height to dune length

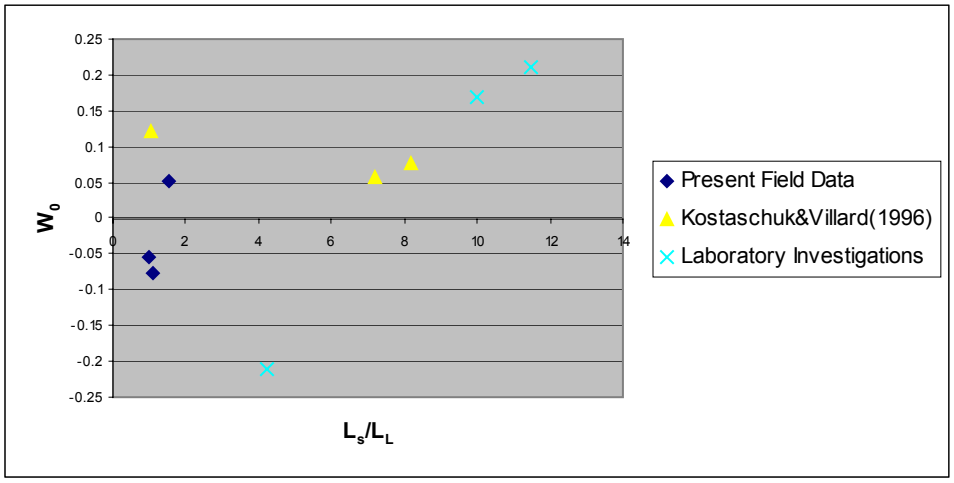

Present Field Data includes KANK-1, MO-1, MO-2; Laboratory Investigations includes: Nelson and others (1993), Lyn (1993) Case 3, and Bennett and Best (1993)

Figure 4.52—Coles wake parameter as a function of the bedform symmetry ratio

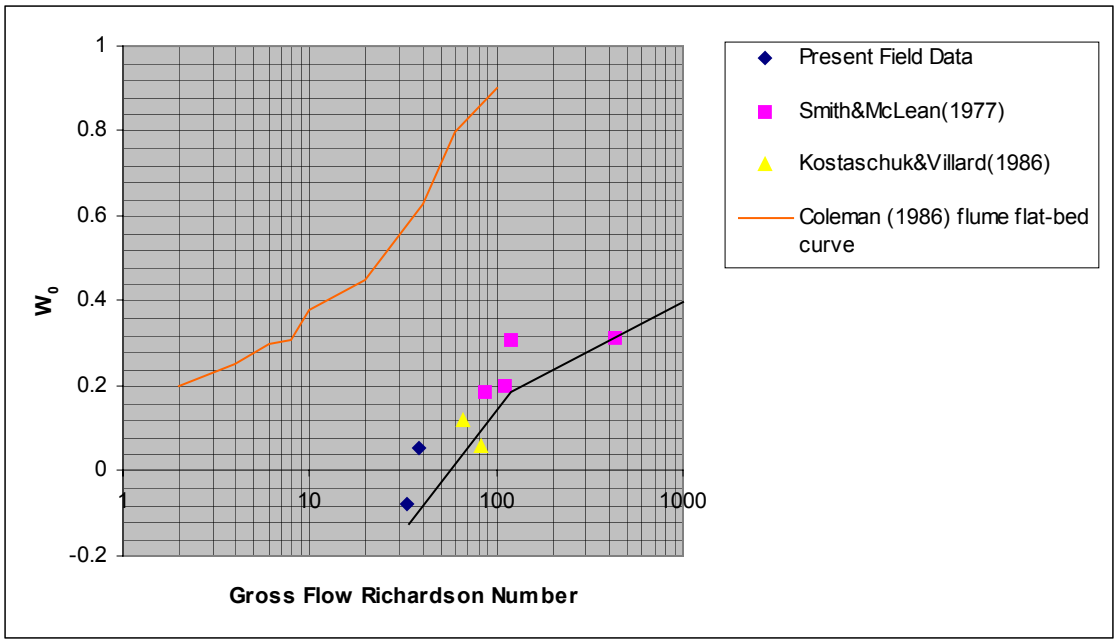

Present Field Data includes KANK-1, MO-1;

Figure 4.53—Coles wake parameter as a function of the gross flow Richardson number

The vertical average of the sediment-water mixture density $\langle \rho \rangle$ was determined for the data plotted on figure 4.53 by using the one sample of sediment concentration collected for each data set (except for MO-2) [3] and using the well-know Rousean distribution to estimate the vertical distribution of sediment concentration. The density at each location in the vertical was then computed as

$$\rho_f = \rho_s c + \rho \ (1 - c) \quad , \qquad [4.35]$$

where c is the volumetric sediment concentration.

[3] For the MO-2 data set, the reference sediment concentration for use in the Rousean distribution was estimated to be equal to that of the MO-1 data set.

The original laboratory flume work of Coleman (1986) where flat beds were used are shown in in figure 4.53. There is an obvious scale difference between the work of Coleman and field situations. As was discussed in Section 2.2.2.4, the Coles wake parameter is used to help account for pressure and inertial forces. With the presence of bedforms, there should be appreciable pressure and inertial effects. However, it is seen that the presence of sediment at capacity suspension has a greater effect on Coles wake parameter.

A two-segment linear relation is fit through the data and shown in figure 4.53. Using this two-segment linear relation, the Coles wake parameter can be estimated. Computing the bulk shear velocity from equations 2.55 and 4.33 and assuming that the maximum velocity and total depth are known, computation of the velocity profile can proceed from equation 2.89. Plots of the model performance in comparison to the field observed data of MO-2; Smith and McLean (1977), 69-W1; and Kostaschuk and Villard (1996), June 29 are shown in figures 4.54-4.56. A summary plot of observed velocity versus modeled velocity for these validation data sets is shown in figure 4.57. The velocity-defect model performs well away from the bed ($z/H>0.1$), where the error is +/- 10 % in all cases (figure 4.58). The accuracy decreases near the bed ($z/H<0.1$). This accuracy decrease is especially true for those situations where the bed becomes more dune-like (increasing lee vortices) and the flow separation is strong resulting in a definitive two-segment, log-linear velocity profile, such as the case of Smith and McLean (1977) 69-W1 data set (figure 4.36). The increased lee vortices also cause more sediment to be entrained into the flow, thus increase the gross flow Richardson number.

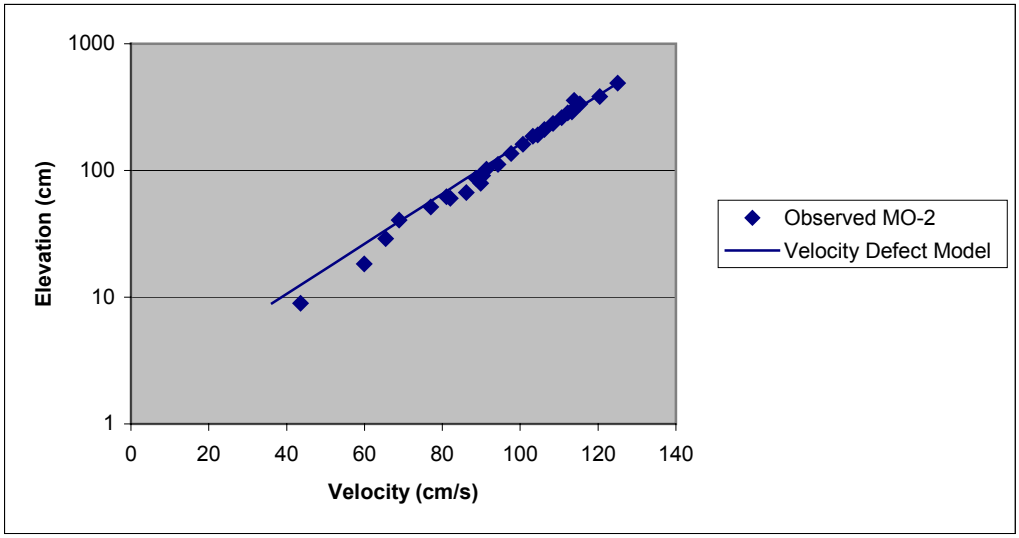

Figure 4.54—Observed and velocity-defect modeled velocity profiles for MO-2 data

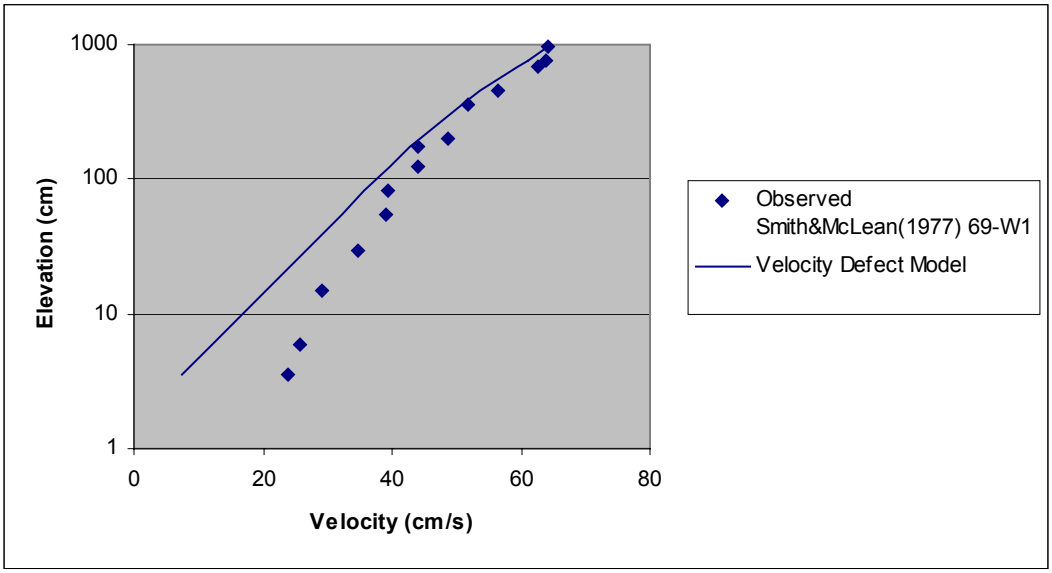

Figure 4.55—Observed and velocity-defect modeled velocity profiles for Smith and McLean (1977) 69-W1 data

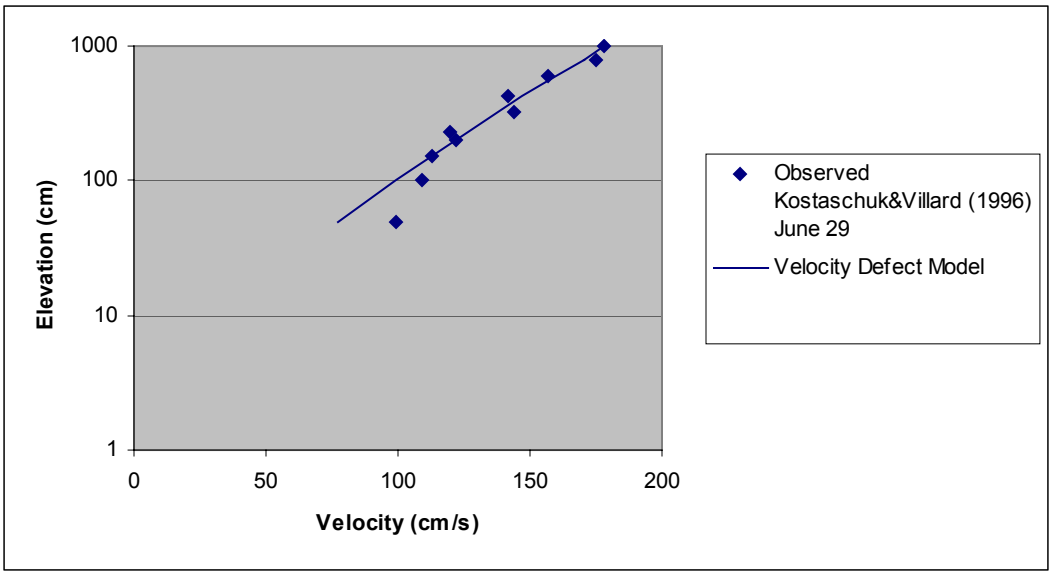

Figure 4.56—Observed and velocity-defect modeled velocity profiles for Kostaschuk and Villard (1996) June 29 data

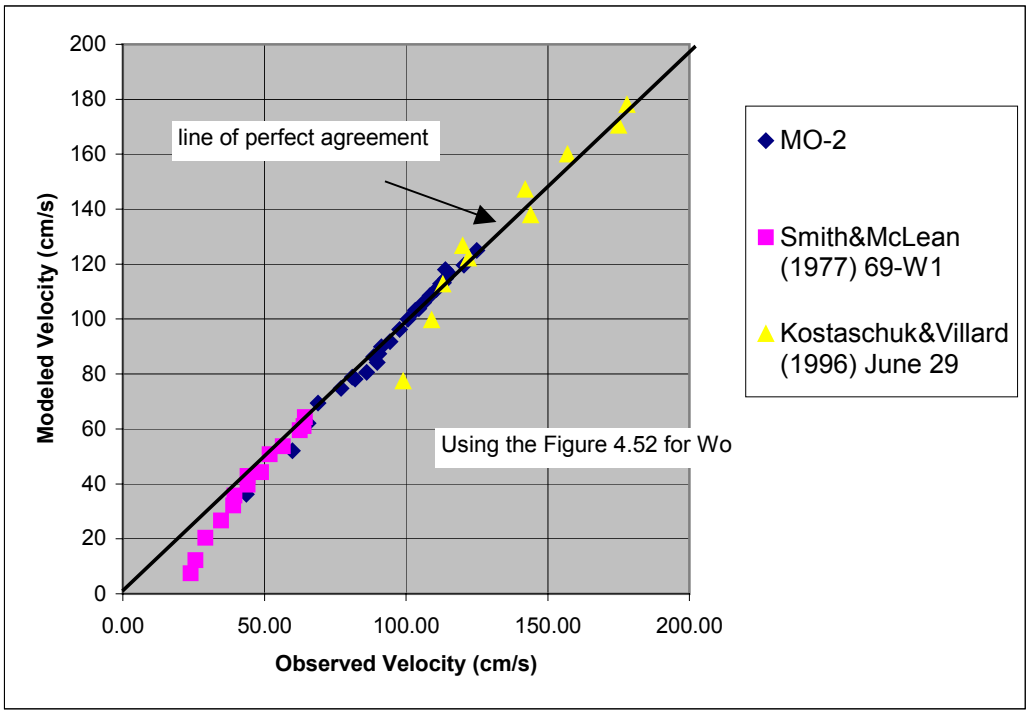

Figure 4.57—Observed and modeled velocity for the velocity-defect model using the Coles wake parameter relation

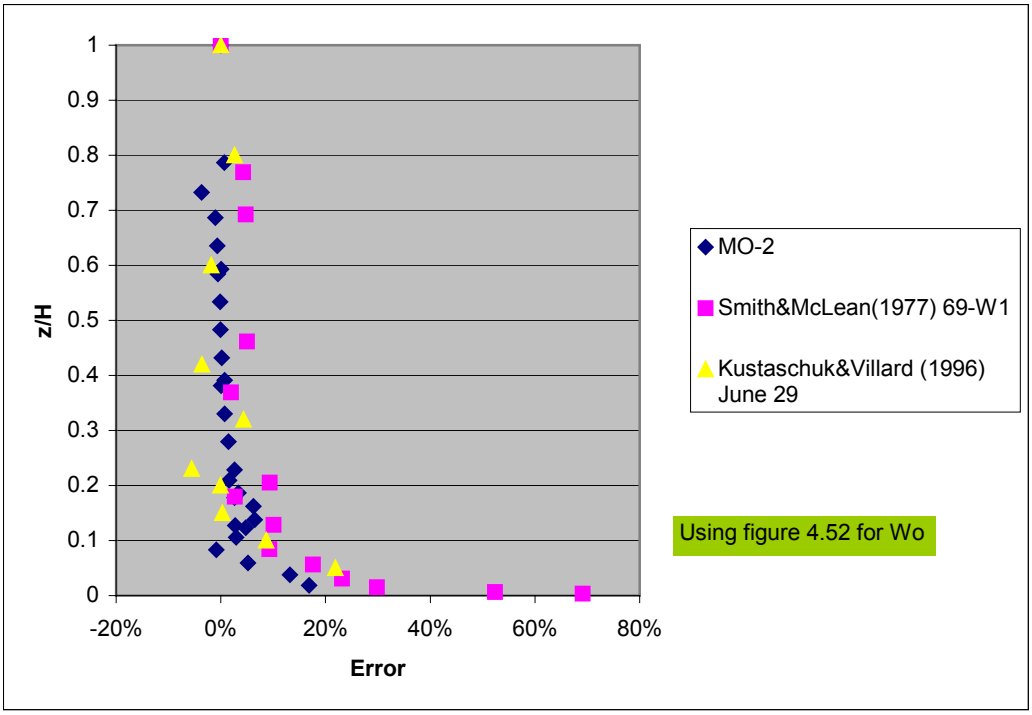

Figure 4.58—Velocity-defect model error as a function of dimensionless elevation above the bed

The vertically averaged mean velocities for modeled and observed velocity profiles are shown in table 4.11. In all cases, modeled mean velocity is within +/- 2% of observed mean velocity.

Data Set	**Obs. U (cm/s)**	**W_0[1]**	**Model U[2] (cm/s)**	**Model U[3] (cm/s)**
KANK-1	74.63	-0.035	74.37	73.94
MO-1	152.05	-0.08	151.78	149.85
MO-2	102.93	0.02	102.58	103.01
S-M 69-W1	54.81	0.36	54.12	56.84
S-M 72-W1	145.70	0.16	147.13	147.13
K-V June 21	182.90	0.09	179.50	182.08
K-V June 27	122.80	0.14	121.20	124.66
K-V June 29	151.80	0.079	150.00	152.13

[1] W_0 estimated from figure 4.52

[2] Mean velocity for the velocity-defect model using the tabulated W_0 values estimated from figure 4.52
[3] Mean velocity for the velocity-defect model using W_0 equal to 0

Table 4.11—Mean velocities computed by the velocity-defect model for the associated Coles wake parameter

Simply estimating W_0 from figure 4.53 alone solves the problem of having to know dune geometry; however, some knowledge of the sediment concentration distribution must be known. Assuming equilibrium conditions, as was done in computing the gross flow Richardson number used in constructing figure 4.53, the sediment concentration distribution could be estimated from a combination of the Rousean distribution[4] and an entrainment function, such as that of Garcia and Parker (1991)[5]. However, the accuracy of such an approach is questionable (Robert R. Holmes, Jr., unpublished work on the Missouri River). Therefore, the velocity-defect model was used assuming $W_0 = 0$ for all data sets to determine the degradation of the results if the Coles wake parameter was neglected.

---

[4] $c = c_b \left[\frac{(H-z)/z}{(H-b)/b} \right]^{Z_R}$, where $Z_R = \frac{v_s}{\kappa u_*}$; also own as the Rouse number, v_s = terminal fall velocity of sediment in quiescent fluid,

[5] $E_s = \frac{A Z_u^5}{\left(1 + \frac{A}{0.3} Z_u^5\right)}$, where A=1.3x10^{-7} and $Z_u = \frac{u'_*}{v_s} R_{ep}^{0.6}$

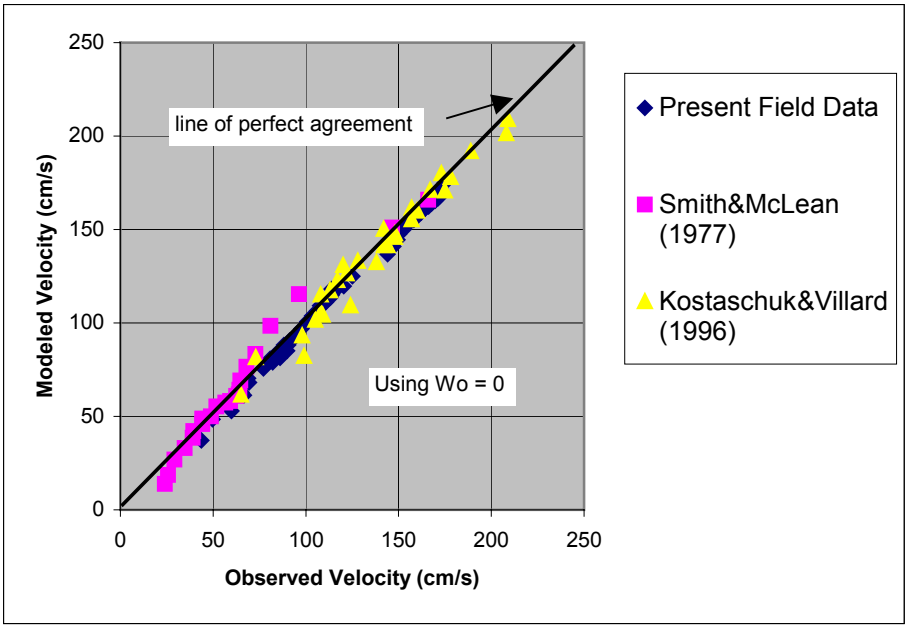

Figure 4.59-- Observed and modeled velocities (with the Coles wake parameter neglected) for all field data

A summary plot of observed velocity versus modeled velocity with the Coles wake parameter neglected (W_0=0) is given in figure 4.59. Even neglecting the wake parameter, the velocity-defect model still performs well away from the bed (z/H>0.3), where the error is +/- 10% in all cases (figure 4.60). This seems to indicate that the influence of bedforms on the spatially averaged velocities in the outer-flow region is less than what would have been previously thought.

The model accuracy decreases in the range z/H <0.3. In this near-bed range, the data all are within +/- 20% error, with the exception of the Smith and McLean (1977) 69-W1 data. When the vertically averaged mean velocities computed using the velocity-defect model with the wake parameter neglected in table 4.11 are examined, the modeled mean velocities have an averaged absolute error value of 1.15 % with all modeled mean

velocities within 2% of the observed vertically averaged mean velocities. The exception to these results is the 69-W1 data set, where the percent error was +3.7 percent.

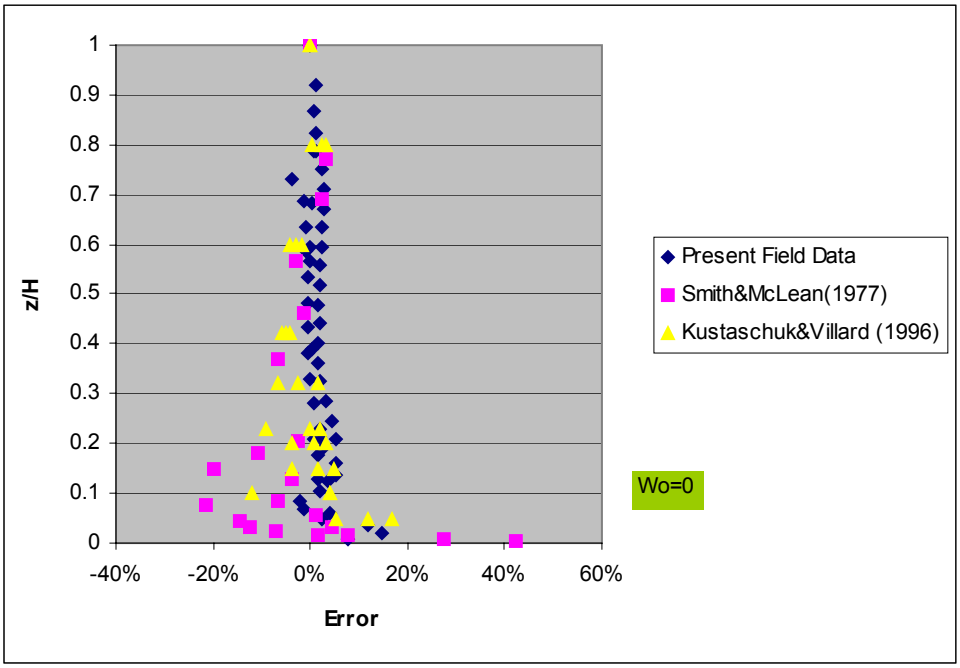

Figure 4.60-- Velocity-defect model error (with the Coles wake parameter neglected) as a function of dimensionless elevation above the bed

It is notable to compare the velocity-defect model performance with that of the Smith and McLean (1977) model (figure 48B) and the Nelson and Smith (1989A) model (figure 49B). The velocity-defect model consistently describes the velocities of the observed field data better than either that of the Smith and McLean (1977) or the Nelson and Smith (1989A) models.

4.7. Conclusions

Detailed measurements of velocity fields over bedforms were made successfully for both the Kankakee and Missouri Rivers. The bedforms for the Kankakee River (KANK-1)

data set consisted of elongated non-symmetrical bedforms. Two data sets were collected on the Missouri River, with the first being symmetrical bedforms (MO-1) and the other having non-symmetrical larger bedforms with smaller superimposed bedforms (MO-2). Field data sets from Smith and McLean (1977) and Kostaschuk and Villard (1996) also were used in this research. The MO-2 data set, the Smith and McLean data sets, and the June 27 and June 29 data sets of Kostaschuk and Villard (1996) were determined to be near-equilibrium dunes. The KANK-1 and MO-1 data sets, along with the June 21 data set of Kostaschuk and Villard (1996), had bedforms that did not fit into the equilibrium dune category.

The MO-2 data set provides the best velocity data detail, as the ADV was deployed every 0.1 m, for the first meter above the bed, and every meter from there to the water surface. Interspersed with the ADV data were those of the ADCP, which provided good, valid mean velocity information every 0.25 m, from 1.5 m above the bed to within 1 m of the water surface.

MO-2 and MO-1 (figures 4.14 and 4.16) both had detectable flow separations downstream of the dune crest, with negative velocities being recorded for MO-2 (figure 4.124). The larger bedforms in MO-2 have bedform geometry scale ratios similar to those for the bedforms of KANK-1; however, KANK-1 (figure 4.15) had no detectable flow separation, as the lee slope is gradual and not conducive for flow separation. The

traditional model of flow separation, flow reattachment, diffusion of momentum defect, and boundary-layer development is confirmed in flow situations like MO-2 with the dunes superimposed on larger waves. The presence of the superimposed dunes induces flow that appears to detach and reattach at numerous points along the large wave structure.

Marked decreases in velocity throughout the water column downstream of the dune crest are noted for MO-1 (figure 4.16) with a weaker decrease apparent for the MO-2 (figure 4.14) and KANK-1 data (figure 4.15). These decreases are believed to be the result of pressure-gradient (topographically induced) effects felt for the entire depth of flow (H increasing locally). This "wavelike" response of the flow to the bedforms was apparent in these field scale experiments as in laboratory flume experiments.

For the local velocity profiles, the velocity was found to be logarithmic with good collapse of the data in both inner and outer regions (using the typical scales) except in the near bed ($z/H < 0.15$) and in MO-1, where the profiles immediately downstream of the dune crest do not collapse well. In all cases, the local shear velocity enabled good collapse of the velocity data above $z/H>0.15$. For $z/H<0.15$, MO-1 and MO-2 had no universal structure to the velocity profiles, which is consistent with the findings of Lyn (1993), who noted that this region would "exhibit only weakly (if at all) any universal structure".

Coles wake parameter for the local velocity profiles was found to vary from as much as +0.252 at the crest of a dune to –0.286 in the trough. In most cases, the wake coefficient was positive in locations where the bed elevation was increasing (adverse pressure gradient) and negative in locations where the bed elevation was decreasing (favorable pressure gradient). There appears to be some sort of lag present, as the wake coefficient does not change from positive to negative until some point after the bedform crest (figure 4.29).

The spatially averaged velocity profiles for those experiments with bedforms that do not approximate a equilibrium dune can be well characterized with a single logarithmic function. The spatially averaged velocity profiles for those experiments with bedforms that approximate equilibrium dunes have a two-segment logarithmic relation. All the field data collected in this research collapse sufficiently well when plotted in inner scales (bulk shear velocity and the composite roughness length) (figure 4.32); however, the collapse is better when the data are plotted in velocity-defect form (figure 4.33). The absence of universal flow structure close to the bed in the local velocity data from MO-1 and MO-2, is not apparent in the spatially averaged data.

The spatially averaged laboratory velocity data appear to have similarity parameters equivalent to those for field data; however, the capacity of the laboratory data to collapse is not as good (figure 4.34). The inability to collapse is thought to be the result of higher sensitivity of the laboratory data to boundary conditions such as bedform geometry ratio, bedform to flow depth ratio, etc.. The laboratory data (which have equilibrium dunes for

bedforms) have two-segment log-linear velocity profiles similar to the field data collected over equilibrium dunes (figure 4.37). The portion of momentum extracted by the bedform is similar for both the laboratory- and field-scale flows.

The local velocity profiles of the lab results collapse well on the field data near bedform crests. The lab results for Lyn (1993) collapse well with the field data in near bedform troughs, however, the results of Bennett and Best (1995) do not collapse well in this region. This result likely is attributable to the larger ratio of dune height to flow depth for the Bennett and Best (1995) data (table 4.2) that was discussed earlier. This good collapse of the Lyn laboratory data at both the crest and the trough indicates that the flume accurately simulates field velocity profiles over dunes of similar geometry and flow. It is apparent by examining the bedform geometry of KANK-1, MO-1, and MO-2 that the bedforms encountered in the field are more complicated in nature than those often studied in the laboratory. Field-scale flows sometimes present bedform geometries that cannot be classified as dunes in the classical sense, and thus are different from many of the bedforms present in laboratory studies. In examining the available methods for predicting bedform type, it is apparent that current methods are lacking in their ability to accurately predict the type of bedform present in the field flow.

When evaluating the available spatially averaged velocity-profile models, the models of Smith and McLean (1977) and Nelson and Smith (1989A) perform adequately when properly applied to flow with appropriate bedform type (figures 4.48 and 4.49). These models are highly sensitive to the bottommost roughness parameter estimation. As such,

the Smith and McLean (1997) model works best when the bedforms approximate equilibrium dunes, where form roughness is an important part of the overall roughness. The Nelson and Smith (1989A) model works best when the bedforms are not equilibrium bedforms and grain roughness predominates (form roughness is less important).

The standard velocity-defect-wake model was tested for the spatially averaged velocity profiles of field data, with bedforms present. Coles wake parameter was presented as a function of the gross flow Richardson number, which requires some knowledge of the vertical-density distribution (sediment concentration being the predominate factor in the density). The model estimates the vertically averaged mean velocity to within 2%, and estimates the point velocities to within +/- 10% for z/H>0.1 (figure 4.58). If sediment concentration cannot be estimated, the model was tested with the assumption that the wake effect was negligible. The vertically averaged mean velocity was found to be within 2% for all but one data set (+3.7%), but the point velocities accuracies decrease to +/- 10% for z/H>0.3 (figure 4.60). The velocity-defect-wake model was found to consistently describe the velocities of the observed field data better than either the Smith and McLean (1977) (figure 4.48B) or the Nelson and Smith (1989A) models (figure 4.49B).